



**POLITECNICO**  
**MILANO 1863**

DIPARTIMENTO DI  
INGEGNERIA CIVILE E AMBIENTALE

# Finite Element Model Updating for Digital Twin Development using Operational Modal Analysis: The JRC Atmospheric Tower Case Study

TESI DI LAUREA MAGISTRALE IN  
CIVIL ENGINEERING - INGEGNERIA CIVILE

Author: Haseeb Ali  
Student ID: 222834

Advisor: Prof. Luca Martinelli  
Co-advisors: Eng. Flavio Bono, Prof. Federico Perotti

Academic Year: 2024-25



# Abstract

The development of accurate numerical replicas of existing civil structures is challenged by the many inherent uncertainties, such as the precise identification of the material elastic properties or the correct boundary conditions. This thesis presents the development of an accurate model that replicates the actual structure behaviour (digital twin) of the 100 m-tall Atmospheric Observatory tower, a steel truss structure located at the European Commission (EC) Joint Research Centre (JRC) in Italy, part of the European Research Infrastructures on climate change and air quality. To monitor the tower, wireless autonomous accelerometers have been positioned at different elevations of the tower structure to acquire structural vibrations continuously. Operational modal analysis Operational Modal Analysis (OMA) techniques are implemented to identify the dynamic properties of the tower from field sensor measurements, and a numerical model of the tower structure has been developed to provide additional insight into the status of the structure and its dynamics. In this thesis, we implement model updating techniques to minimize the errors between the real structure and the Finite Element (FE) model based on the modal properties calculated from the vibration sensors data. With the adoption of model updating techniques, the improved numerical model is shown to reproduce the tower's dynamic response accurately. The present work highlights the importance and challenges of model updating using OMA, from real-time vibration sensor measurements to develop accurate digital twins, with the real-world test case of the JRC Atmospheric Observatory tower. The study gives an idea of the importance of model updating in enhancing the accuracy of digital twins of complex reticular structures, thus providing a valuable tool for accurate digital twins to improve structural health monitoring and support predictive maintenance strategies.

**Keywords:** structural health monitoring, operational modal analysis, modal updating, finite element method, damage detection



# Abstract in lingua italiana

Lo sviluppo di repliche numeriche accurate di strutture civili esistenti è sfidato dalle molte incertezze intrinseche, come l'identificazione precisa delle proprietà elastiche dei materiali o la corretta definizione delle condizioni al contorno. Questa tesi presenta lo sviluppo di un modello accurato che replica il comportamento reale della struttura (digital twin) della torre Atmospheric Observatory, una struttura reticolare in acciaio alta 100 m situata presso il EC JRC in Italia, parte delle Infrastrutture di Ricerca Europee sul cambiamento climatico e la qualità dell'aria. Per monitorare la torre, accelerometri autonomi wireless sono stati posizionati a diverse altezze della struttura per acquisire continuamente le vibrazioni strutturali. Tecniche di analisi modale operazionale OMA sono state implementate per identificare le proprietà dinamiche della torre a partire dai dati raccolti dai sensori in campo, e un modello numerico della struttura è stato sviluppato per fornire ulteriori informazioni sullo stato della struttura e sulla sua dinamica. In questa tesi, vengono applicate tecniche di aggiornamento del modello per minimizzare gli errori tra la struttura reale e il modello ad elementi finiti FE, basandosi sulle proprietà modali calcolate dai dati dei sensori di vibrazione. Grazie all'adozione delle tecniche di aggiornamento del modello, il modello numerico migliorato è in grado di riprodurre accuratamente la risposta dinamica della torre. Il presente lavoro evidenzia l'importanza e le sfide dell'aggiornamento del modello utilizzando OMA, a partire dalle misurazioni in tempo reale dei sensori di vibrazione per sviluppare digital twin accurati, con il caso di studio reale della torre Atmospheric Observatory del JRC. Lo studio fornisce un'idea dell'importanza dell'aggiornamento del modello per migliorare l'accuratezza dei digital twin di strutture reticolari complesse, fornendo così uno strumento prezioso per migliorare il monitoraggio della salute strutturale e supportare strategie di manutenzione predittiva.

**Parole chiave:** monitoraggio della salute strutturale, analisi modale operativa, aggiornamento modale, metodo degli elementi finiti, rilevamento dei danni



# Contents

<b>Abstract</b>	i
<b>Abstract in lingua italiana</b>	iii
<b>Contents</b>	v
<b>1 Introduction</b>	1
1.1 Objectives of Thesis . . . . .	2
1.2 Motivation of Thesis . . . . .	3
1.3 Structure of Thesis . . . . .	4
<b>2 Literature Review</b>	7
2.1 Bibliometrics . . . . .	7
2.2 Key Studies . . . . .	17
2.3 Model Updating . . . . .	18
2.3.1 Iterative model updating . . . . .	18
2.3.2 Manual model updating . . . . .	19
2.3.3 Sensitivity model updating . . . . .	19
2.3.4 Stochastic model updating . . . . .	20
2.4 Key terms in the FEMU (Finite Element Model Updating) procedure and their interrelationships . . . . .	21
2.5 Choosing the Updating Parameters and Model Class . . . . .	23
2.5.1 Selection method . . . . .	24
2.5.2 Clustering method . . . . .	25
2.6 Douglas-Reid Model Updating . . . . .	27
2.6.1 Mathematical formulation of DR method . . . . .	28
2.7 Modal Analysis . . . . .	30
2.8 Operational Modal Analysis . . . . .	30
2.8.1 Overview of operational modal analysis techniques . . . . .	31

<b>3 Validation of DR Method for FEMU for Test Structure</b>	<b>41</b>
3.1 Description of test structure . . . . .	41
3.1.1 Members dimensions . . . . .	44
3.1.2 Material properties . . . . .	45
3.1.3 Dynamic testing . . . . .	46
3.2 Numerical Model of Testing Structure . . . . .	47
3.3 Algorithm for Model Updating by DR Method . . . . .	51
3.3.1 Young's modulus of L-shaped wall ( $E_c$ ) as MU parameter . . . . .	53
3.3.2 Bending stiffness of L-shaped wall ( $EI_b$ ) as MU parameter . . . . .	56
<b>4 Conceptualizing the Real-World Structure and Numerical Simulation</b>	<b>61</b>
4.1 Insights into Real-World Structure . . . . .	61
4.2 Tower Geometry . . . . .	63
4.3 Base Building . . . . .	69
4.4 Sensors Monitoring for Ambient Vibration Test . . . . .	72
4.5 Tower Dynamics Assessment during the Delivery Phase . . . . .	75
4.6 Finite Element Modeling of Tower . . . . .	77
4.7 Finite Element Modelling of Base Building . . . . .	82
4.8 Complete Finite Element Model of Structure . . . . .	85
4.9 Modal Analysis of Numerical Model of the Complete Structure . . . . .	89
<b>5 Ambient Vibration Testing</b>	<b>93</b>
5.1 Processing of sensor data . . . . .	93
5.1.1 Detrending . . . . .	93
5.1.2 Noise reduction using smoothing methods . . . . .	97
5.2 Modal Parameter Estimation with Operational Modal Analysis . . . . .	99
<b>6 Model Updating for Real-World Structures</b>	<b>111</b>
6.1 Purpose of Model Updating . . . . .	111
6.2 Model Updating of Real-World Structure . . . . .	112
6.2.1 Manual tuning . . . . .	114
6.2.2 Sensitivity analysis . . . . .	115
6.3 Model Updating Results . . . . .	118
<b>7 Wind Analysis of Atmospheric Tower</b>	<b>125</b>
7.1 Wind Load Calculation . . . . .	126
7.1.1 Peak velocity pressure . . . . .	126
7.1.2 Basic wind velocity . . . . .	126

7.1.3	Exposure coefficient:	128
7.1.4	Aerodynamic coefficient	129
7.1.5	Dynamic coefficient	130
7.2	Wind Load Calculation in Midas Gen	130
7.3	Response of Structure Under Wind Loading	130
7.4	Modal Updating for FEM4	133
7.5	Modal Analysis with wind loading	134
<b>8</b>	<b>Conclusion and Way Forward</b>	<b>137</b>
<b>Bibliography</b>		<b>141</b>
<b>A</b>	<b>Appendix A</b>	<b>151</b>
<b>B</b>	<b>Appendix B</b>	<b>155</b>
<b>List of Figures</b>		<b>157</b>
<b>List of Tables</b>		<b>161</b>
<b>List of Symbols</b>		<b>163</b>
<b>Acknowledgements</b>		<b>165</b>



# 1 | Introduction

Ensuring the proper functioning of civil structures and infrastructure is critical for any country. Key structures such as skyscrapers, offshore platforms, bridges, and telecommunication towers are essential components of this system, and their failure can have widespread, severe consequences. A significant concern is that many of these structures have surpassed their designed lifespan. For instance, according to the United States Federal Highway Administration (2021) [6], the country has 619,622 bridges, with more than 40% exceeding an intended service life of approximately 50 years. Moreover, 43,578 bridges have been classified as structurally deficient. This situation poses significant challenges for citizens, government agencies, and infrastructure management authorities. With limited resources for maintaining these aging structures, there is an increasing focus on Structural Health Monitoring (SHM). SHM provides researchers and engineers with essential tools to assess the condition of structures and prioritize maintenance, thereby preventing sudden failures and extending the lifespan of critical infrastructure.

The primary goal of SHM is to continuously monitor a structure's behaviour throughout its lifetime. It relies on systematic data collection, interpretation, and processing to evaluate structural integrity and long-term performance. In the early 20<sup>th</sup> century, structural inspections were predominantly conducted visually. However, recent technological advances have introduced sophisticated instruments such as sensors, data storage devices, and transmission hardware, significantly enhancing data collection and processing capabilities.

These advancements now allow for precisely measuring complex parameters, including three-dimensional vibrations. In SHM, vibration data is typically obtained through Operational Modal Analysis (OMA), which measures the modal properties of a structure, such as natural frequencies, mode shapes, and damping ratios under actual operating conditions. This information forms the foundation for understanding a structure's dynamic behaviour.

Over time, structures are often subjected to extreme events, such as earthquakes, to evaluate their performance and gain insights into both routine and extraordinary maintenance

requirements under severe loading conditions. This data is crucial for understanding how a structure responds to extreme seismic forces, thereby informing optimized maintenance strategies to ensure long-term resilience and safety.

Finite Element Model Updating (FEMU) is crucial for aligning a structure's physical and digital representations. FEMU involves adjusting a numerical model so that its output modal properties match those obtained from OMA, thereby creating a more accurate digital twin of the structure. This process enhances the reliability of predictive analysis and supports more informed decisions regarding maintenance and safety interventions.

FEMU's primary function is to update the physical and mechanical properties of structure parameters that may vary over time or for which precise information is unavailable by treating them as random variables and adjusting them using different iterative methods available in the literature. This tool is handy for older structures that have exceeded their intended lifespan, as it facilitates timely and efficient maintenance decisions. By providing accurate details about a structure's condition, FEMU enables prompt scheduling of repairs, ensuring continued safety and preventing potential failures.

Considering these challenges, this research applies SHM techniques to large structures, such as the 100-meter-tall steel trussed *Atmospheric Tower* located at the EC JRC at ISPRA, Italy. Although the study is not exclusively tailored to this structure, it offers a robust mathematical and experimental framework applicable to the general maintenance and monitoring of large structures. The methods and approaches developed herein aim to improve existing techniques for assessing structural health and optimizing maintenance strategies.

## 1.1. Objectives of Thesis

The primary objective of this thesis is to develop a *digital twin*, a digital replica of a real-world structure. This involves creating a numerical model of the structure and applying a Finite Element Model Updating (FEMU) approach to adjust the structural properties, ensuring the model accurately replicates the behaviour of the actual structure. The specific objectives of the study are as follows:

- **Understanding the Structure:** Analyze the geometry, orientation, surrounding environment, and physical and mechanical properties of each structure component.
- **Numerical Model Development:** Develop a numerical model of the case study structure, incorporating key assumptions regarding the behaviour of 1D, 2D, and 3D structural components used in the analysis.

- **Mathematical Framework for DR Method:** Formulate a mathematical framework for the Douglas-Reid (DR) method to be applied in the FEMU process.
- **Challenges in FEMU Implementation:** Identify and address the challenges encountered when implementing mathematical strategies in FEMU.
- **Model Validation and Updating:** Compare the modal data from the numerical model with OMA results, and update the model properties to ensure it closely replicates the behaviour of the actual structure.
- **Boundary Conditions Analysis:** Investigate the effect of boundary conditions by replacing them with three-dimensional springs at the foundation.
- **Joint Section Analysis:** Examine the impact of joint sections by reducing the bending stiffness at these sections, simulating scenarios such as bolt loosening at certain locations.
- **Static Wind Analysis:** Conduct a static wind analysis on the updated finite element model. Given that the EC JRC Atmospheric Tower is a tall structure, wind loading is critical in defining its dynamic behaviour.

This research aims to enhance the accuracy and effectiveness of FEMU in structural health monitoring by leveraging the DR method. The study seeks to provide a robust framework for creating digital twins that can reliably predict the behaviour of real-world structures.

## 1.2. Motivation of Thesis

Much of the existing research on FEMU emphasizes sensitivity-based model updating, an iterative approach that minimizes discrepancies between numerical models and experimental data through least-squares optimization [61]. While computational tools have supported such methods for over half a century, recent advances in computational mathematics have introduced innovative strategies to streamline the FEMU process over the past decade. These modern techniques prioritize simplicity of implementation and reduced computational demands, addressing longstanding challenges in structural engineering.

A notable example is the application of the Douglas-Reid (DR) method in structural engineering, as demonstrated by [6]. Initially developed for finite element optimization, the DR method offers a systematic framework for parameter identification and model refinement. This study investigates its potential to enhance FEMU workflows and advance Structural Health Monitoring (SHM) systems. The DR method enhances the efficiency of model updating by integrating it into the process, thereby improving both the accuracy

and practicality of FEMU. These advancements play a crucial role in developing robust digital twins that accurately replicate real-world structural behaviour under different operational conditions.

### 1.3. Structure of Thesis

This thesis is organized into several chapters, each addressing a key aspect of the research.

- **Chapter 1** provides a general introduction to the topic, outlining the motivation behind the study and its significance.
- **Chapter 2** presents a detailed review of previous studies on similar subjects, highlighting different strategies used in model updating formulations and their mathematical foundations. The objective is to explore existing methodologies and emerging trends in research that could be applied to the case study.
- **Chapter 3** focuses on the implementation of the *Douglas-Reid (DR)* model updating method on a simple structure to validate its effectiveness. This step ensures a clear understanding of the model properties and updating parameters before applying the technique to the case study.
- **Chapter 4** describes the case study structure, the EC JRC *Atmospheric Tower*. The chapter begins with an overview of the tower's primary geometry along with its secondary elements, such as stairs, elevator mast, and parapets. A numerical model of the structure is then developed using MIDAS software [57], followed by a *modal analysis* to determine the structure's modal properties. These properties are a foundation for model updating, ensuring accurate calibration of the structure's physical and mechanical characteristics. Additionally, three different finite element models are created to examine specific factors such as foundation conditions, joint behaviour, and wind analysis.
- **Chapter 5** focuses on Ambient Vibration Testing (AVT), through which the structure's experimental frequencies are determined using OMA. This process establishes the actual dynamic properties of the structure under operational conditions, providing benchmark modal parameters for subsequent model updating.
- **Chapter 6** details the application of the DR model updating procedure to the *JRC Atmospheric Tower*. Multiple finite element models are developed to address uncertainties, particularly concerning the foundation conditions and joint flexibility (potentially due to bolt loosening). The objective is to refine the numerical model

until it accurately replicates the actual structural behaviour, resulting in a digital twin, a precise computational replica of the physical structure.

- **Chapter 7** extends the analysis by performing *static wind analysis* on the digital twin, incorporating the updated physical and mechanical properties. This assessment evaluates the structure's dynamic response under wind loading and investigates the impact of wind on its modal properties.
- **Chapter 8** presents the conclusions of the research, summarizing key findings and offering recommendations for future studies.

This structured approach ensures a systematic progression from theoretical foundations to practical implementation, ultimately developing an accurate digital twin of the JRC *Atmospheric Tower*.



# 2 | Literature Review

This chapter provides a comprehensive overview of previous studies on this topic, emphasizing identifying emerging trends relevant to our research on tall steel truss tower structures. For this, we explore key concepts that are important in that thesis, including Structural Health Monitoring (SHM), Operational Modal Analysis (OMA), Experimental Modal Analysis (EMA), and model updating methods. By analyzing bibliometric data, we aim to cover current research trajectories and trends in this field, which offers valuable insights that will enhance the relevance and applicability of our study. Graphical representations will be employed to visualize these trends, allowing for a clearer understanding of the research landscape and its implications for our investigation.

## 2.1. Bibliometrics

A vast amount of bibliometric data is available in Structural Health Monitoring (SHM), with over 49,000 documents indexed in *Scopus* alone. Analyzing this large dataset to identify current trends presents a significant challenge. To address this, we utilize VOSviewer, a tool developed by Nees Jan van Eck and Ludo Waltman from Leiden University [84]. VOSviewer is widely used for mapping relationships between research papers based on keywords, authorship, co-citation, country of origin, and other metadata marked by the authors. This tool provides an interactive visual map, offering insights into the various research domains within SHM, highlighting areas with concentrated research activity, and identifying emerging trends in a highly accessible and visually engaging format.

Now, we are performing different searches on Elsevier's Scopus regarding SHM. In today's world, extensive research is being done on the built environment, which requires ongoing maintenance to ensure the proper functioning of the structure throughout its life span. Structural monitoring has become a crucial aspect of this process, as it helps prevent undesirable events that occur under extreme events like earthquakes, such as causes of structural collapse. Structures that have reached the end of their intended lifespan cannot always be sustainably demolished. Therefore, we need to adopt strategies that extend the life of these structures, monitor their health, and apply interventions as required. This

need has led to a significant increase in research in this area.

Figure 2.1 clearly shows that interest in this field began in the early 2000s, with a notable rise in publications and research in recent years.

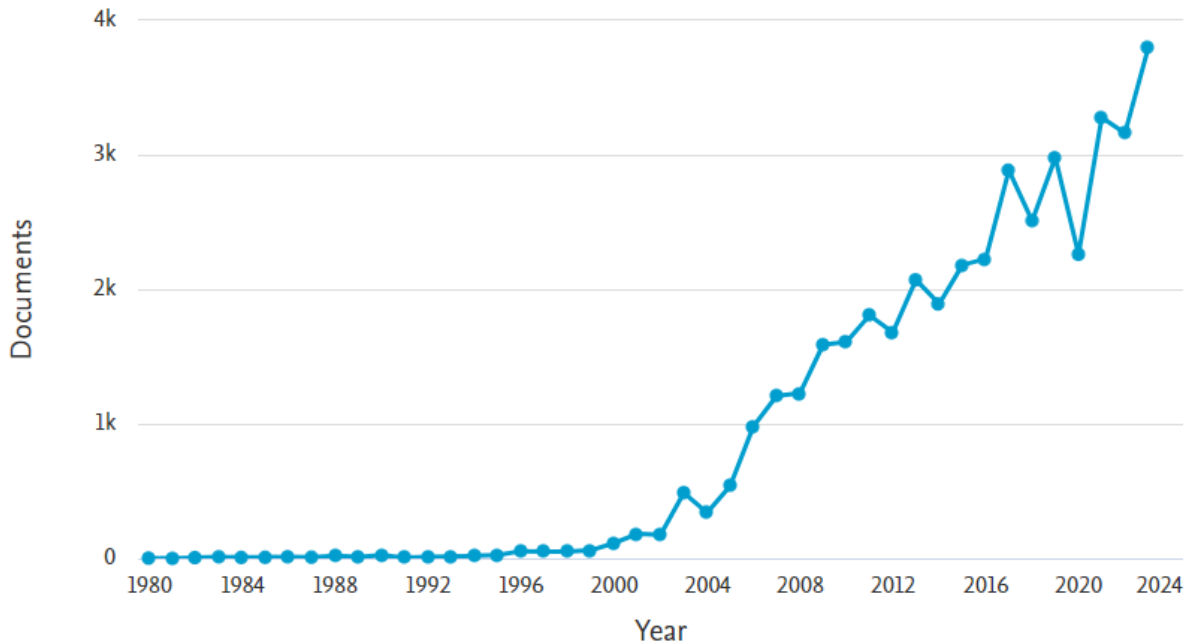


Figure 2.1: Yearly trend of structural health monitoring (SHM).

Next, we examine the dataset related to modal updating techniques in Structural Health Monitoring (SHM). The primary objective of this analysis is to develop a digital twin [26, 30], which serves as a virtual replica of the actual structure. This digital representation enables an accurate assessment of the structure's behaviour.

During the modeling process, it is crucial to compare the finite element analysis (FEA) results with experimental data obtained using Operational Modal Analysis (OMA). However, discrepancies often arise between numerical simulations and experimental findings. Model updating techniques are commonly employed to address these inconsistencies. These techniques adjust certain numerical model parameters, such as mechanical properties, to ensure that the computed results closely align with the observed experimental data.

According to Elsevier's Scopus database, there are over 400 publications on model updating for SHM, as illustrated in Figure 2.2. This trend highlights the growing research interest in this field in recent years.

### Documents by year

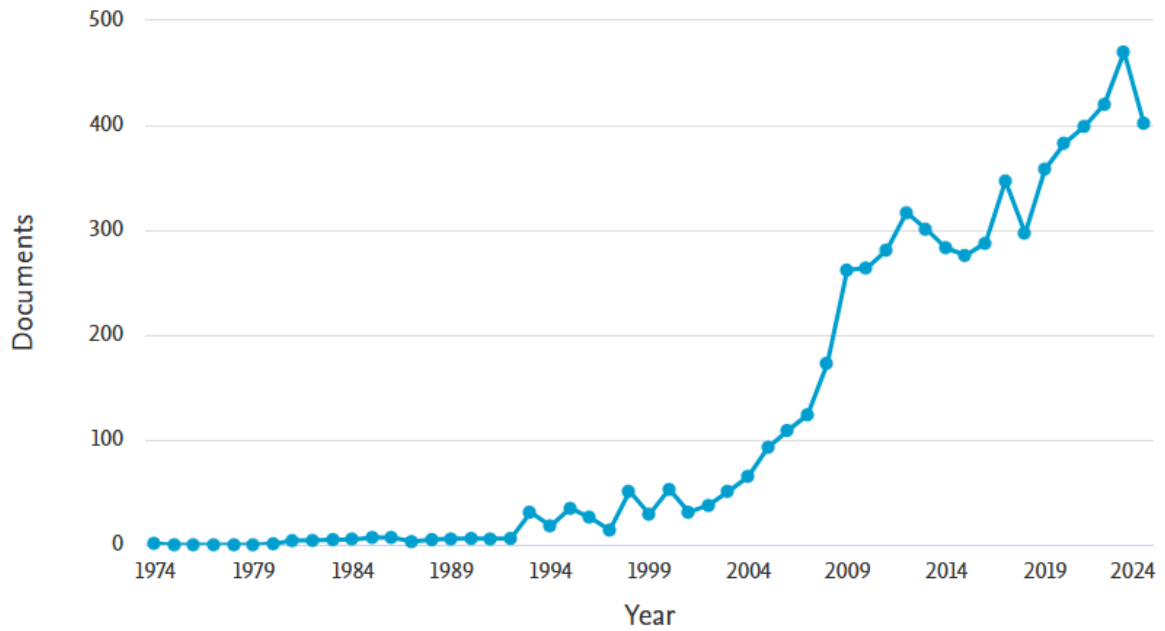


Figure 2.2: Yearly trend of model updating in (SHM).

Finally, we analyze a dataset from Elsevier's Scopus, which includes studies on high-rise structures, steel structures, and frame structures in the context of Structural Health Monitoring (SHM), while excluding research on masonry and bridge structures. Our study specifically focuses on a tall steel tower structure, considering only engineering-related publications. This analysis enables us to identify key research trends in the field, which began to emerge in the early 2000s and have seen significant advancements over the past two decades.

According to Elsevier's Scopus, more than 100 publications explore model updating techniques for tall structures under SHM, as depicted in Figure 2.3.

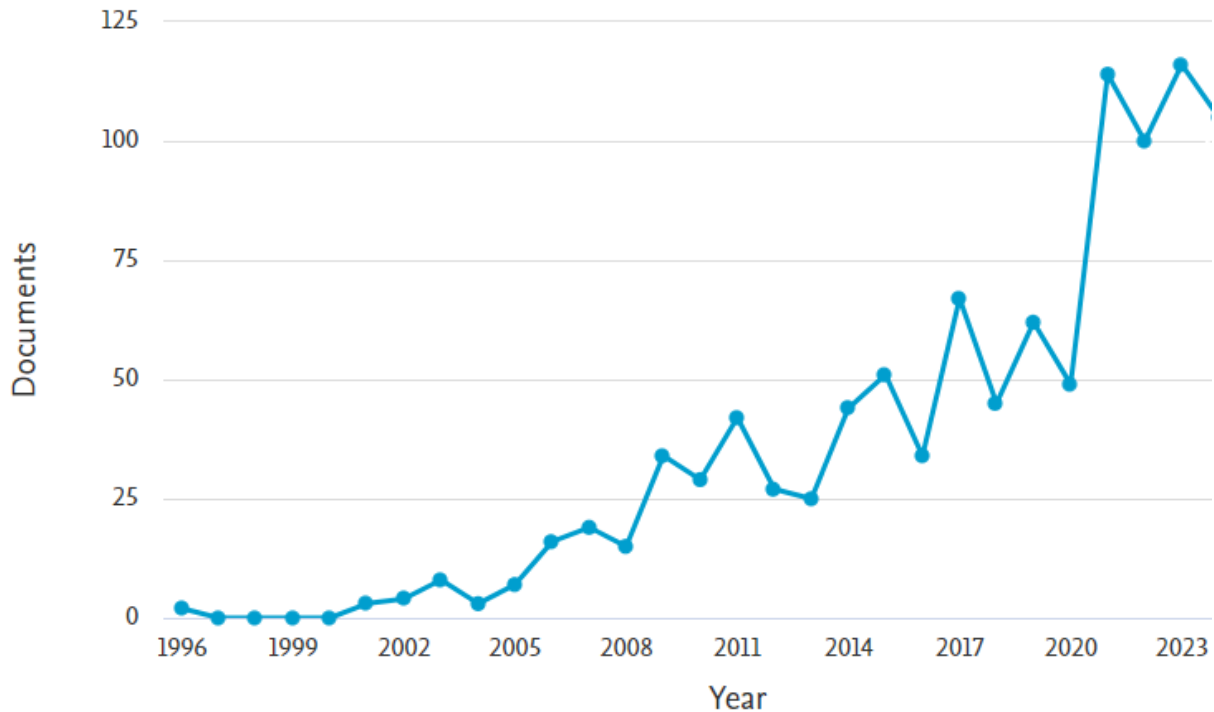


Figure 2.3: Yearly trend of model updating tall structures in (SHM).

Using VOSviewer, we can generate an interactive map highlighting emerging trends and interconnected topics in Structural Health Monitoring (SHM). This visualization is based on various parameters, including keywords, authorship, co-citations, countries of origin, and other metadata specified by researchers. A thesaurus file containing all the keywords used in different research papers is referenced in (cfr. Appendix A.1), facilitating the identification of synonyms and related terms to ensure consistency in mapping. Focusing on the Structural Health Monitoring keyword, we analyze a dataset comprising 546 frequently used keywords, each appearing at least three times and originating from 37 countries. This provides a comprehensive overview of the evolving research landscape in SHM.

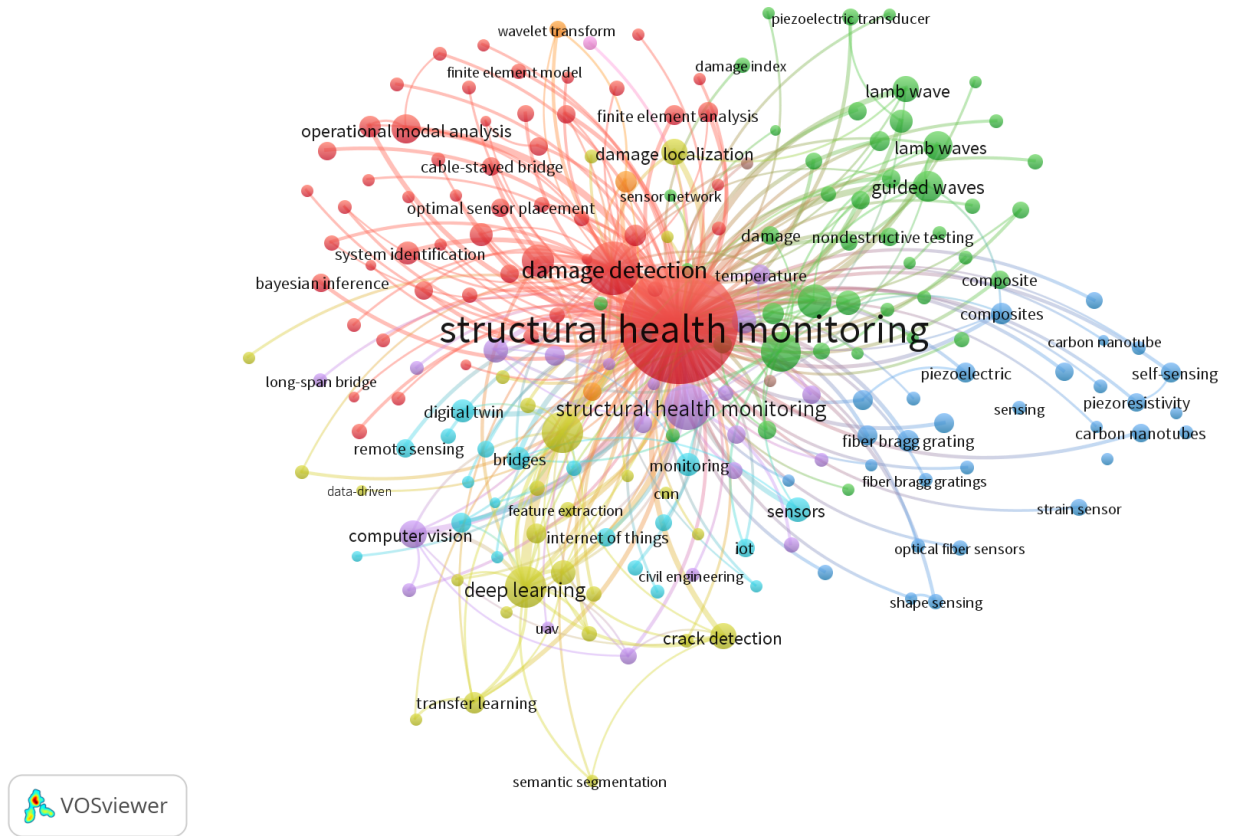


Figure 2.4: VOSviewer analysis map on keyword co-occurrence of Structural Health Monitoring (SHM).

In Figure 2.4, we observe clusters around keywords like structural health monitoring and subtopics that have become focal points of recent research, such as damage detection, damage localization, and damage index. These terms highlight the various severities that occur in a structure due to damage during its service life, informing maintenance strategies. Additionally, terms like finite element method, finite element analysis, and digital twin emphasize the critical role of numerical modeling in SHM. Numerical models are developed using FEM software, and the results from these models are then validated against data from Operational Modal Analysis (OMA) or Experimental Modal Analysis (EMA). The ultimate goal is to create digital twins that accurately replicate the actual dynamic properties of the structure.

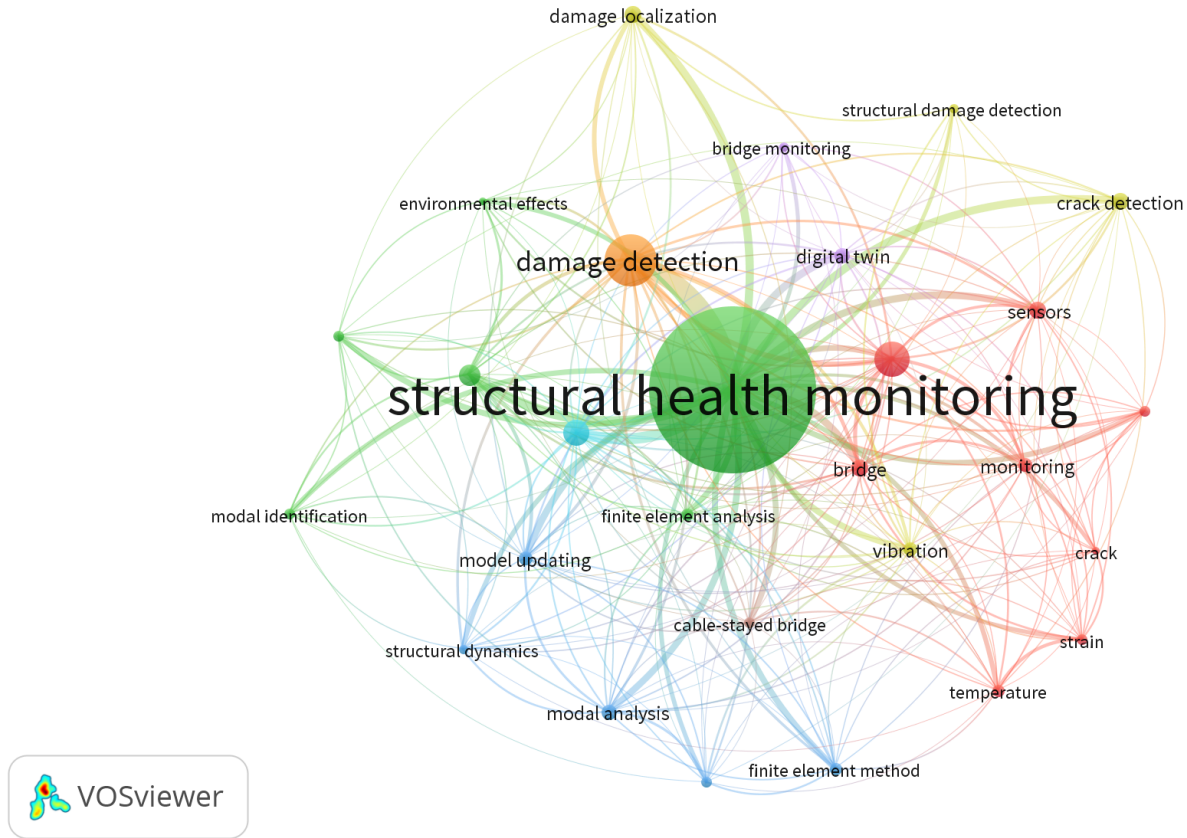


Figure 2.5: VOSviewer analysis map on important keyword co-occurrence of Structural Health Monitoring (SHM).

In Figure 2.5, after removing some of the less relevant keywords, the map is simplified to highlight the most important terms in the development of the field, such as damage detection, digital twin, sensors, monitoring, model identification, finite element analysis, and crack detection. Among these keywords, sensors play a crucial role in Operational Modal Analysis (OMA). Specifically, for the JRC tower, a 3-dimensional tri-axial accelerometer is used to capture the structural dynamics properties.

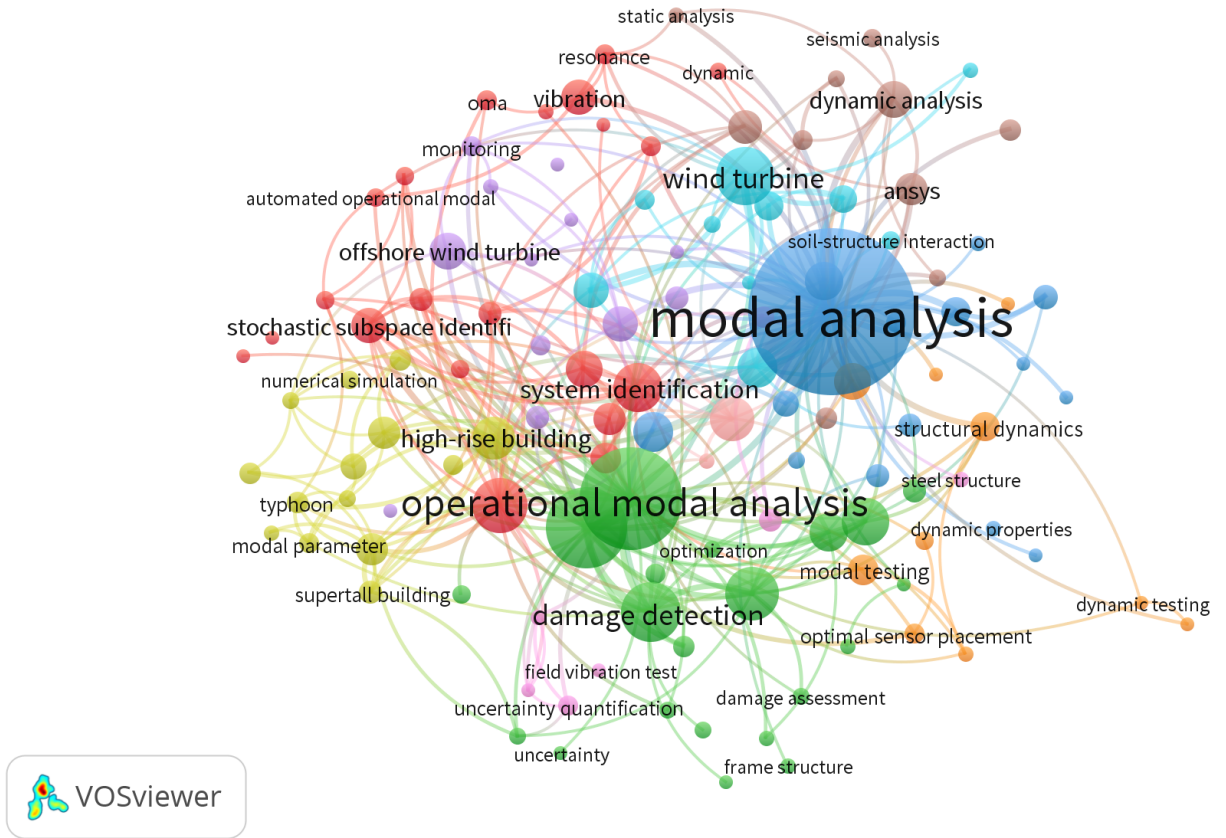


Figure 2.6: VOSviewer analysis map on keyword co-occurrence of modal analysis of tall and steel structure.

In this section, we extend our analysis using the VOSviewer application, explicitly focusing on modal analysis, as shown in Figure 2.6. This analysis targets the computation of modal properties in tall steel structures. Our findings reveal that Operational Modal Analysis (OMA) prominently appears in the literature, indicated by a larger node in the VOSviewer network, signifying its widespread application across numerous studies.

The main key terms in the map include modal identification, modal analysis, and modal parameters, which are centered on determining a structure's dynamic properties, such as natural frequencies, mode shapes, and damping ratios. These properties are fundamental for understanding the dynamic behaviour of structures. Two primary methods are commonly employed to determine the modal properties of a structure: Experimental Modal Analysis (EMA) and Operational Modal Analysis (OMA). EMA involves actively exciting the structure with a known force and computing the modal properties under experimental conditions, such as wind tunnel testing. In contrast, OMA measures the

structural responses of a structure in its natural environment using sensors without applying any external forces. For the JRC tower, a 3-dimensional tri-axial accelerometer with a solar-powered antenna captures acceleration along the x, y, and z axes under ambient conditions.

To determine the modal properties of the structure, sensors and base stations were strategically placed at various heights. Data acquisition was performed at multiple intervals, using tri-axial accelerometers to capture vibrations in three directions. Various techniques exist for extracting modal properties, relying on different software tools and packages. In this study, we used the PyOMA [67] graphical interface application to facilitate the identification of modal properties.

Both frequency and time-domain methods can be applied to compute these modal properties. In the frequency domain, techniques such as Frequency Domain Decomposition (FDD), Enhanced Frequency Domain Decomposition (EFDD), and Frequency Spatial Domain Decomposition (FSDD) are commonly used. Methods like Covariance-Driven Stochastic Subspace Identification (SSI-Cov) and Data-Driven Stochastic Subspace Identification (SSI-Dat) are employed for time-domain analysis. These methods will be explored in more detail in subsequent sections of this thesis to provide a comprehensive understanding of their application in modal property identification.

Accurately determining a tower's modal properties is highly dependent on the optimal placement of sensors. This includes defining a precise reference axis for the structure and calculating the coordinates for each sensor location, including the base station. In this study, three accelerometers were strategically placed at heights of 60m, 80m, and 100m along the northeast side of the tower. This configuration was chosen to ensure high fidelity in capturing the tower's dynamic responses, thereby improving the accuracy of modal analysis and structural monitoring.

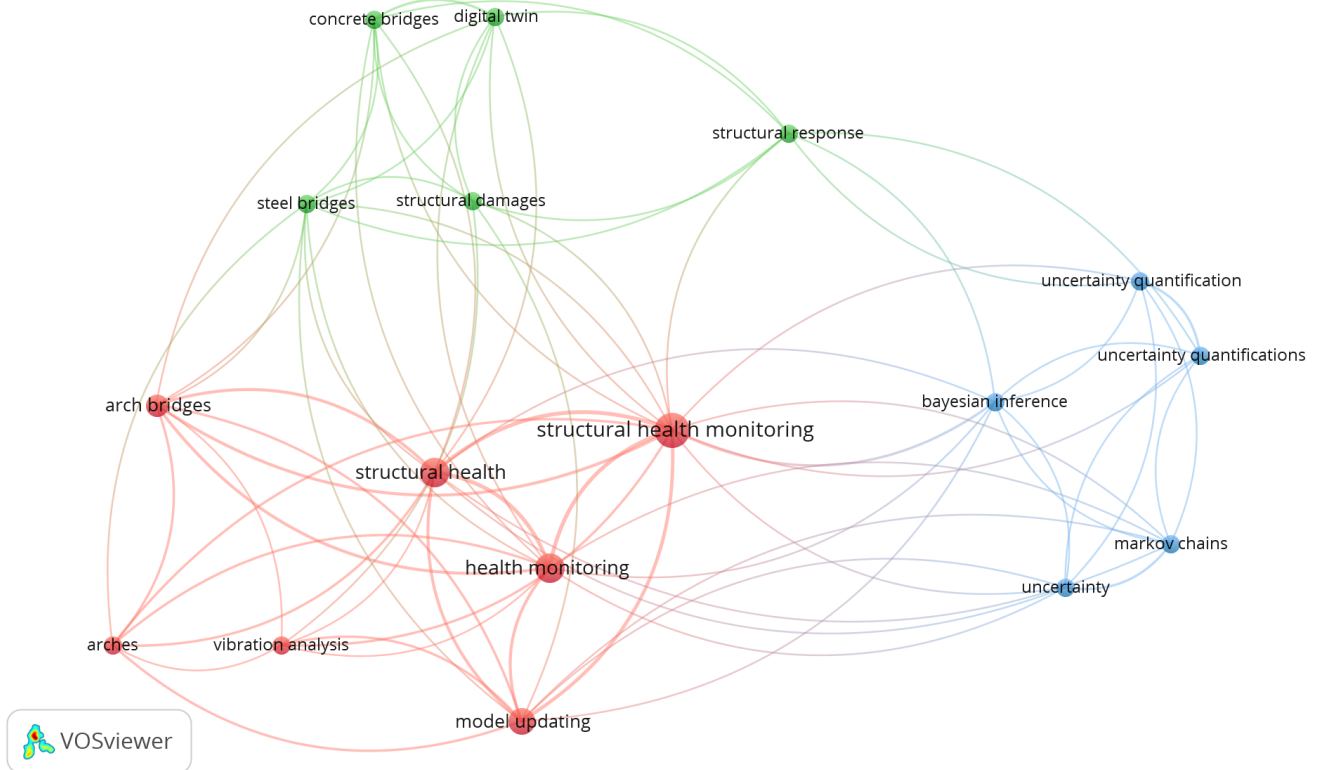


**Figure 2.7:** VOSviewer analysis map on keyword co-occurrence of model updating of tall structure.

In the following analysis, we utilize the VOSviewer application to perform modal updating, explicitly focusing on tall structures, excluding masonry constructions. Modal updating plays a central role in this thesis as it allows for refining our FE model, as depicted in Figure 2.7. This process involves comparing the numerical model of the structure with experimental results obtained through Experimental Modal Analysis (EMA) or Operational Modal Analysis (OMA).

The primary objective of this process is to iteratively update the FE model by adjusting its physical and mechanical properties to achieve a closer alignment with the experimental data. To achieve this, we apply the Douglas-Reid method, a second-order approximation technique that enables the refinement of natural frequency estimations. Through this iterative approach, we adjust the model parameters to minimize the discrepancies between the model's predictions and the experimental observations, thus reducing errors and improving the accuracy of the model.

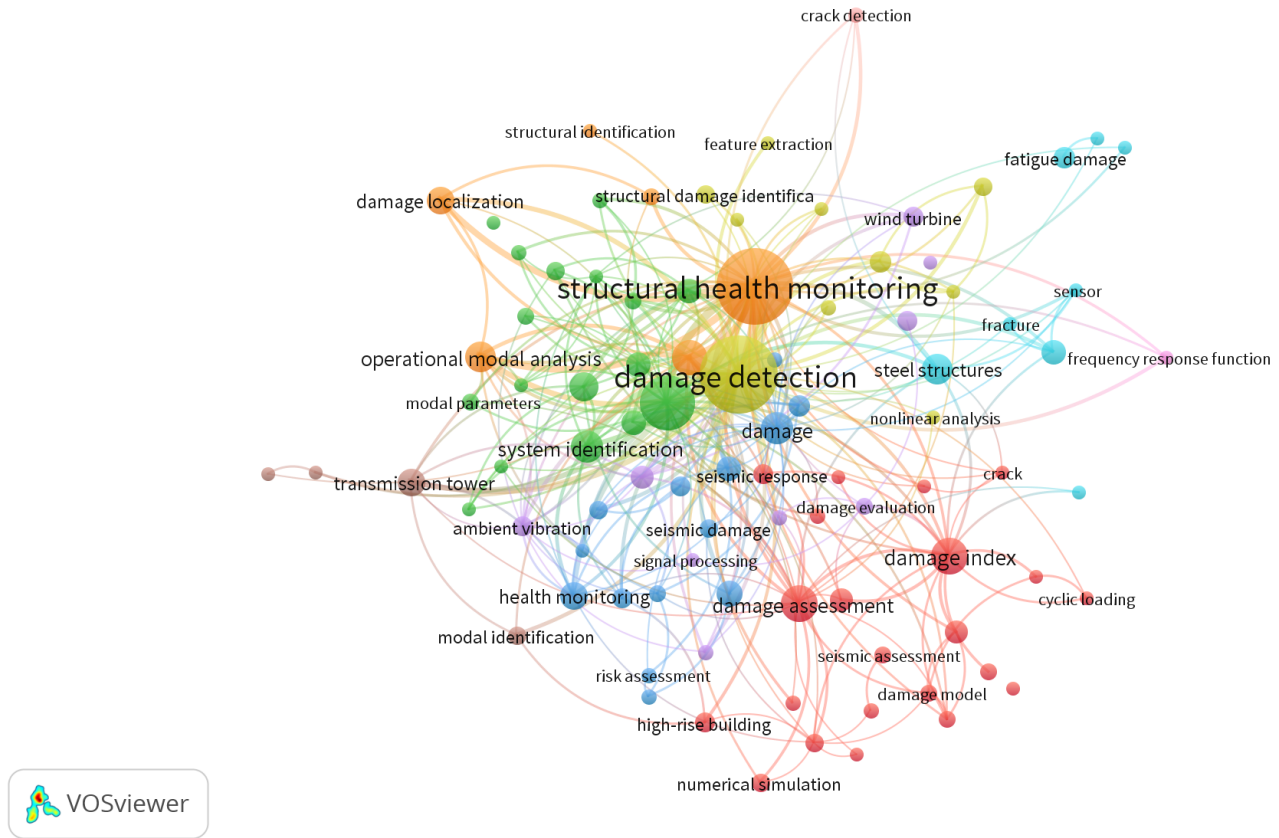


**Figure 2.8:** VOSviewer analysis map on keyword co-occurrence of damage detection in structure.

In the final analysis, the VOSviewer application is used to perform a co-occurrence analysis of key terms frequently found in structural health monitoring studies, such as damage detection, seismic damage, and damage index, as illustrated in Figure 2.8. This approach is particularly relevant for tall structures, such as steel and transmission towers, within the domain of structural health monitoring. By identifying damage categories and potential sources of damage, this analysis aids in developing targeted intervention strategies throughout the lifespan of these structures. For steel structures, regular maintenance typically involves periodic inspections, tightening bolts, and preventing the development of rust.

## 2.2. Key Studies

Modeling and simulation play a crucial role in Structural Health Monitoring (SHM), particularly in assessing high-rise steel structures, which present unique challenges. As demonstrated in the work of Y. Q. Ni in monitoring the Canton Tower in China [62], SHM involves strategically placing various sensors on the structure to calculate its modal properties. Environmental factors such as wind, seismic activity, and corrosion are also considered to ensure accurate calibration of the structure. Subsequently, algorithms are applied to determine the damage index associated with these factors, facilitating the development of targeted intervention strategies to enhance the structure's resilience.

Structural Health Monitoring (SHM) is essential for preserving a structure's integrity against a variety of environmental factors throughout its lifespan. By analyzing the structure's behaviour and applying statistical methods to the measured data, SHM enables early damage detection and quantification, ensuring safety and preventing potential failures [41]. Over time, cumulative environmental loads can significantly degrade structural performance, underscoring the importance of regular monitoring.

Implementing SHM in high-rise structures, such as steel buildings, presents several challenges, with one of the main difficulties being the accurate placement of sensors to capture the structure's dynamic behaviour. While the Global Positioning System (GPS) is a standard method for sensor positioning, its application is often limited by environmental factors, such as electromagnetic interference and satellite movement. The Laser Doppler Vibrometer (LDV) [51] provides an alternative with high precision, but its high installation cost limits its use to high-priority projects. In contrast, accelerometers are widely used due to their ease of installation and ability to operate without a relative reference system, making them ideal for capturing acceleration data under operational conditions [92]. Additionally, the growing adoption of wireless networks (WN) has improved the efficiency of SHM systems by simplifying sensor deployment and enhancing data acquisition accuracy [45].

Accelerometer signals inherently include offsets, and although frequency noise is typically minimal, these raw signals are often unsuitable for direct analysis. Unknown initial conditions and inherent offsets can lead to drift during numerical integration. To address these challenges, various drift-free integration techniques have been proposed in the literature [34]. For example, one approach for eliminating drift from frequency-based data is discussed in [82], while baseline correction is another standard method [92]. However, baseline correction tends to remove critical low-frequency components and requires careful selection of the window frame for the input data, limiting its practicality for real-time

estimation [2, 85].

In high-rise structural health monitoring, vibration data from accelerometers provide valuable insights into damage accumulation. Changes in these data reflect alterations in the structure's stiffness and damping properties. Although research in this area is limited, recent studies have employed data-mining techniques to extract model properties such as natural frequencies, mode shapes, and damping coefficients from the vibrational response of structures under dynamic loading [31]. Moreover, to enhance drift-free integration, a multiple baseline correction approach has been proposed. Unlike single baseline correction, which may not entirely eliminate drift, the multiple baseline correction method, supported by a low-pass filter, provides a more consistent time reference and minimizes drift effects compared to traditional integrators [34].

## 2.3. Model Updating

Rosati [77] highlights an essential aspect of Structural Health Monitoring (SHM): conducting non-destructive assessments while maintaining low computational demands. The study utilizes an existing numerical model to investigate the effects of continuous vibrations on the Tower of the Nation in Naples, Italy. Various model updating techniques are applied, including the Douglas-Reid (DR) method, and these are compared with other methods from the literature, such as the Inverse Eigen-sensitivity and grid search methods. The primary objective is to assess the performance of the DR method within the SHM framework, thereby exploring different model updating strategies that are crucial for optimizing SHM applications.

### 2.3.1. Iterative model updating

Iterative model updating is further divided into two primary approaches: direct and indirect methods [21]. In the early stages of Finite Element (FE) model updating, direct methods [29, 32, 60] were the most prevalent. This approach involves updating the structure's mass and stiffness matrices based on experimental modal data. The main advantage of direct methods is their simplicity and low computational demand. However, they often result in mass and stiffness matrices that lack a meaningful physical interpretation of the structure. Additionally, direct methods are generally limited in capturing localized effects within the structure, and error tends to accumulate with numerous iterations due to the iterative process.

In contrast, the indirect model updating method [4, 29] also adjusts the mass and stiffness

matrices but does so by refining the physical and mechanical properties of the structure, such as Young's modulus, member stiffness, joint stiffness, and boundary conditions. This approach produces a more physically representative mass and stiffness matrix. It is more widely used due to its accuracy and reduced scatter between experimental results and FE model updating outcomes. Consequently, the indirect method has become a preferred choice in the iterative model updating process for Structural Health Monitoring applications.

### 2.3.2. Manual model updating

A trial-and-error approach is employed to refine specific physical or mechanical parameters in manual and automated model updating [9]. This method relies on engineering judgment to select parameters by comparing the modal properties obtained from numerical solutions with those from experimental data. It is beneficial in cases where the numerical model closely approximates the experimental model. By iteratively adjusting certain parameters, this approach aims to minimize scatter and achieve greater alignment between the experimental and numerical results, thereby enhancing the accuracy of the updated model.

### 2.3.3. Sensitivity model updating

Sensitivity model updating is explored as a widely adopted technique in FE model updating, gaining significant traction from the late 20th century to the present. This approach utilizes a linear least-squares method [39] to solve the iterative updating process. Typically, model properties are non-linear; however, sensitivity model updating linearized the problem by expanding the system's Taylor series and retaining only the linear terms, disregarding higher-order terms relative to the model updating parameters. This linearization improves computational efficiency while allowing for precise adjustments in the model, making it a popular choice for model updating [61].

$$x(\alpha) \approx x_i + S_i \Delta \alpha_i \quad (2.1)$$

$$S_i = \begin{bmatrix} \frac{\partial x_1}{\partial \alpha_1} & \dots & \frac{\partial x_1}{\partial \alpha_n} \\ \vdots & \ddots & \vdots \\ \frac{\partial x_m}{\partial \alpha_1} & \dots & \frac{\partial x_m}{\partial \alpha_n} \end{bmatrix}_{\alpha=\alpha_i} \quad (2.2)$$

In Equation (2.1),  $\alpha$  represents the updating parameter in the analysis, while  $x_i$  is a vector containing all modal properties obtained from the numerical analysis. The term

$\Delta\alpha_i$  denotes the residual after each iteration, and  $S_i$  is the sensitivity matrix. Here,  $n$  refers to the number of updating parameters considered in the analysis, and  $m$  represents the modal properties as shown in Equation (2.2).

$$\mathbf{r}_i = (x_m - x_i) - S_i \Delta\alpha = \Delta x_i - S_i \Delta\alpha_i \quad (2.3)$$

$$\min_{\Delta\alpha_i} \|\Delta x_i - S_i \Delta\alpha_i\|^2 \quad (2.4)$$

To compute the residual vector  $r_i$ , we arrange it in the standard form necessary to apply the linear least-squares method. Following this, we take the Euclidean second norm( $l_2$ ), ensuring the solution is unique. In this approach, it is common to include a weighting function or matrix to emphasize the significance of each modal property in the analysis. Afterward, a regularization technique is applied, with Tikhonov regularization [39] being one of the most widely used methods. This process enables us to solve the analytical problem and obtain the variations in the updating parameters at each iteration.

$$\min_{\Delta\alpha_i} \|W(\Delta x_i - S_i \Delta\alpha_i)\|^2 \quad (2.5)$$

$$W = [\text{diag}(x_m)]^{-1} \quad (2.6)$$

$$\min_{\Delta\alpha_i} \|W(\Delta x_i - S_i \Delta\alpha_i)\|^2 + \lambda^2 \|\Delta\alpha_i\|^2 \quad (2.7)$$

$$\Delta\alpha_i = [S_i^T W^T W S_i + \lambda^2 I]^{-1} S_i^T W^T W \mathbf{r}_i \quad (2.8)$$

where  $\lambda > 0$  is the regularization parameter that controls the relative weighting between the two terms of the objective criterion. The selection of an appropriate regularization parameter  $\lambda$  is crucial for a desirable updating process. In each iteration, the update increment  $\Delta\alpha_i$  is computed and applied to the current parameter value,  $\alpha_{i+1} = \alpha_i + \Delta\alpha_i$ . This iterative process continues until the difference between successive iterations is below a prescribed tolerance, indicating convergence.

### 2.3.4. Stochastic model updating

The term “stochastic” implies that the model updating parameters are treated as random variables. When deriving modal properties through Experimental Modal Analysis (EMA) or Operational Modal Analysis (OMA), it is well understood that the results do not precisely match the actual structural modal properties. Inaccuracies in the computed experimental modal properties can arise from different noise sources, such as sensor

malfunctions or suboptimal sensor placement in OMA.

In the works of Blitzstein [12, 54], the model updating parameters are considered random variables, with their statistical characteristics described by their mean and variance. Similarly, Friswell [33] proposed an approach in which both the model updating parameters and the experimental modal properties are modeled as random variables, assuming that these datasets are statistically independent.

This stochastic approach gained significant traction at the beginning of the 21<sup>st</sup> century, particularly with the introduction of Monte Carlo simulations [38, 54]. Monte Carlo methods facilitate the generation of numerous realizations of experimental modal data and model updating parameters, thereby enabling modifications to the system's sensitivity matrix.

Furthermore, Govers [38] introduced an iterative approach where the updating parameters are adjusted to minimize the differences between the mean values of the model updating parameters and those of the experimental modal properties. This method also accounts for differences in covariance between the two datasets, aiming to achieve an accurate and reliable representation of the structure's modal characteristics.

## 2.4. Key terms in the FEMU (Finite Element Model Updating) procedure and their interrelationships

Before discussing our Finite Element Model Updating (FEMU) method, we will discuss some essential analogies that need to be clear before approaching the definition of FEMU. In that, we first have to understand the basics like a model, model class, and computed data, and then finally, we see the model updating in that we highlight some mathematical formulation in that regard.

Initially, we considered our dataset, let's call it  $\tilde{N}$  as our vector in which we have the n-component that can contain one type of dataset, which we generally call the homogenous data or it can have a different kind of dataset which we call the heterogeneous data, this dataset relay on the structure model properties that is natural frequency and mode shapes or it can also depend on the kinematic property of the structure that is our displacement and strains.

Now, consider that the system's input depends on structural properties such as physical or mechanical characteristics, while the numerical model outputs include variables like natural frequencies and mode shapes. In this framework, the system operates as an

input-output model, where the input is given by the updating parameter, and the output comprises the resulting data. Here,  $\alpha$  represents the model updating parameter, and  $z$  denotes the system response (e.g., natural frequencies, mode shapes, displacements, strains, etc.) for any spatial vector  $x$ . By combining this input-output relationship, we obtain Equation (2.9).

$$z = \mathcal{N}(x, \alpha) \quad (2.9)$$

Here,  $N$  is our operator that performs the model updating procedure between our input and output variables. One interesting thing is that in a finite element model updating operation,  $N$  is not dependent on the vector  $x$  of the space variable, so the above equation will be like Equation (2.10)

$$z = \mathcal{N}(\alpha) \quad (2.10)$$

The model updating parameter  $\alpha$  belongs to the class of models that is  $\mathcal{N}_n$  and which belongs to the subset class  $P_N$ , so the model class of the structure can be represented as:

$$\mathcal{N}_n = \{\mathcal{N}_n(\alpha) \mid \alpha \in P_N\} \quad (2.11)$$

Now as we know we define the dataset which we get from the experimental results and also the model class, then the model updating procedure is just now estimating the parameter of the model in a specifically defined model class, and during that, we will also be expected that there will be some uncertainties that are model uncertainties  $\varepsilon$  and the another is calculation uncertainties  $\mu$  after adding those uncertainties in our system the final form is represented in Equation (2.12).

$$\tilde{N} = N(\alpha) + \varepsilon + \mu \quad (2.12)$$

Now as know the model updating parameter optimal value  $\alpha_{\text{opt}}$ , and the value that we get from our output numerical that is  $N(\alpha_{\text{opt}})$  which represent the model which is  $\mathcal{N}_n(\alpha_{\text{opt}})$  align with the result we get from the experimental dataset  $\tilde{N}$ .

Afterward, we will see the basics in which we choose design variables, that is, the model updating parameter during the finite element model is updated.

## 2.5. Choosing the Updating Parameters and Model Class

Incorporating updating parameters in the finite element model is not straightforward, as it can sometimes lead to non-trivial solutions. The selected parameters should effectively represent the structure's unknown properties. A key challenge in model updating is determining the appropriate number of updating parameters. The system may become ill-conditioned if too many parameters are chosen, leading to numerical instability.

Several methods have been proposed in the literature to mitigate this issue. One approach involves conditioning the stiffness matrix using the cut-set basis method [47]. Another technique is preconditioning the conjugate gradient method. When dealing with the flexibility matrix, which is the inverse of the stiffness matrix, the cycle bases of a network can be generated to improve conditioning [46].

While using any of the above-discussed methods, there will be issues like the parametrization of the model while performing the updating technique, leading to a non-unique solution. Estimation of the parameter will be affected if we don't have sufficient measure data, which causes the system to remain under-determined in our deterministic method, and during the application of the stochastic iterative method [11, 61], there is an unidentified parameter. Usually, the regularization technique is used to update our deterministic finite element model. Still, sometimes, depending upon the complexity of our structure in the computational time frame, it's preferred to use parametrization [83]. The parameters in that regard belong to the vast domain, some of which are the mechanical and material properties, cross-sections of the element, boundary conditions, geometry of the model, and the connection provided at the joints. Those are some updating parameters commonly used during the model updating procedure.

The parametrization of the model has a very significant effect on simplifying the numerical model and also reducing the errors between the modal properties of the real structure and the finite element model. As Mottershead and Friswell [32] have discussed, to achieve better accuracy and reliability from the model updating procedure, the parameter of the model should satisfy these parametrization conditions:

- The selection of the model updating parameters should be such that it will affect the system's output.
- There should be updating parameters selected so there will be no ill-condition problem.

- If some uncertainties are available in the model, those uncertainties should be resolved by using the parametrization technique.

Performing a sensitivity analysis on model parameterization offers several advantages. It helps identify the most influential parameters while reducing the risk of inadequacy issues in the system. This type of parameterization can be further categorized into two subtypes: the selection method [87] and the clustering method [44].

### 2.5.1. Selection method

The first sensitivity-based approach is the selection method. Consider a substructure composed of  $n$  individual finite elements (FEs). Let  $a$  be the updating parameter of the substructure, while  $a_1, a_2, \dots, a_n$  represent the updating parameters associated with the individual FEs that constitute the substructure [87].

Assuming that the updating parameters of both the substructure and the individual FEs correspond to the same physical property, such as the substructure parameter, Young's modulus, mass density, or stiffness, the objective function can be expressed as:

$$F(a) \quad \text{or} \quad F(a_1, a_2, \dots, a_n). \quad (2.13)$$

Since  $F(a_1, a_2, \dots, a_n)$  simplifies to  $F(a, a, \dots, a)$  when  $a_i = a$  for all  $i = 1, 2, \dots, n$ , a Taylor series expansion allows us to approximate the objective function as:

$$F(a_1, a_2, \dots, a_n) = F(0, 0, \dots, 0) + \frac{\partial F}{\partial a_1} a_1 + \frac{\partial F}{\partial a_2} a_2 + \dots + \frac{\partial F}{\partial a_n} a_n + \dots \quad (2.14)$$

Equation (2.14), the sensitivity of the objective function concerning the updating parameter  $a$  can be derived as:

$$\left. \frac{\partial F}{\partial a} \right|_{a_i=a} = \frac{F(a, a, \dots, a) - F(0, 0, \dots, 0)}{a} = \frac{\partial F}{\partial a_1} + \frac{\partial F}{\partial a_2} + \dots + \frac{\partial F}{\partial a_n} = \sum_{i=1}^n \frac{\partial F}{\partial a_i}. \quad (2.15)$$

Equation (2.15) establishes that the sensitivity of the objective function for the updating parameter of the substructure is equivalent to the sum of the sensitivities of the objective function for the updating parameters of the individual FEs comprising the substructure [20]. This allows us to determine the influence of the objective function sensitivity on individual FEs based on two key observations:

1. The sensitivity of the objective function varies for each individual FE.
2. Individual FEs within the substructure can be grouped based on the calculated sensitivity values, considering the overall sensitivity of the FE mesh.

### 2.5.2. Clustering method

The second sensitivity-based approach is the clustering method. This technique commonly identifies equivalent elastic parameters by comparing measured and analytically predicted natural frequencies [8]. It formulates an inverse problem aimed at updating the equivalent parameters. In the FEMU-based parameter identification process, the optimization is framed as a least-squares problem to minimize the objective function.

$$J(p) = r^T W r, \quad r = f^e - f^a(p) \quad (2.16)$$

where  $J(p)$  represents the objective function, and  $T$  denotes the transpose operation. The residual vector,  $r$ , captures the difference between the experimental ( $f^e$ ) and analytically predicted ( $f^a$ ) natural frequencies. The diagonal weighting matrix  $W$  accounts for the significance of each term in the residual vector, particularly in cases where specific values are given more importance. The optimization problem can thus be formulated as:

$$\min J(p) \quad \text{s.t. } p_l \leq p \leq p_u, \quad (2.17)$$

Where  $p_l$  and  $p_u$  define the lower and upper bounds of the physical parameters to be identified.

Despite the nonlinear relationship between the objective function and the parameters, a well-conditioned model can be obtained with prior knowledge of the equivalent modeling. In the standard FEMU-based method, selecting physical parameters is intuitive and direct. However, excessive parameters can lead to an ill-conditioned system, impacting sensitivity analysis and potentially introducing uncertain parameters. To mitigate this, clustering techniques can be applied to reduce the number of independent parameters while preserving their structural influence.

Through clustering, sets of directly linked parameters are grouped into representative cluster parameters. Each cluster parameter, denoted as  $p^k$ , is defined with the initial parameters as:

$$p^k = p_0(1 - t\theta), \quad k = 1, 2, \dots, q \quad (2.18)$$

where  $k$  represents the  $k^{th}$  cluster, and  $q$  is the total number of cluster parameters. Initially,  $\theta$  is set to zero. It is important to note that the superscript  $k$  distinguishes the clustered parameters from their original counterparts. The transformation matrix/vector  $L$  is then introduced to relate the original and clustered parameters:

$$\mathbf{p} = \begin{bmatrix} p_1 \\ \vdots \\ p_n \end{bmatrix} = L_{n \times q} \begin{bmatrix} p^1 \\ \vdots \\ p^q \end{bmatrix} \quad (2.19)$$

In the field of sensitivity analysis, various parameterization methods exist in the literature, including Bayesian parameterization [25] and particle swarm parameterization [49].

Despite the availability of multiple approaches, selecting the most suitable method for model updating depends on a thorough understanding of structural behaviour, sound engineering judgment, and the specific objectives of the test [7, 61]. Ultimately, a limited number of updating parameters must be chosen in alignment with the test objectives to achieve an accurate physical model while ensuring rapid convergence and avoiding ill-conditioning issues. This process leads to the development of a numerical model, commonly referred to as the digital twin of the actual structure.

To effectively implement parameterization and select the appropriate model updating parameters, it is crucial first to identify the correct class of the structural model. This step is essential to ensure that the model updating process is both efficient and effective. Additionally, defining the finite element (FE) model class is necessary as it provides a structured approach to input-output modeling for the pre-modeled structure concerning various parameterization techniques [55]. The literature offers a wide range of sensitivity-based methods [44] for selecting the most suitable model class for a given structure. Among these, Bayesian methods [88] and Particle Swarm Optimization [49] are commonly employed.

In practical applications, the Bayesian approach is widely used for selecting the appropriate model class due to its straightforward quantitative procedure, which is computationally less expensive than other methods [25]. This method involves selecting a model class with the highest probability for further analysis. However, despite its simplicity, the Bayesian approach often favors highly complex models that incorporate numerous system uncertainties, even when only minor parameter modifications are necessary. In

scenarios where the objective is to minimize the fitting error between the output dataset and the predicted model updating parameters, selecting a model class with significant parameters becomes crucial. However, when dealing with complex structural models, it is essential to implement penalization strategies to avoid unnecessary complexity, though their application is not always straightforward.

Ultimately, selecting an appropriate model class is critical to ensuring the accuracy of the finite element model in representing the physical behaviour of the actual structure. The chosen model should be efficient and effective while maintaining computational feasibility [86]. This approach is fundamental in model updating, as it enhances the reliability of the numerical model and enables the handling of highly complex systems through appropriate refinement techniques, leading to improved model properties.

## 2.6. Douglas-Reid Model Updating

The Douglas-Reid (DR) model updating [27] was introduced in 1982, and it belongs to the class of iterative model updating; this method is getting intensive consideration in research areas where we want the model updating of the structure under continuous vibration which we take for the structural health monitoring, this method is based on the second-order quadratic interpolation technique which causes this method very straight forward and less computational, due to that advantage this method use for model updating of different structures like bridges [23, 35, 93] and also for the old historical buildings [70], in regarding the application of that method is we were considering our updating parameter which can be the physical and mechanical property of the structure and perform the analysis so which gave us the updated properties which we can use to compare with the experimental results.

The main goal is to update the model properties based on the outcome of their dynamic behaviour to the model that is already being modeled, for that use the objective function that gives information about the scatter between the computed model behaviour from the numerical model and the actual behaviour that comes from the OMA. Usually, we take model properties to update natural frequencies [36, 70] and the modes shape [10, 23]. Still, our studies only consider the natural frequency, not the modes shape, because the updating parameter has little influence on the modes shape [70]. Following the same procedure, we can apply this method to modes shape[10].

### 2.6.1. Mathematical formulation of DR method

The mathematical development behind this method is explained in this section, so initially, we need the experimental data of the natural frequencies  $f_i^{\text{exp}}$ ; for this we can carry on the experimental campaigns by actually oscillating the structure by external forces or we can also perform the OMA technique, for finding the model properties of the structure which is our natural frequencies as in Equation (2.20). M here is the number of modes. Similarly, we have  $f_i^{\text{FEM}}$  that is the natural frequency computed from the numerical model developed for the structure as shown in Equation (2.21).

$$f_i^{\text{exp}} \quad (i = 1, \dots, M) \quad (2.20)$$

$$f_i^{\text{FEM}} = f_i^{\text{FEM}}(x_1, x_2, x_3, \dots, x_k, \dots, x_N) \quad (2.21)$$

Here, N is the number of updating parameter  $x_k$ ; now, as we want to minimize the scatter between the computed natural frequency from the Equation (2.21) w.r.t the experimental, for this, we define the range of updating parameters. Then, the DR method uses the second-order interpolation on natural frequency by varying the updating parameters.

$$f_i^{\text{DR}} = C_i + \sum_{k=1}^N (A_{i,k}x_k + B_{i,k}x_k^2) \quad (2.22)$$

Here in Equation (2.22) we have the general formulation of DR method for second-order approximation of natural frequency  $f_i^{\text{DR}}$ , and that  $C_i$ ,  $A_{i,k}$  and  $B_{i,k}$  is our unknown of the system which we find by using some preliminary analysis so our system has  $(2N + 1)$  unknowns in the Equation (2.22). So, to find those unknowns, we initially define the nominal value  $x_k^B$  and its upper  $x_k^U$  and lower  $x_k^L$  range for updating parameter and then we normalize it by the nominal value as shown in Equation (2.23).

$$\frac{x_k^L}{x_k^B} \leq \frac{x_k^B}{x_k^B} \leq \frac{x_k^U}{x_k^B} \quad (2.23)$$

Now to compute the  $(2N + 1)$  unknowns of Equation (2.22), we first solve Equation (2.24) in which we vary our one updating parameter at a time within its predefined upper and lower bound and keeping the nominal value for the other updating parameters same, and than equated them with natural frequencies that we get from a numerical model  $f_i^{\text{FEM}}$  as shown in the Equation (2.24).

$$\begin{cases} f_i^{\text{DR}}(x_1^B, \dots, x_k^B, \dots, x_N^B) = f_i^{\text{FEM}}(x_1^B, \dots, x_k^B, \dots, x_N^B) \\ f_i^{\text{DR}}(x_1^U, \dots, x_k^B, \dots, x_N^B) = f_i^{\text{FEM}}(x_1^U, \dots, x_k^B, \dots, x_N^B) \\ f_i^{\text{DR}}(x_1^L, \dots, x_k^B, \dots, x_N^B) = f_i^{\text{FEM}}(x_1^L, \dots, x_k^B, \dots, x_N^B) \\ f_i^{\text{DR}}(x_1^B, \dots, x_k^U, \dots, x_N^B) = f_i^{\text{FEM}}(x_1^B, \dots, x_k^U, \dots, x_N^B) \\ f_i^{\text{DR}}(x_1^B, \dots, x_k^L, \dots, x_N^B) = f_i^{\text{FEM}}(x_1^B, \dots, x_k^L, \dots, x_N^B) \\ f_i^{\text{DR}}(x_1^B, \dots, x_k^B, \dots, x_N^U) = f_i^{\text{FEM}}(x_1^B, \dots, x_k^B, \dots, x_N^U) \\ f_i^{\text{DR}}(x_1^B, \dots, x_k^B, \dots, x_N^L) = f_i^{\text{FEM}}(x_1^B, \dots, x_k^B, \dots, x_N^L) \end{cases} \quad (2.24)$$

with  $i = 1, \dots, M$

Now we can express this Equation (2.24) in matrix form as shown below

$$\{f_i^{\text{FEM}}\} = [C]\{K_i\} \quad (2.25)$$

with:

$$[C] = \begin{bmatrix} 1 & x_1^B & (x_1^B)^2 & \dots & x_N^B & (x_N^B)^2 \\ 1 & x_1^U & (x_1^U)^2 & \dots & x_N^B & (x_N^B)^2 \\ 1 & x_1^L & (x_1^L)^2 & \dots & x_N^B & (x_N^B)^2 \\ \vdots & \vdots & \vdots & \ddots & \vdots & \vdots \\ 1 & x_1^B & (x_1^B)^2 & \dots & x_N^U & (x_N^U)^2 \\ 1 & x_1^B & (x_1^B)^2 & \dots & x_N^L & (x_N^L)^2 \end{bmatrix} \quad (2.26)$$

$$\{K_i\} = \begin{Bmatrix} C_i \\ A_{i,1} \\ B_{i,1} \\ \vdots \\ A_{i,N} \\ B_{i,N} \end{Bmatrix} \quad (2.27)$$

Now, the unknown vector of  $K_i$  is:

$$\{K_i\} = [C]^{-1}\{f_i^{\text{FEM}}\} \quad \text{with } i = 1, \dots, M \quad (2.28)$$

After knowing all the  $(2N + 1)$  unknowns, we can use our Equation (2.24) and compute the second-order approximated DR natural frequency, which we can use in place of our frequencies calculated from the numerical model  $f_i^{\text{FEM}}$  and minimize the objective function. The objective functions considered in those studies are given below, and  $PMR_i$  is

the participation mass ratio for each mode that acts as a weighing function.

$$J'_f = \frac{100}{M} \sum_{i=1}^M \left| \left( \frac{f_i^{\text{FEM}} - f_i^{\text{exp}}}{f_i^{\text{exp}}} \right) \right| \quad (2.29)$$

$$J''_f = \frac{100}{M} \sum_{i=1}^M \left( \frac{f_i^{\text{FEM}} - f_i^{\text{exp}}}{f_i^{\text{exp}}} \right)^2 \cdot \text{PMR}_i \quad (2.30)$$

## 2.7. Modal Analysis

The modal analysis encompasses several key characteristics that must be thoroughly understood, particularly in the study of structural behaviour. It serves various purposes, including identifying sources of error in the analysis [15, 24, 40, 89], validating numerical models, and facilitating structural dynamic modifications. Additionally, it plays a crucial role in load sensitivity assessments, structural health monitoring (SHM), substructure coupling, and sensitivity analysis [15, 91].

There are different methods available for modal analysis. The three common methods are Experimental Modal Analysis (EMA) and Operational Modal Analysis (OMA). These two are widely used, and the third method, now under development, is known as Impact Synchronous Modal Analysis (iSMA). The oldest method is Experimental Modal Analysis (EMA), which is around 60 years old; in this method, structural vibration is excited artificially by the impact of a hammer or shaker, and it is usually performed in a controlled environment like in a laboratory. We can excite a large structure discussed in it [58, 71]. The main difference between EMA and OMA or iSMA is that the OMA and iSMA method is applied to the working condition of the structure, or we can say the ambient condition. The main difference between our OMA and iSMA is that in OMA technique, we consider the ambient excitation of the structure, which is our unknown parameter; on the other hand, iSMA uses the artificial excitation similar to the case of EMA as its input parameter that is known.

## 2.8. Operational Modal Analysis

In [73], Rainieri and Fabbronicino highlight some important concepts regarding the operational modal analysis used for defining the dynamic characteristic of the structure and also discuss some considerations or assumptions used for simplifying this method, which are listed below.

- *Observability*: The sensor's location should be such that we can produce all mode shapes of the structure.
- *Stationarity*: The dynamic property of the structure under observation will remain the same in the time domain.
- *Linearity*: If our input system has a linear combination, we will also get the linear combinations in the output.

Operational Modal Analysis (OMA), also known as output-only modal analysis, operational modal analysis, and ambient modal identification, is a technique used to determine the modal properties of a structure under ambient vibrations. These vibrations are typically caused by natural environmental factors, such as wind, traffic, or machinery, and are captured by sensors installed at different structure elevations. This method is beneficial when conventional Experimental Modal Analysis (EMA) is unsuitable, such as when artificial excitation is difficult or impossible to apply due to the structure's large slenderness.

In contrast to EMA, which requires controlled excitation of the structure, OMA relies on the structure's response to ambient vibrations, which are typically caused by cyclic loads in the environment. Since the input excitation in OMA is unknown, specialized algorithms are used to extract the modal properties of the structure from the recorded vibrational data. This makes OMA a valuable tool for identifying the dynamic characteristics of structures under random excitation generated by ambient environmental conditions.

OMA techniques are developed based on several algorithms used for data processing. It is seen that processing the data through OMA leads to several types of errors as discussed here [3], so to overcome this disadvantage of OMA, research has developed different methods to perform the OMA, through which we can compare the results between different methods and find the optimal results for the dynamic characteristic of the structure, this method we see in the later sections of this development.

### 2.8.1. Overview of operational modal analysis techniques

The use of operational modal analysis has one issue: this method is very computationally expensive because, in that method, we have a large amount of output data collected from the sensors. Analyzing this extensive data takes more time, and the efficiency of the system is also reduced for such comprehensive data computation; then, to overcome this disadvantage, a lot of research was carried out in the late 19th century, and some software which can help to efficiently process this immense data, and compute the model properties [75].

Broadly, the OMA techniques or methods are divided into two domains, namely *time domain methods* and *frequency domain methods*. In the time domain method, we use the correlation functions or the time histories. In contrast, in the frequency domain method, we generally use the concept of Power Spectral Density (PSD), which defines the relation between the input and output dataset. Some techniques are discussed below.

## Peak picking (PP)

The first and most commonly used method of OMA is the peak picking method [42], and it belongs to the class of frequency domain technique. In this method, we initially produced the PSD curve, and to find the modal properties, like natural frequencies, we were peaking the picks of the curve, which are our natural frequencies that excite the structure most. In this technique, we assume that the mode shapes of our model are widely separated and the damping coefficients of the system are low. This method has shown excellent accuracy for the structure in which the mode shapes are widely separated [56, 91]. This method is straightforward and easy to implement and less computationally heavy, but the results from this method can be misleading if the mode shapes are closely spaced, and as we know, in the fundamental structure, most of the modes of the structure are very closely spaced which is the drawback of this method, so to overcome this drawback research has developed another method that is frequency domain decomposition (FDD).

## Frequency Domain Decomposition (FDD)

In Frequency Domain Decomposition (FDD) method, we can overcome the drawback of the peak picking method, so in FDD [16] as its name indicates, this technique also belongs to the frequency class of the method. That technique is simple to implement, and it is also the most common technique that is usually used for identifying the modal properties of the structure. The FDD method is the extension of the Peak Picking (PP) method. In that method, we use the Singular Value Decomposition (SVD) of PSD matrix to identify the multiplicity of the modes. While considering the SVD of PSD matrix, PSD matrix is decomposed into several small sets of auto-spectral densities, and this small set of auto-spectral densities represents the Single Degree of Freedom System (SDOF) system.

Now, to develop a relationship between input, which is unknown ambient excitation  $x(t)$ , and output is the response of the structure  $y(t)$  that is discussed in [1].

$$[G_{yy}(j\omega)] = [H(j\omega)]^* [G_{xx}(j\omega)] [H(j\omega)]^T \quad (2.31)$$

Here,

\* in the superscript indicate the complex conjugate, and

T in the superscript indicates the transpose

$[G_{yy}(j\omega)]$  is output's PSD matrix,  $[G_{xx}(j\omega)]$  is input's PSD matrix and  $[H(j\omega)]$  is Frequency Response Function (FRF) matrix. Performing SVD of the output's PSD matrix at discrete frequencies  $\omega = \omega_i$  gives [16, 74].

$$\left[ \hat{G}_{yy}(j\omega_i) \right] = [U]_i [S]_i [U]_i^H \quad (2.32)$$

Here,

$H$  in the superscript is conjugate transpose, or it is also known as the Hermitian transpose,  $[U]_i$  Unitary matrix that contains the vector proportional to eigenvectors of a matrix, and  $[S]_i$  Unitary matrix that contains the vector proportional to eigenfrequencies of a matrix.

So, as we know, by using FDD, we can correctly compute the model properties of the system even for the closely spaced modes or even for the repeated modes, but this method also has one drawback that is by using this method we can not compute the damping coefficients for the structure so, to overcome this drawback another method is developed that is Enhanced Frequency Domain Decomposition (EFDD).

## Enhanced Frequency Domain Decomposition (EFDD)

EFDD [17], is just the advanced version of the FDD, which is developed to overcome the drawback of the FDD, that is the damping coefficients, so by the EFDD method we can compute the all modal properties of the structure like natural frequencies, mode shapes or even the damping ratios with much higher accuracy as compared to the FDD method. In FDD, we use the strategy of the Inverse Discrete Fourier Transform (IDFT), which converts PSD function in the time domain, and in time domain response, the peak of the system lies at the resonance frequency of the structure which we get from the zero-crossing times. Then, finally, to obtain the damping, we take the logarithmic decrement of the corresponding normalized auto-correlation function.

EFDD is also the most common method and widely used strategy for the computation of modal property due to its more straightforward implementation and very user-friendly, which computes the natural frequency and mode shapes with higher accuracy and also for closed space modes. In addition, it also computes the damping ratio, but the accuracy of the computation of the damping ratio is still an open question. There are several other

methods available in the literature for accurately computing the damping ratio for this reader can refer to those papers [18, 50, 91].

## Time Domain Decomposition (TDD)

As the name indicated of Time Domain Decomposition (TDD) belongs to the time domain method for computing modal properties, we will incorporate the technique of OMA, which is the time domain [48]. In this method, the basic approach is that we have the SDOF system, which should be in the time domain. In this method, we will extract all the undamped mode shapes using the SVD method for the output correlation matrix, which is based on the location of sensors; by using this method, we get all the modal properties of the structure that is natural frequencies, mode shapes and damping ratios that we extract from the SDOF system by using the predefined strategy that is PP method.

The output response of the system, which is under the action of ambient vibration forces, can be represented by the mode shapes as in Equation (2.33) [48].

$$y(t) = \sum_{i=1}^{\infty} c_i(t) \varphi_i \quad (2.33)$$

Here,  $y(t)$  is the displacement profile vector of the output,  $\varphi_i$  is the  $i$ th mode shape, and  $c_i(t)$  is the  $i$ th modal contribution factor of the displacement at time  $t$ . As we know, the number of modes resolved in a continuous response of the structure is unlimited, so the output response of acceleration of time history will be given as [48].

$$\ddot{y}(t) = \sum_{i=1}^{\infty} \ddot{c}_i(t) \varphi_i \quad (2.34)$$

Here, the double dot on the  $c$  represents the second order of derivative with respect to time.

There is only one mode in the SDOF approach, which is generally opposed to the Multi Degree of Freedom System (MDOF) approach. Hence, it eliminates the chances of the false identification of the spurious modes. In addition, in the actual structure, measured time response belongs to the class of the MDOF signal. So initially in TDD, we will define our band-pass filter for an appropriate frequency range that takes into account only one mode of the structure at a time; however, for visually identified frequency bandwidth, a filter can be designed, and a mode isolated discrete time response can be created [48]. So, if any mode-isolated signals are present at the  $i$ th acceleration, the response of the SDOF can be given as in Equation (2.35) [48].

$$\ddot{y}_i(k) = \ddot{c}_i(k)\varphi_i + \tilde{\epsilon}_i(k) \quad (2.35)$$

Here,  $\ddot{y}_i(k)$  is the acceleration response at sampling time  $k$ ,  $\tilde{\epsilon}_i(k)$  is the noise at time sample  $k$ . In addition, the TDD method is to form an output energy correlation matrix with mode-isolated time history signals. The cross-correlation matrix  $E_i$  can be disturbed as the energy correlation of the  $i$ th mode concerning the correct location of the sensors [48].

$$E_i = Y_i Y_i^T \quad (2.36)$$

Where  $Y_i$  is the mode-isolated output acceleration time history that contains only the  $i$ th mode, in the next step, SVD is performed of the matrix  $E_i$  as [48].

$$E_i = U \Omega U^T \quad (2.37)$$

Here  $U$  is the singular vector matrix of  $Y_i$ , and the diagonal matrix  $\Omega$  is the singular value matrix of  $Y_i$  [48]. Finally, the first column vector of  $U$  is designated as the undamped mode shape for the isolated mode. The PP method can extract each mode's natural frequency and damping ratio from the SDOF signal. The reader may refer to [48] for more details on this method.

TDD is a computationally efficient method when many sensors are involved in structure analysis. The mode isolation task achieved by using a digital band-pass filter dramatically reduces operator interaction during the analysis process, making this method suitable for automated online health monitoring system applications. On the other hand, since this method is based on the SDOF approach, it isn't easy to extract modal parameters from closely spaced modes [48].

## Stochastic subspace identification (SSI)

Stochastic Subspace Identification (SSI) is a time-domain Operational Modal Analysis (OMA) technique first developed by Van Overschee and De Moor in 1991 [59]. Its primary advantage is determining an effective state-space model for even highly complex dynamic systems under stochastic excitation using only data acquired during an OMA campaign [65]. Moreover, the simplicity of SSI allows for a significant reduction in computational complexity compared to methods such as ARMA [74].

Two commonly used variants of SSI are available [68]:

- Stochastic Subspace Identification by Data-Driven (SSI-DATA)
- Stochastic Subspace Identification by Covariance-Driven (SSI-COV)

In the SSI-COV approach, Singular Value Decomposition (SVD) is typically employed to extract the deterministic system characteristics and reduce noise [64]. In this method, a Hankel matrix, denoted by  $H$ , is constructed from the Frequency Response Function (FRF) dataset gathered during the OMA campaign. For implementation purposes, techniques such as Canonical Variate Analysis (CVA), Unweighted Principal Components (UPC), or Principal Components (PC) can be utilized. Initially, the Hankel matrix is weighted using one of these approaches before being decomposed via SVD. These weighting strategies are essential for enhancing the performance of the decomposition process [69, 90].

The first step in the Covariance-Driven Stochastic Subspace Identification (SSI-Cov) is to find the output covariance  $R_i$  as explained in [72].

$$R_i = \lim_{N \rightarrow \infty} \frac{1}{N} \sum_{k=0}^{N-1} y_{k+i} y_k^T \quad (2.38)$$

where  $N$  is the data sample. The Toeplitz matrix, the output covariance matrix  $T_i$ , is also explained in [72].

$$T_i = \begin{bmatrix} R_i & R_{i-1} & \cdots & R_1 \\ R_{i+1} & R_i & \cdots & R_2 \\ \vdots & \vdots & \ddots & \vdots \\ R_{2i-1} & R_{2i-2} & \cdots & R_i \end{bmatrix} \quad (2.39)$$

The Toeplitz matrix can also be decomposed into the product of observability matrix  $O_i$  and controllability matrix  $\Gamma_i$  as discussed in [72].

$$T_i = \begin{bmatrix} C \\ CA \\ CA^2 \\ \vdots \end{bmatrix} \begin{bmatrix} A^{-1}G & A^{-2}G & \cdots & G \end{bmatrix} = O_i \Gamma_i \quad (2.40)$$

The SVD gives  $T_i$  as shown in Equation (2.41) [72].

$$T_i = USV^T \quad (2.41)$$

where  $S$  is a singular matrix with diagonal values,  $U$  and  $V$  are orthogonal matrices. The system matrices  $A$  and  $C$  can be solved by solving Equation (2.42) and Equation (2.43) simultaneously. To get modal parameters, eigenvalue decomposition is applied to state matrix  $A$  as [72].

$$A = \Psi \Lambda \Psi^{-1} = \sum_{k=1}^n \psi_k \lambda_k \psi_k \quad (2.42)$$

Where  $\lambda_k$  is the eigenvalue of a discrete-time system. The natural frequency  $\omega_k$ , damping ratio  $\zeta_k$  and mode shape  $\varphi_k$  are obtained from Equation (2.43) [72].

$$\omega_k = \frac{|\lambda_k|}{2\pi}, \quad \zeta_k = \frac{-100 \operatorname{Re}(\lambda_k)}{|\lambda_k|}, \quad \varphi_k = C\psi_k \quad (2.43)$$

Where  $\lambda_k$  is the eigenvalue in a continuous time system, obtained from Equation (2.44) [72].

$$\lambda_k = \frac{\ln \lambda_k}{\Delta T} \quad (2.44)$$

Another method of Stochastic Subspace Identification (SSI) is Data-Driven Stochastic Subspace Identification (SSI-Dat), which was initially developed by Van Overschee and De Moor [63]. If we compare this method with the SSI-Cov, in SSI-Dat, the covariance is not computed from the data that we get from the outputs that are the primary difference in SSI-Dat. In SSI-Dat, we use a different decomposition, which is the QR decomposition of the dataset of Hankel Matrix, which is used to project the row space of future outputs into the row space of past outputs [66, 68, 90]. In the end, we will use the SVD method for the decomposition of the projection matrix through which we will understand the parameters of the system as we see in SSI-Cov (Principle Component (PC), Canonical Variant Analysis (CVA) and Unweighted Principle Component (UPC)) methods which are generally used for the weighing the matrix.

It is generally preferred that we use the method CVA when we have data that consist of a low signal-to-noise ratio and modes with varied strength, and in UPC method when our data indicates a high signal-to-noise ratio and the modes have the same strength overall, and for our last method PC which is the compromise between this two methods

CVA and UPC [73]. The mode strength reflects the dominance of the mode that excites the structure most in the time domain, so the modes that have the high strength will indicate the high excited modes, and low strength mode will indicate the low excited modes during the test, and for the system in which we have the varying strength that means the few modes are excited high and, few were excited low, so to overcome this low and high strength modes we generally adopt the weighing phenomena which distribute the strength on each mode, similarly as we use weighting function in CVA method. The advantage of this method is that we will get the information about those modes also which are excited less in our operation working campaign [59, 63].

Another common difference between SSI-Cov and SSI-Dat from the computational point of view is that SSI-Cov is faster to compute as compared to the SSI-Dat, since SSI-Cov uses the Fast Fourier Transform (FFT), on the other hand, the SSI-Dat use the QR factorization which is slower than the FFT [37]. Now, for computing the SSI-Cov, we have the two methods [68].

1. By converting raw time histories of the data Hankel matrix to the covariances of the Toeplitz matrix assuming ergodicity.
2. By computing the covariances as the IDFT of the auto and cross-spectral density of the output.

SSI method has the advantages of high accuracy on parameter estimation and high computational efficiency compared to other OMA methods [76]. Due to these advantages, SSI has become a standard OMA method [53, 69, 75, 76] and SSI-Cov is a commonly used OMA method [76]. However, in a recent study, several new methods called correlation signal subset-based SSI like Component-Specific Stochastic Subspace Identification (CoS-SSI) presented in [52], also its implementation in SHM. The method aims to analyze systems with strong non-stationary vibration responses and nonlinearity. The method was tested on a car on a rustic road to identify vehicle suspension-related modal parameters. It was reported that this method can effectively handle signals with a low signal-to-noise ratio to identify modal parameters accurately and has better accuracy than SSI-Cov.

The OMA techniques discussed in this section are summarized in Table 2.1.

Table 2.1: Summary of different OMA techniques with their pros and cons.

Method	Type	Pros	Cons	References
PP	Frequency domain	Less computation, easiest and good for the widely separated mode	Inaccurate if a system has closely spaced modes which is the case in most real structures	[42, 56, 91]
FDD	Frequency domain	Can identify natural frequencies and closely spaced mode shapes accurately	Cannot estimate damping ratios	[1, 16, 74]
EFDD	Frequency domain	User-friendly and fast processing method. Can identify damping ratios along with mode shapes and natural frequencies with higher accuracy than FDD	Exact computation of modal damping is still an issue which may often lead to biased estimates	[17, 50, 91]
TDD	Time domain	Computationally efficient method. Reduces operator interaction greatly during modal analysis process	Difficult to extract modal parameters from closely spaced modes	[48]
NExT	Time domain	Provides a good ground to extend EMA techniques in OMA	Nature of the data in OMA is stochastic, while NExT methods have deterministic framework	[19, 37, 43]
ARMA	Time domain	Output measurements can be utilized directly	Computationally intensive method	[5, 14, 37, 69, 74]
SSI	Time domain	High parameter estimation accuracy and high computational efficiency compared to other OMA methods	Mathematically complex method	[37, 52, 59, 65, 74, 75]



# 3 | Validation of DR Method for FEMU for Test Structure

As in the previous chapter, we discussed in detail the DR model updating method and its framework for implementation on a structure; this method gives us a much wider range of possibilities for model updating like geometrical and mechanical properties of the structure, as compared to other methods. So, now we implement this method on the testing structure before proceeding towards the actual structure, which is a case study of the *Atmospheric Tower* of EC JRC, which is a steel truss structure that is 100m tall. In this chapter, we will adopt DR model updating techniques on our real-world structure.

The goal of the finite element model updating problem is to eliminate the discrepancies between the experimental modal data (see section 2.7), and the corresponding modal properties we get from the numerical model of the structure are updated by the model updating procedure, and appropriate model properties were computed which can able to perform the similar response as actual structure.

To check the accuracy of the model updating technique, we will apply this to a simple structure to know about this method accurately and whether this method can meet our requirements and eliminate the discrepancy between the modal properties.

## 3.1. Description of test structure

We have the 4-story structure in which we apply the DBD design procedure on one side of the dual structure as indicated in Figure 3.4. This structure consists of a 3-bay frame with two shear walls, the first one is an L-shaped shear wall with the dimensions of  $1.0\text{ m} \times 0.5\text{ m} \times 0.25\text{ m}$  and the second shear wall is rectangular with the dimensions of  $1.0\text{ m} \times 0.25\text{ m}$ , and this was joined by the coupled beam that is 0.45 m deep beam and the length of it is 1.0 m and the depth of the slab is 0.25 m, in addition to that we also have the two columns in our frame structure which have a depth of 0.4 m which is made for the pseudo-dynamic (PsD) that is testing parallel to the frame in ELSA(European Laboratory

of Structural Assessment) which has the facility of European Commission at ISPRA, all the dimension are in Table 3.1 also the real test scenario shown in Figure 3.3. The one important thing is that in the design of this structure, it is tested for the additional masses, which we add by considering the width instead of 2.0 m as 5.0 m, which increases the additional load during testing. The floor plan and the section at A-A are shown in Figure 3.2.

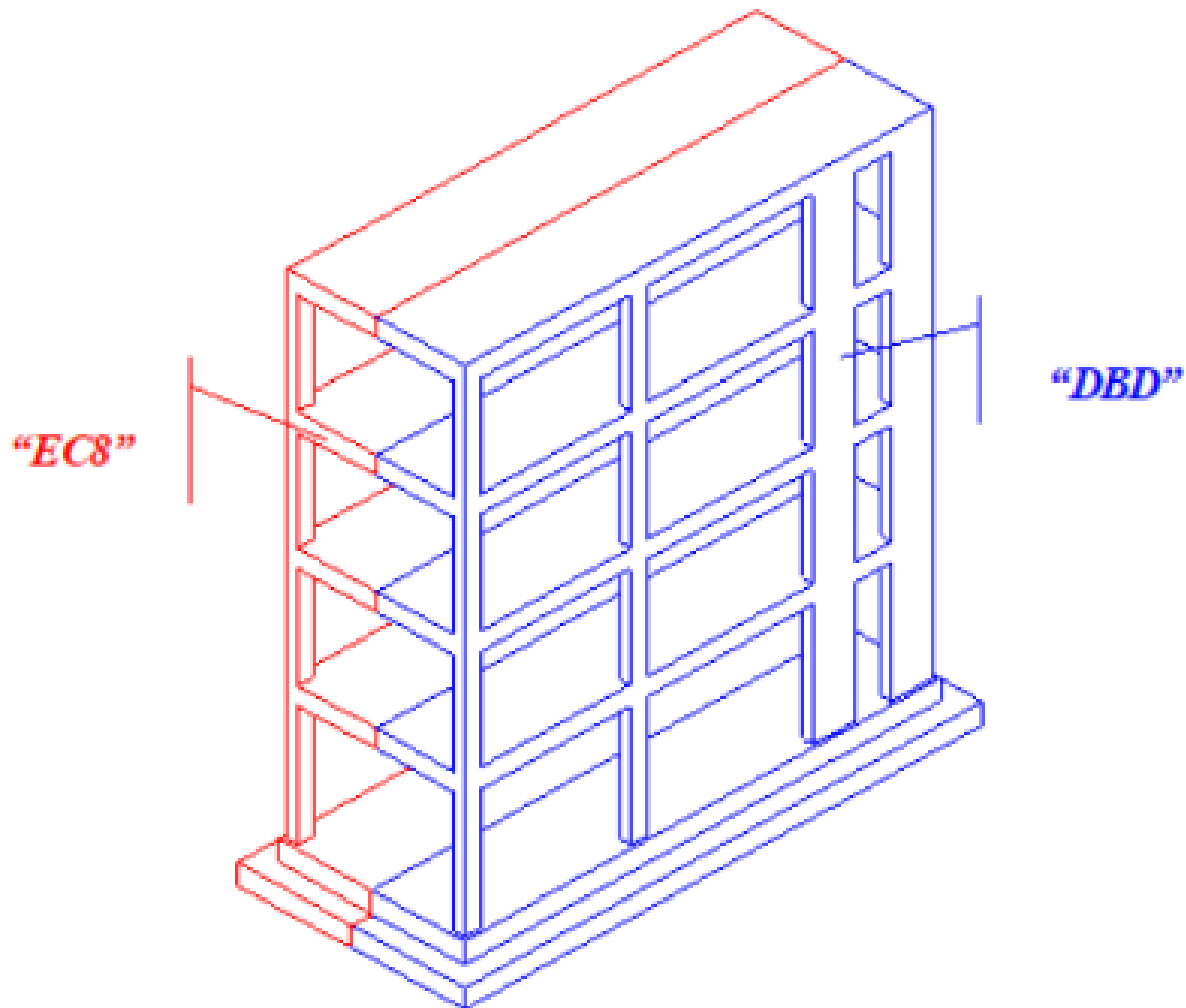
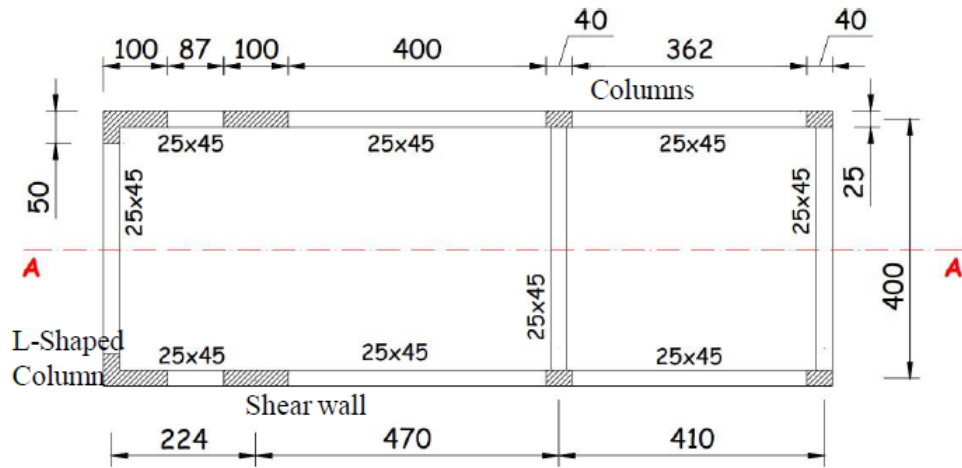
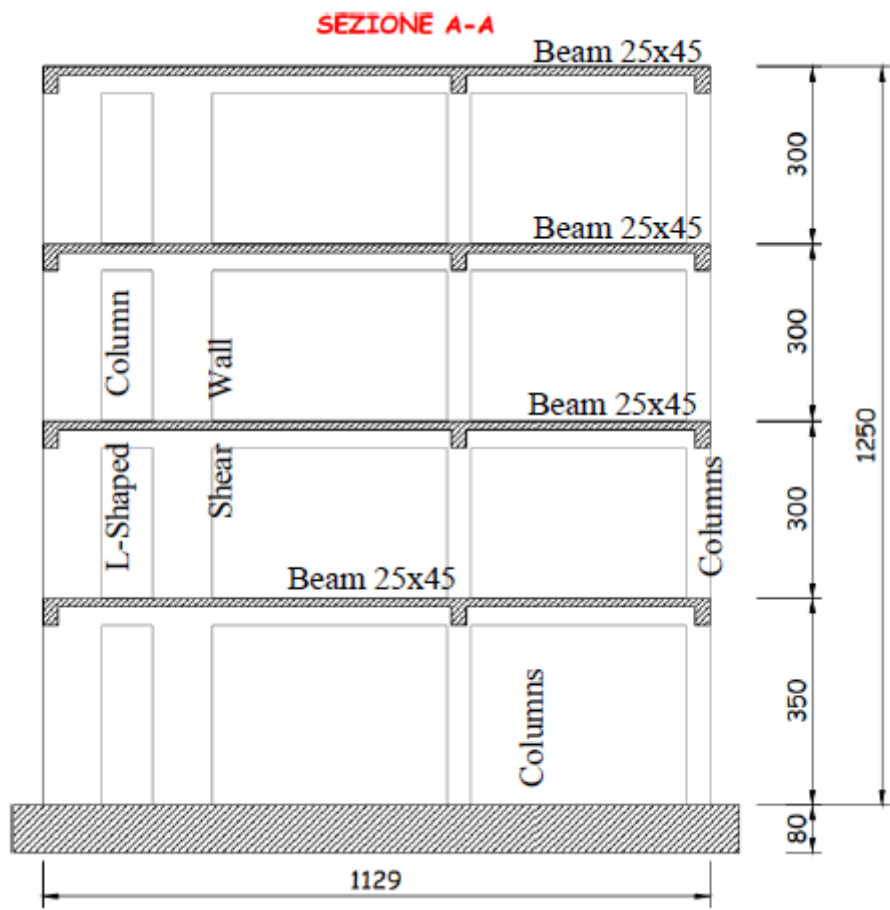


Figure 3.1: 3D model of dual design structure.



(a) Floor plan.

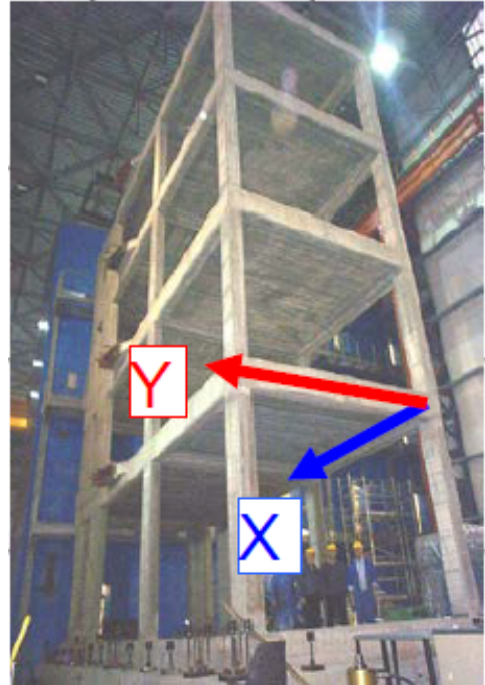


(b) Section A-A.

Figure 3.2: Floor plan and cross-section of the testing structure.



(a) Testing structure.



(b) Reference system for test.

Figure 3.3: This is the real structure under the testing condition with its reference system

### 3.1.1. Members dimensions

The dual structure (frame-wall) system resists the horizontal forces partially by shear walls and partially by moment-resisting frames. The geometry of each member is mentioned in the Table 3.1

Table 3.1: Table of members geometry.

Member	Model Identification
Beams	B 25x45
Columns	C 25x40
Shear wall	C 25x100
L-shaped wall	L 100x25

### 3.1.2. Material properties

#### Concrete

The concrete class used in structural design is C20/25, and the following are the results obtained from compressive tests performed on the cylindrical specimens, which are tabulated in Table 3.2.

Table 3.2: Concrete cylindrical strength (MPa).

Location	28-day Cubes (Average of 2 Specimens)	7-month Cores (at PsD Test)	12-month cores (5 Months After PsD Test)
Columns	22.5	-	-
Columns	21.2	-	-
Columns	19.7	26.5 (1 Core)	-
Columns	24.0	-	-
Slab, Beams	22.2	29.3	32.4 (average, 3 cores)
Slab, Beams	13.7	31.3	31.2 (average, 3 cores)
Slab, Beams	19.8	31.3	34.0 (average, 2 cores)
Slab, Beams	18.5	31.9	-
Walls	22.4	-	-
Walls	20.1	-	-
<b>Average</b>	<b>20.5</b>	<b>31.0</b>	<b>32.8</b>

Henceforth, the average value (mean compressive strength) will be 20 MPa. From mean compressive strength, the characteristic value (lower fractile value) was obtained as, For the modulus of elasticity, reference can be made to “EN1992-1-1,” which gives the following formula for calculation as shown in Equation (3.1) and Equation (3.2).

$$\begin{cases} f_{ck} = f_{cm} - 8 \quad (\text{MPa}) \\ f_{ck} = 20 - 8 \quad (\text{MPa}) \\ f_{ck} = 12 \quad \text{MPa} \end{cases} \quad (3.1)$$

$$\begin{cases} E_{cm}[\text{MPa}] = 22000 \times \left(\frac{f_{cm}}{10 \text{ MPa}}\right)^{0.3} \\ E_{cm}[\text{MPa}] = 22000 \times \left(\frac{20}{10} \text{ MPa}\right)^{0.3} \\ E_{cm} = 27.085 \text{ GPa} \end{cases} \quad (3.2)$$

## Steel

Tensile tests on the S500 steel class were performed with different sizes of steel specimens whose results are tabulated in Table 3.3.

Table 3.3: Strength and ultimate elongation of steel bars.

Diameter (mm)	Yield Strength (Mpa)	Tensile Strength (MPa)	Ultimate Elongation A5 (%)
8	557.5	642.1	23.7
10	525.2	617.2	24.2
12	516.5	615	24.8
14	521.9	615.2	26.2
16	506.4	627	24
<b>Average</b>	<b>525.5</b>	<b>623.3</b>	-

### 3.1.3. Dynamic testing

A dynamic test considering only the self-weight of the structure with the assumption of only linear elastic modelling was carried out. The first 9 Natural frequencies obtained are the experimental frequencies we use for the model updating, which are given in Table 3.4.

Table 3.4: Experimental natural frequencies of the structure under its self-weight.

Modes	Frequency (Hz)	Type	Ordering
1	2.06	Direction Y	1
2	3.94	Torsion	1
3	4.31	Direction X	1
4	6.37	Direction Y	2
5	11.62	Direction Y	3
6	12.9	Torsion	2
7	15.32	Direction X	2
8	16.56	Direction Y	1
9	24.31	Torsion	3

## 3.2. Numerical Model of Testing Structure

For the development of the numerical model, finite element model development software is used, which is MIDAS Gen [57]. The testing structure is a reinforced concrete frame structure designed based on two design strategies, DBD and EC8; at this stage, we will define the member's properties as the linear beam finite elements, and the connection between the member is considered the perfectly clamped connection between the member. Now, we will consider the four sections that we needed to define the structure's geometry in which we have the beams, columns, rectangular shear wall, and L-shaped shear wall as (cfr. section 3.1.1). In addition to that, all the sectional properties of each section are mentioned in Table 3.5. Beams and columns are used for defining the geometry, and two shear walls are also provided, as two L-shaped walls and the material is assumed to be perfectly elastic and isotropic; a complete model of the structure is shown in the Figure 3.4.

Table 3.5: Properties of different section types.

Section Types	A [m <sup>2</sup> ]	I <sub>y</sub> [m <sup>4</sup> ]	I <sub>z</sub> [m <sup>4</sup> ]	I <sub>t</sub> [m <sup>4</sup> ]
<b>Beam</b>	0.1125	$5.9 \times 10^{-4}$	$1.9 \times 10^{-4}$	$1.5 \times 10^{-3}$
<b>Column</b>	0.10	$1.3 \times 10^{-3}$	$5.2 \times 10^{-4}$	$3.2 \times 10^{-3}$
<b>Shear wall</b>	0.25	$2.1 \times 10^{-2}$	$1.3 \times 10^{-3}$	$8.3 \times 10^{-2}$
<b>L-shaped wall</b>	0.3125	$9.01 \times 10^{-3}$	$5.4 \times 10^{-3}$	$3.8 \times 10^{-2}$

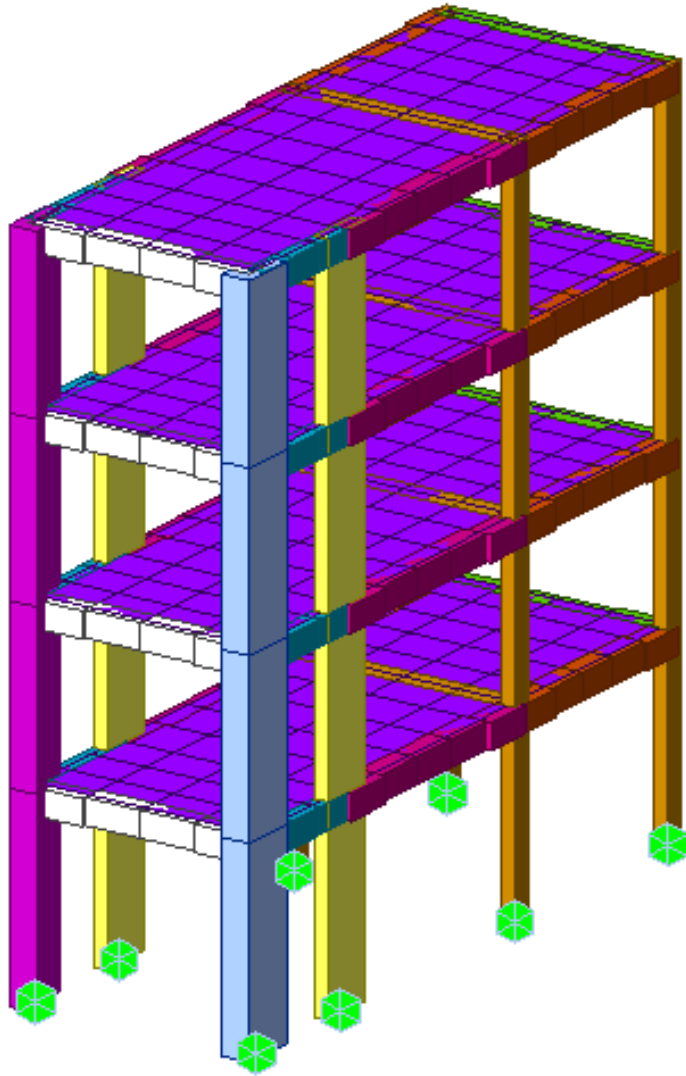


Figure 3.4: Initial numerical model of testing structure.

Now that we know that our structure is reinforced concrete structure, we will consider the mechanical properties of the structure that were adopted, and for that, we will consider that our material properties are perfectly elastic and isotropic).

- Young's modulus:  $E = 27 \text{ GPa}$ ;
- Poisson's ratio:  $\nu = 0.2$ ;
- Density:  $\rho = 2500 \frac{\text{kg}}{\text{m}^3}$ .

The finite element (FE) model is configured with a fixed support at the base, indicating that there is no displacement or rotation at the foundation. This model comprises 254 nodes, 274 line elements, and 48 plane elements.

Given the geometry, sectional properties, material properties, and boundary conditions, the developed model computes the mass matrix and the stiffness matrix associated with the structure. After performing modal analysis, obtaining the first  $N$  eigenvalues (i.e., natural frequencies) and eigenvectors (i.e., mode shapes) is possible. The results are summarized in Table 3.6 and mode shapes given in Figure 3.5

Table 3.6: Mode shape properties.

Mode	Frequency (Hz)	Participation Mass	Percent Mass (%)	Cumulated Percent (%)	Mode Mass (%)	Type
1	2.34771	29033.3	7.1348	13.3151		Global
2	3.17819	34297.7	8.42852	21.7437		Global
3	4.95205	25872.5	6.35805	28.1017		Global
7	10.4271	56961.4	13.998	42.9009		Global
9	16.3133	21160.6	5.20011	50.4906		Global
10	19.5858	31203.1	7.66802	58.1586		Global
12	24.1946	58464.1	14.3673	73.8636		Global
16	32.3737	26862.4	6.60131	83.0533		Global
23	40.782	45637.2	11.2151	97.4655		Global

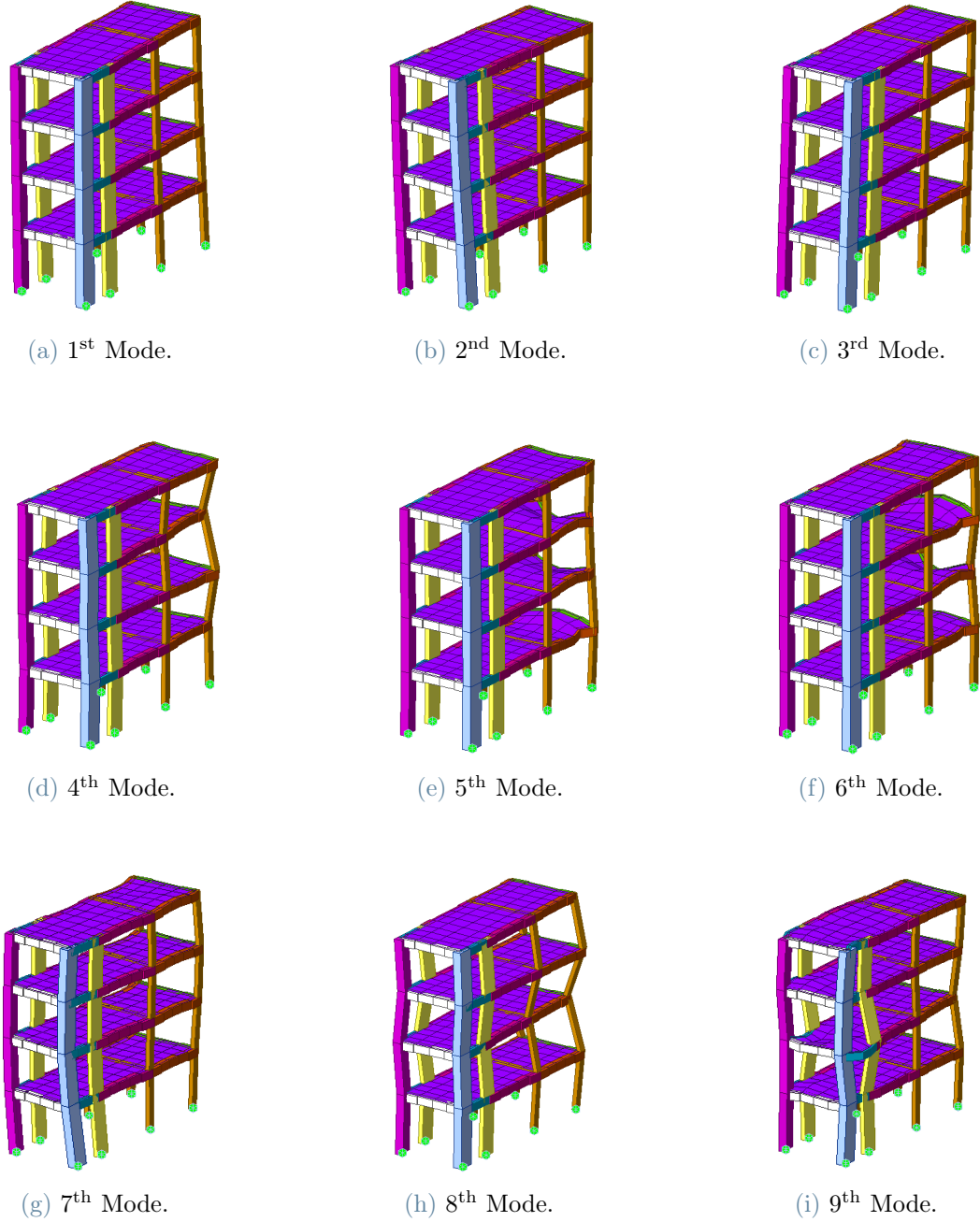


Figure 3.5: Global mode shapes of testing structure.

### 3.3. Algorithm for Model Updating by DR Method

The algorithm we use for the model updating is shown in Algorithm 3.1.

---

**Algorithm 3.1** Model updating of FE model using Douglas-Reid method

---

- 1: Compute the natural frequencies of the numerical model, denoted as  $f_i^{\text{FEM}}$ , as given by:

$$f_i^{\text{FEM}} = f_i^{\text{FEM}}(x_1, x_2, \dots, x_N) \quad (3.3)$$

where  $N$  is the total number of updating parameters  $x_k$ .

- 2: Approximate the natural frequencies using the Douglas-Reid method, denoted as  $f_i^{\text{DR}}$ , which can be expressed as:

$$f_i^{\text{DR}} = C_i + \sum_{k=1}^N (A_{i,k}x_k + B_{i,k}x_k^2) \quad (3.4)$$

where  $C_i$ ,  $A_{i,k}$ , and  $B_{i,k}$  are the coefficients to be determined.

- 3: Define the upper and lower normalized limits for the updating parameters as:

$$\frac{x_k^L}{x_k^B} \leq \frac{x_k^B}{x_k^B} \leq \frac{x_k^U}{x_k^B} \quad (3.5)$$

- 4: Equate the approximated natural frequencies  $f_i^{\text{DR}}$  with the FEM frequencies  $f_i^{\text{FEM}}$  for different sets of parameters, resulting in the system of equations:

$$f_i^{\text{DR}}(x_1^B, \dots, x_k^B, \dots, x_N^B) = f_i^{\text{FEM}}(x_1^B, \dots, x_k^B, \dots, x_N^B) \quad (3.6)$$

for  $i = 1, 2, \dots, M$ .

- 5: Compute the unknown coefficients  $A_i$ ,  $B_i$ , and  $C_i$  using the matrix form:

---


$$\{f_i^{\text{FEM}}\} = [C]\{K_i\} \quad (3.7)$$


---

---

Algorithm 3.1 Model updating of FE model using Douglas-Reid method (continued)

where the matrix  $[C]$  and vector  $\{K_i\}$  are defined as:

$$[C] = \begin{bmatrix} 1 & x_1^B & (x_1^B)^2 & \dots & x_N^B & (x_N^B)^2 \\ 1 & x_1^U & (x_1^U)^2 & \dots & x_N^B & (x_N^B)^2 \\ 1 & x_1^L & (x_1^L)^2 & \dots & x_N^B & (x_N^B)^2 \\ \vdots & \vdots & \vdots & \ddots & \vdots & \vdots \\ 1 & x_1^B & (x_1^B)^2 & \dots & x_N^U & (x_N^U)^2 \\ 1 & x_1^B & (x_1^B)^2 & \dots & x_N^L & (x_N^L)^2 \end{bmatrix} \quad (3.8)$$

and

$$\{K_i\} = \begin{bmatrix} C_i \\ A_{i,1} \\ B_{i,1} \\ \vdots \\ A_{i,N} \\ B_{i,N} \end{bmatrix} \quad (3.9)$$

The unknown coefficients can then be found by:

$$\{K_i\} = [C]^{-1}\{f_i^{\text{FEM}}\} \quad (3.10)$$

Compare the approximated natural frequencies  $f_i^{\text{DR}}$  with the experimental frequencies  $f_i^{\text{exp}}$ . Minimize the objective function to match the experimental and numerical frequencies using:

$$J'_f = \frac{100}{M} \sum_{i=1}^M \left| \left( \frac{f_i^{\text{FEM}} - f_i^{\text{exp}}}{f_i^{\text{exp}}} \right) \right| \quad (3.11)$$

or

$$J''_f = \frac{100}{M} \sum_{i=1}^M \left| \left( \frac{f_i^{\text{FEM}} - f_i^{\text{exp}}}{f_i^{\text{exp}}} \right) \right| \cdot \text{PMR}_i \quad (3.12)$$

where  $\text{PMR}_i$  is the participating mass ratio of the  $i$ -th mode.

---

In this example, we focus on two fundamental mechanical properties of the L-shaped wall, as it exhibits the highest sensitivity compared to other updating parameters. These properties are the Young's modulus ( $E_c$ ) and the bending stiffness of the member ( $EI_b$ ).

### 3.3.1. Young's modulus of L-shaped wall ( $E_c$ ) as MU parameter

For the model updating, we consider our first updating parameter as Young's modulus of L-shaped wall ( $E_c$ ), so first, we will define its upper and lower limit as shown in Table 3.7.

Table 3.7: The first updating parameter is  $E_c$ .

Updating Parameter Limit	Values	Unit	Normalized Value
Upper Limit	35000	MPa	1.296296296
Nominal Limit	27000	MPa	1
Lower Limit	13000	MPa	0.481481481

## Results

- Variation of the natural frequencies computed by the DR method concerning Young's modulus of the L-shaped wall ( $E_c$ ) as shown in Figure 3.6.

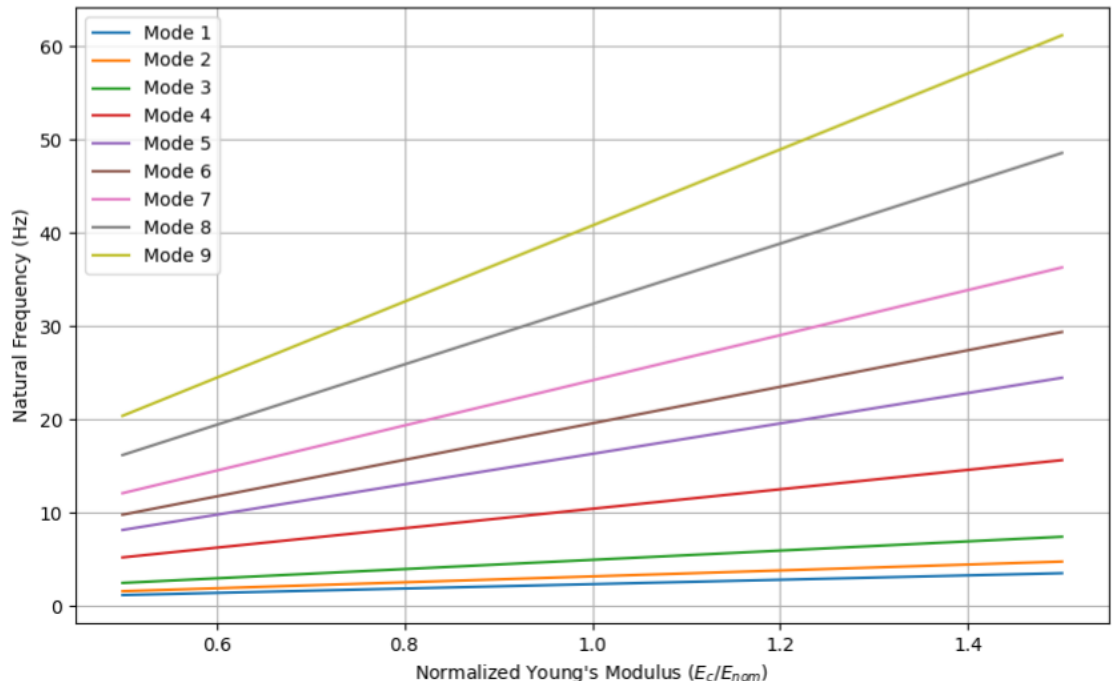


Figure 3.6: Predicted natural frequencies for ( $E_c$ ).

- We will plot our objective function with the PMR and consider the value that has the minimum error that is at the value of 0.63 of ( $E_c$ ) as shown in Figure 3.7.

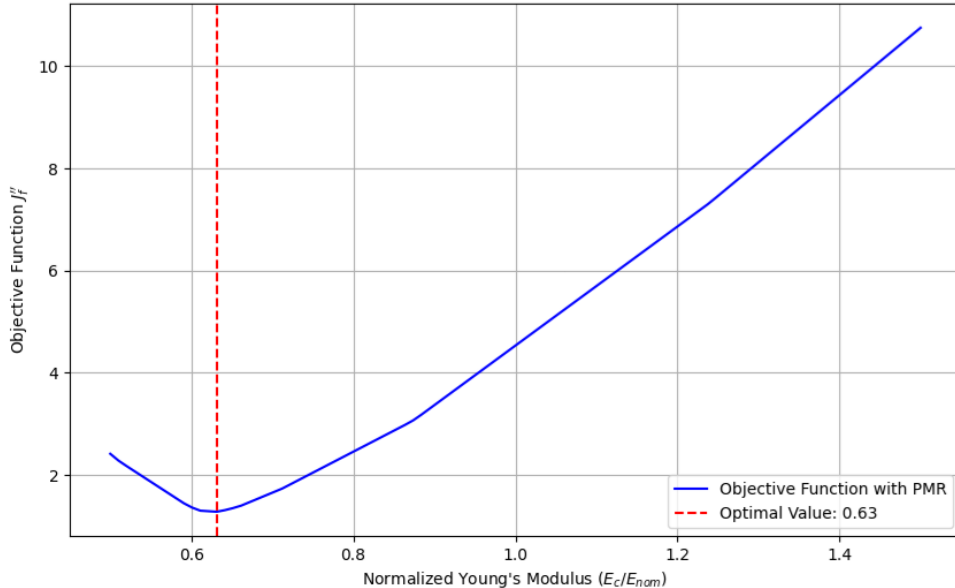


Figure 3.7: Minimization of objective function for ( $E_c$ ).

- Comparison between the predicted and optimal value natural frequencies with the experimental results (cfr. section 3.1.3) as shown in Figure 3.8.

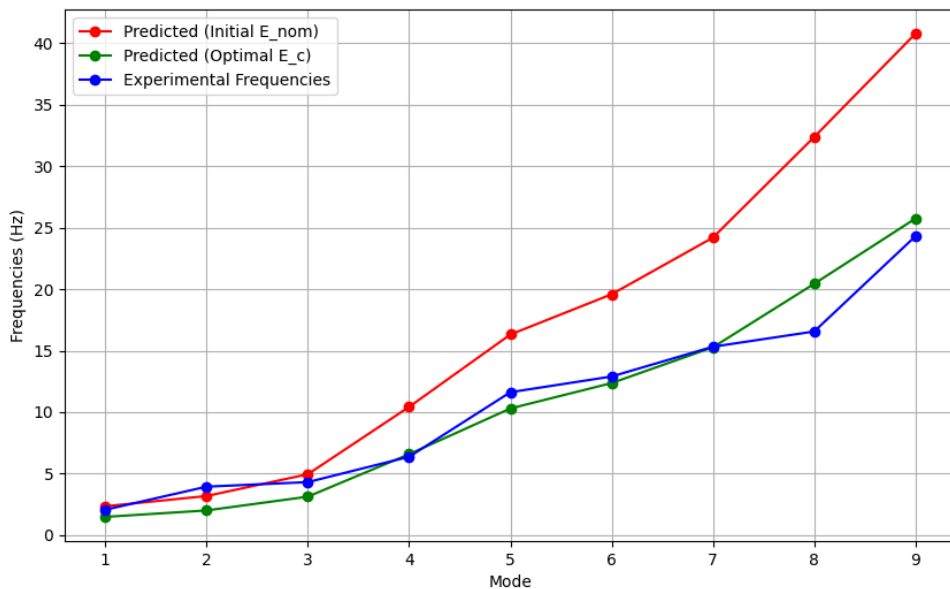


Figure 3.8: Comparison between the predicted and optimal natural frequencies with the experimental results for ( $E_c$ ).

- Absolute error between the nominal value of Young's modulus  $E_{nom}$  and optimal value of Young's modulus  $E_{opt}$  as shown in Figure 3.9.

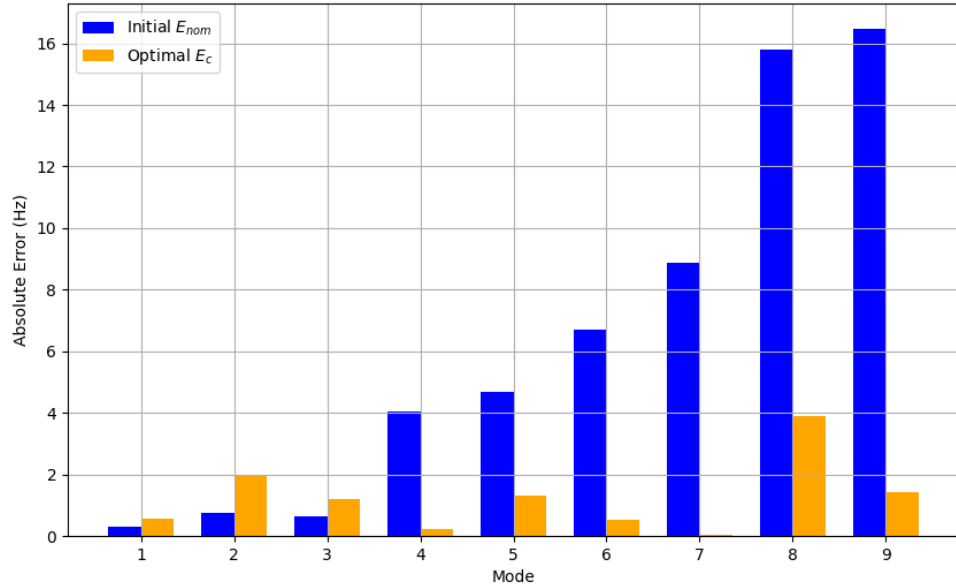


Figure 3.9: Absolute error between the  $E_{nom}$  and  $E_{opt}$ .

### 3.3.2. Bending stiffness of L-shaped wall ( $EI_b$ ) as MU parameter

For the model updating, we will consider our second updating parameter as the bending stiffness of an L-shaped wall ( $EI_b$ ), so first, we will define its upper and lower limit as shown in Table 3.8.

Table 3.8: The second updating parameter is  $EI_b$ .

Updating Parameter Limit	Values	Unit	Normalized Value
Upper Limit	150	%	1.5
Nominal Limit	100	%	1
Lower Limit	50	%	0.5

## Results

- Variation of the natural frequencies computed by the DR method about the bending stiffness of the members ( $EI_b$ ) as shown in Figure 3.10.

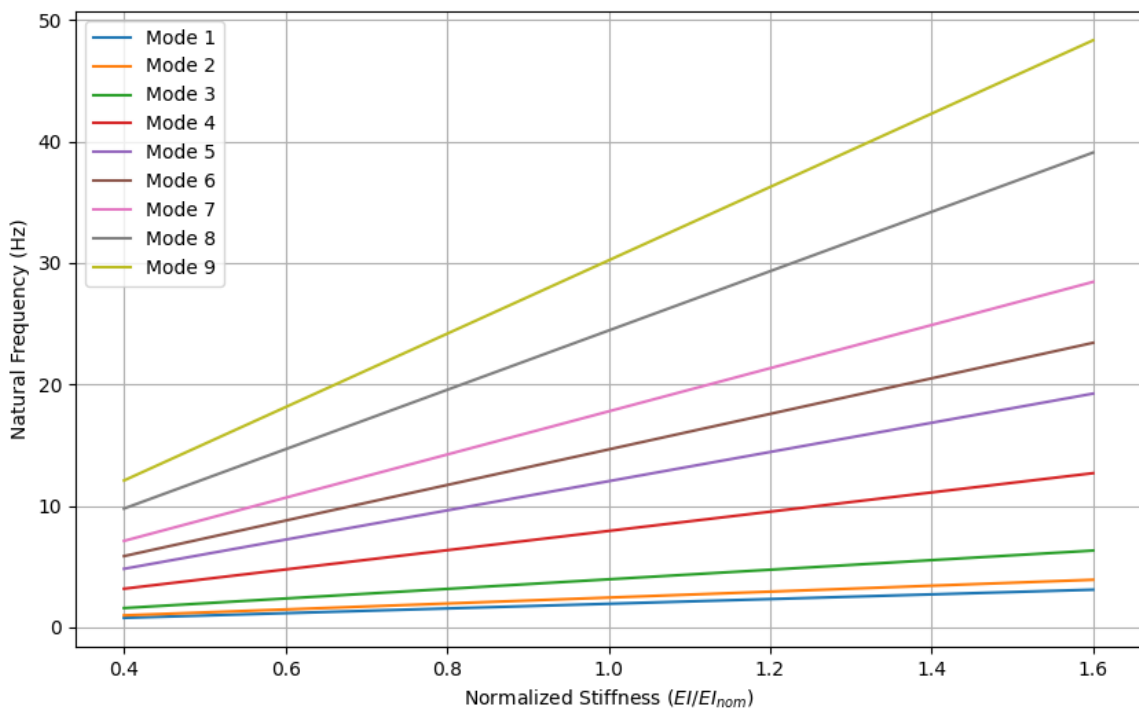


Figure 3.10: Predicted natural frequencies for ( $EI_b$ ).

- We will plot our objective function with the PMR and consider the value that has the minimum error that is at the value of 0.86 of ( $EI_b$ ) as shown in Figure 3.11.

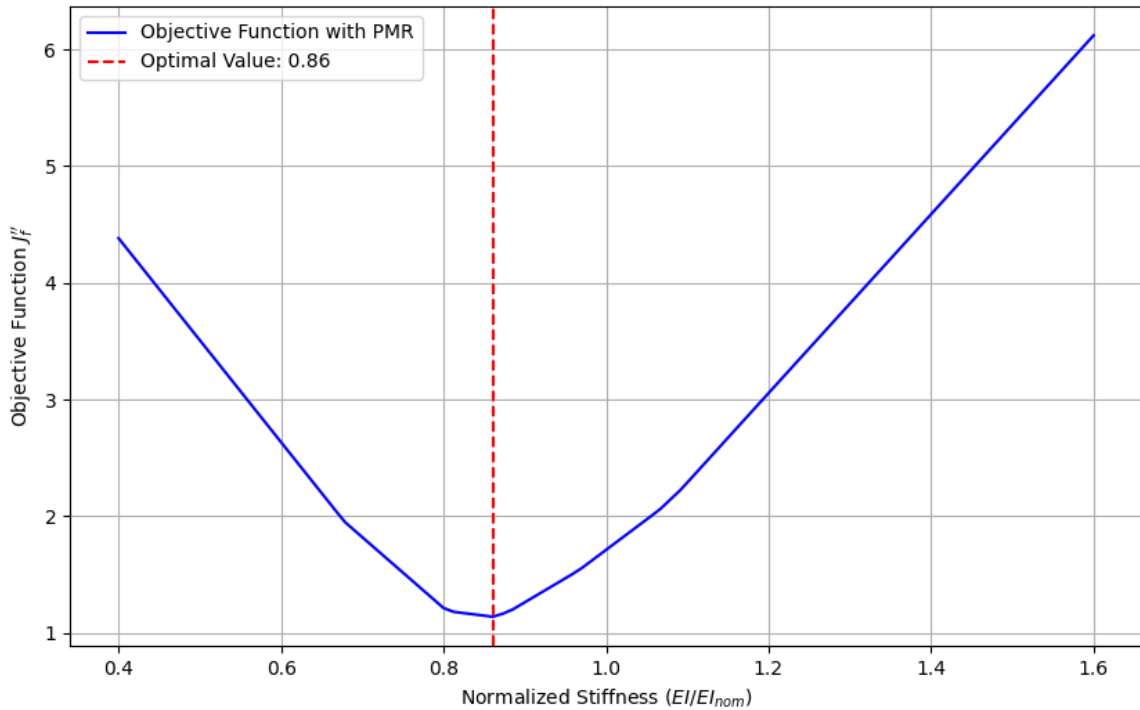


Figure 3.11: Minimization of objective function for  $(EI_b)$ .

- Comparison between the predicted and optimal value natural frequencies with the experimental results (cfr. Section 3.1.3) as shown in Figure 3.12.

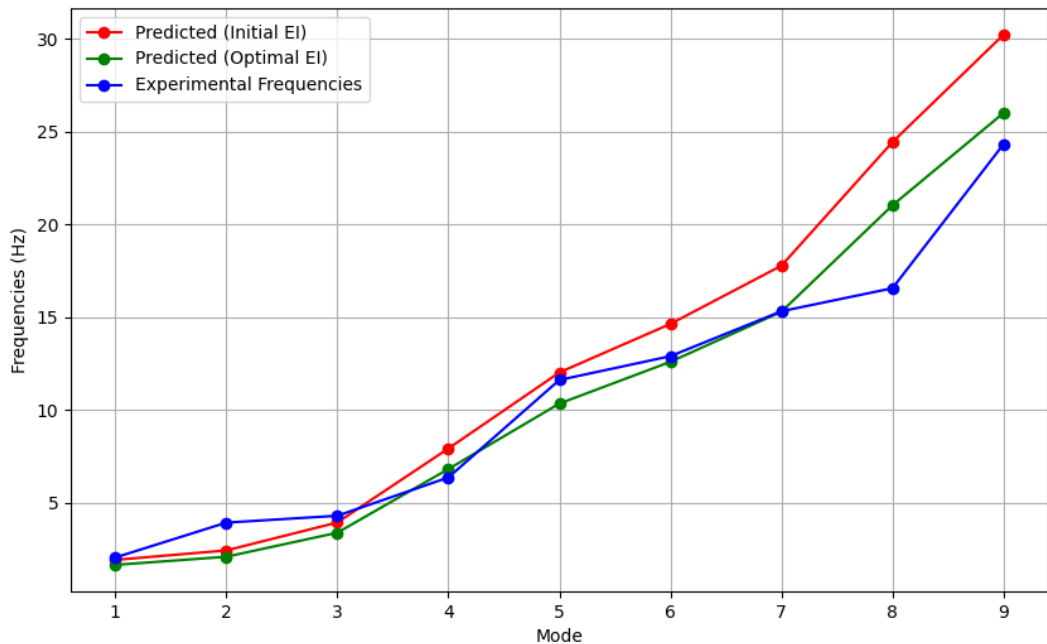


Figure 3.12: Comparison between the predicted and optimal natural frequencies with the experimental results for  $(EI_b)$ .

### 3| Validation of DR Method for FEMU for Test Structure

- Absolute error between the nominal value of bending stiffness  $EI_{nom}$  and the optimal value of bending stiffness  $EI_{opt}$  as shown in Figure 3.13.

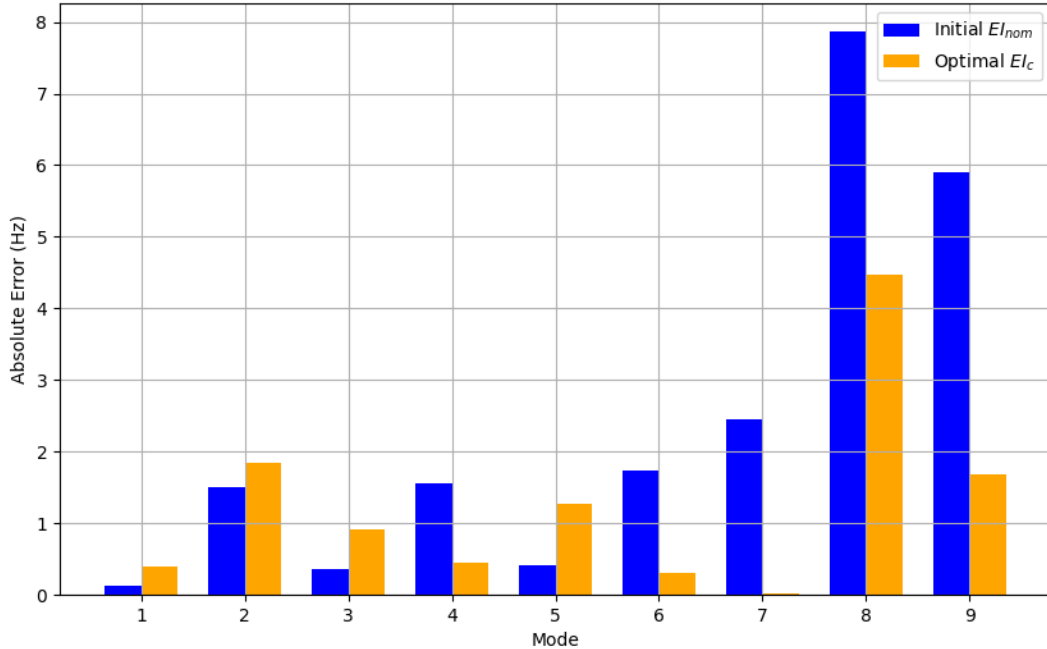


Figure 3.13: Absolute error between the  $EI_{nom}$  and  $EI_{opt}$ .

## Comments

- As our experimental frequencies are lower than the natural frequencies computed from the numerical model, our model is stiffer than the actual structure. To bring the model's frequencies closer to the experimental values, we should decrease the bending stiffness and Young's modulus of the sections in our model. This is because a reduction in stiffness typically results in a decrease in the natural frequencies of a structure, allowing it to approach the lower frequencies observed experimentally. By iteratively adjusting (decreasing) the bending stiffness and Young's modulus, we can bring the numerical model's response closer to the experimental results.
- By comparing both results, it is evident that using Young's modulus of the L-shaped wall ( $E_c$ ) as the updating parameter yields much better results compared to using the bending stiffness of the members ( $EI_b$ ). This is because when  $E_c$  is used as the updating parameter, we obtain better results for higher modes, with a smaller absolute error between the experimental and optimal natural frequencies. In this analysis, only two updating parameters are considered and updated individually, keeping the second parameter constant. However, multiple updating parameters will be considered and updated simultaneously in future developments.
- Applying this DR method of updating the model in the testing structure ensures that the validation of this method can be used correctly to update the numerical model, so after that, we will apply this method to our case study structure, which is a steel truss tower at EC JRC ISPRA.



# 4 | Conceptualizing the Real-World Structure and Numerical Simulation

## 4.1. Insights into Real-World Structure

In Chapter 3, we see the application of the model updating by the DR method using the test structure. Now, we implement all these strategies on a real-world case study problem, which is the 100m tall steel structure *Atmospheric Tower* at EC JRC Ispra. Where the ongoing research on Smart Cities and infrastructure developed different test cases and applications, including Structural Health Monitoring (SHM) system. The E.3 unit – *Safety and Security of Buildings* is responsible for selecting different structures to conduct the research activities for the *Smart Cities* project. The Atmospheric Tower is one of the research project case studies.

The reason for calling it the *Atmospheric Tower* is that it measures the different atmospheric components like wind direction speed, humidity effect, and temperature variation. For this purpose, the tower is equipped with different atmospheric sensors and anemometers. In addition, the tower is also equipped with autonomous sensors, which continuously record the data and transfer it to the smart cities platform. The orientation of the tower is shown in Figure 4.1.

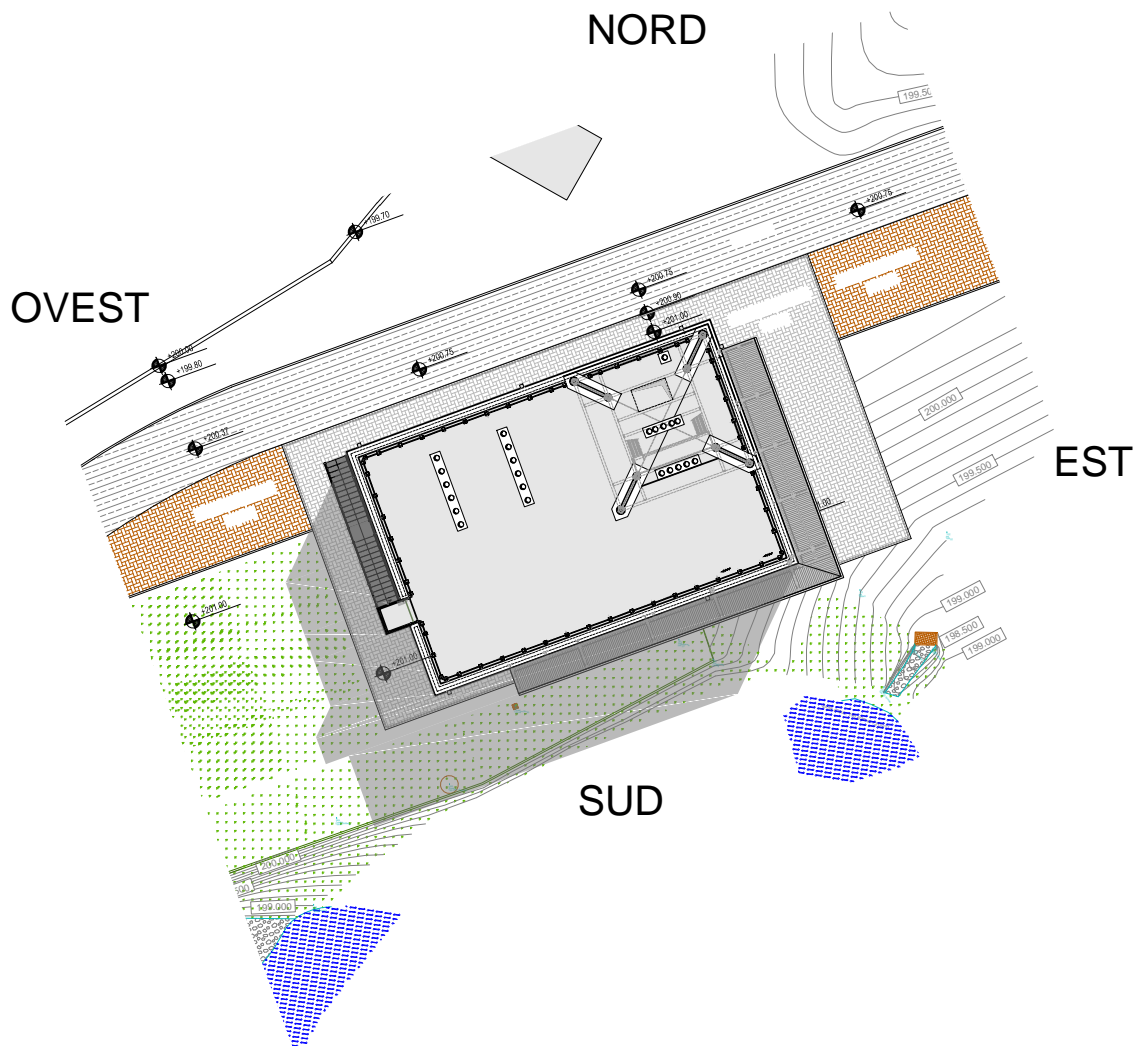


Figure 4.1: Orientation of the tower according to the cardinal directions.

The wireless sensors are placed on the tower at different elevations to measure the acceleration in all three axes correctly. Initially, the three sensors were placed at elevations of 60m, 80m, and 100m; now, recently additional sensors has been installed to better understand the structure's dynamic behaviour. In the actual configuration, two wireless sensors are placed at 100m elevation. one wireless sensor with a base station is placed at 80m elevation; one wireless sensor is placed at 40m elevation, and at last, one base station at the 20m elevation as shown in Table 4.1.

Table 4.1: Sensor information for dynamic behaviour analysis.

Sensor ID	Sensor Type	Elevation	Remarks
1	Wireless Sensor	100m	Dynamic acceleration measurements
2	Wireless Sensor	100m	Dynamic acceleration measurements
3	Wireless Sensor	80m	Base Station with wireless sensor
4	Wireless Sensor	40m	Dynamic acceleration measurements
5	Base Station	20m	Base station for wireless sensors

Therefore, this structure is a good case study for understanding actual structure dynamic behaviour and implementing some of the methods discussed in Chapter 2 regarding the SHM and trying to meet our ultimate goal of developing the digital twin.

Hence, we will get the sensor's data that we placed at different tower elevations. From there, we will compute the real-time dynamic behaviour of the structure by using the OMA techniques which we discuss in section 2.8.

## 4.2. Tower Geometry

The JRC *Atmospheric Tower* is a steel truss structure that is 100 m tall, but the tower is 95 m tall. The base building underneath the tower is 5 m tall, and it is a reinforced concrete structure that supports the whole tower.

Now, see that the tower is supported by four core vertical columns that go from the tower's base up to the top. These four columns are arranged in such a way that they create a square of 4.75 m × 4.75 m as shown in Figure 4.2. These four columns are made up of steel hollow circular sections  $RO\ 244.5 \times 20$ , which goes from the base of the tower up to the 71 m elevation and from there to the top of the tower,  $RO\ 193.7 \times 12.5$  sections are used for internal four core columns. The intermediate height of each floor is 5 m except for the first and the last floor. To connect columns between the intermediate floors, 12 bolts  $M\ 24 \times 85$  are used for the section  $RO\ 244.5 \times 20$ , and  $M\ 18 \times 60$  for the section  $RO\ 193.7 \times 12.5$ .

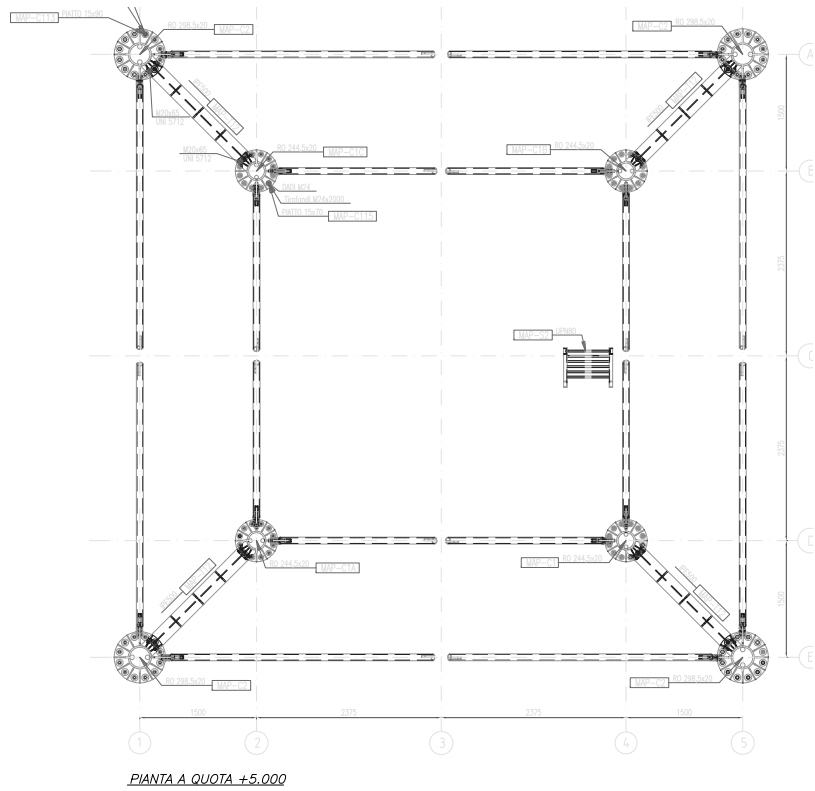


Figure 4.2: Plan view at the elevation of 5 m.,

Besides these four core columns, the tower also has four external columns arranged to create a square of larger dimensions  $7.75 \text{ m} \times 7.75 \text{ m}$ . Hollow steel sections are used for these columns, with a dimension of  $RO\ 298.5 \times 20$ , and connected using  $M20 \times 70$  bolts. These four outer columns go vertically straight up to the elevation of 25 m. Afterward, the section is inclined inward with an angle of  $3.43^\circ$ . A different steel hollow section is used for this inclined portion, denoted as  $RO\ 244.5 \times 20$ , and  $M\ 24 \times 85$  bolts are used for these connections.

As these four outer columns are inclined inward, they meet with the inner columns at the elevation of 50 m. The elevation view of the tower is shown in Figure 4.3.

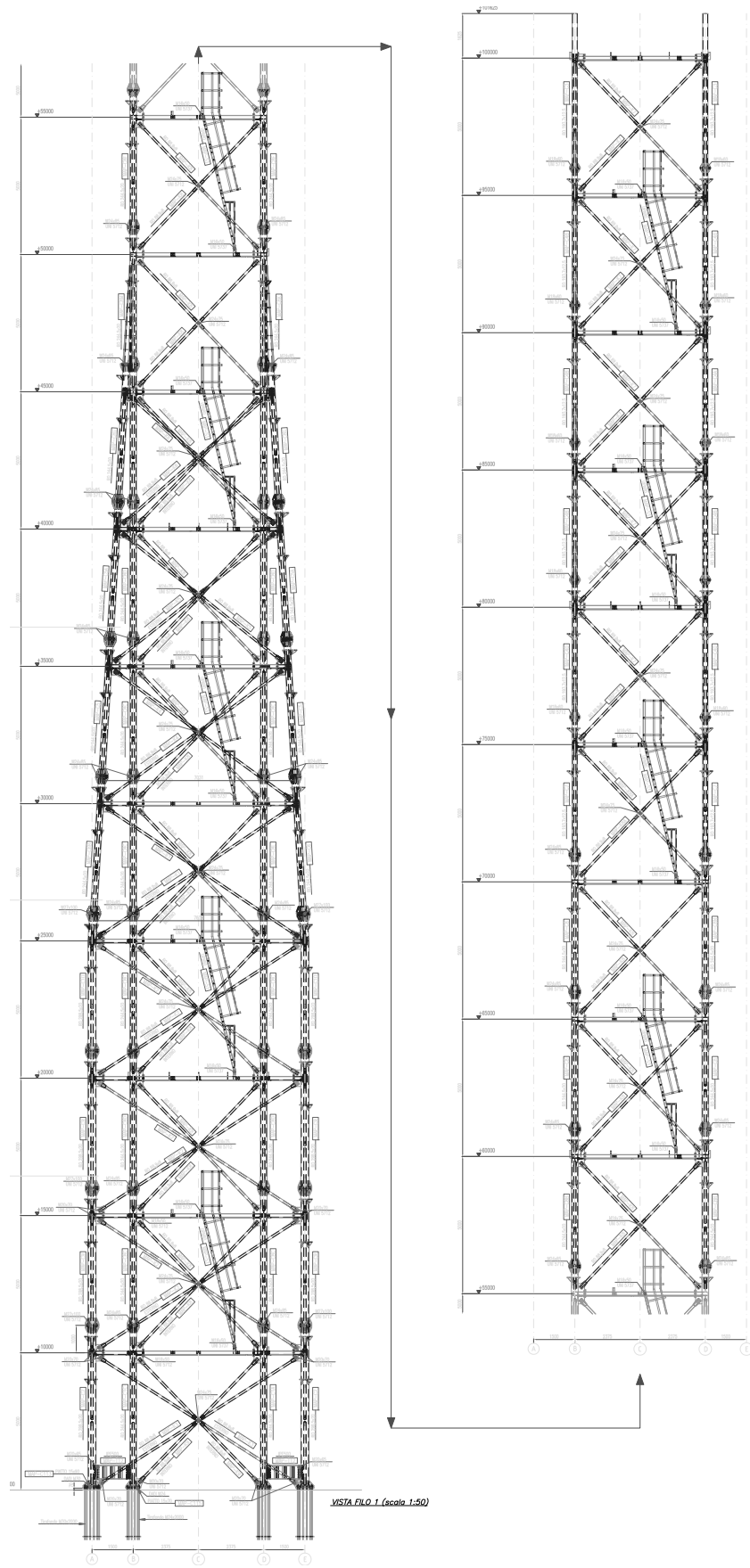


Figure 4.3: Elevation view of the whole tower.

The four internal columns and outer column ends are connected by vertical bracing, as shown in Figure 4.3. This bracing is also a hollow steel section, denoted as  $RO\ 88.9 \times 8$ , and they are connected by using  $M\ 16 \times 50$  bolts at their ends. These bolts are bolted to fin plates welded to the columns.

The floors are formed by the gridwork of the *HEA140* steel section. There are different gridworks of beams for the relative elevations, and a grid of steel beams connects the outer columns with the inner columns up to the elevation of 45 m. After that, the outer columns connect with the internal columns. To connect all this gridwork of beams,  $M\ 12 \times 50$  bolts are used, and for connecting the beams with the columns,  $M\ 18 \times 50$  bolts are used, as shown in Figure 4.4.

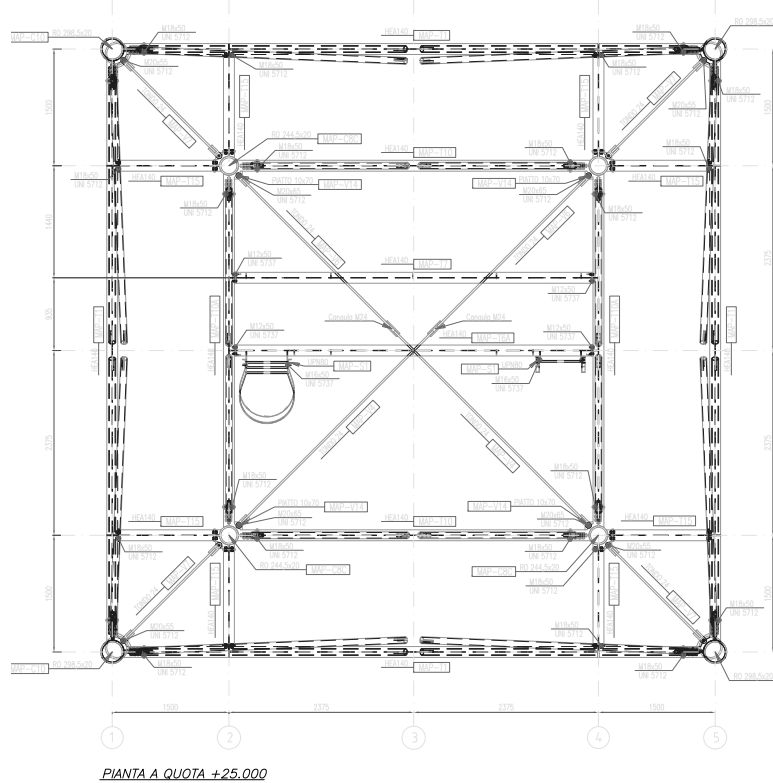
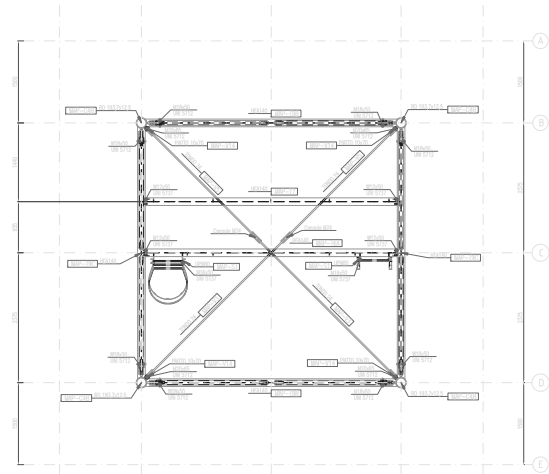
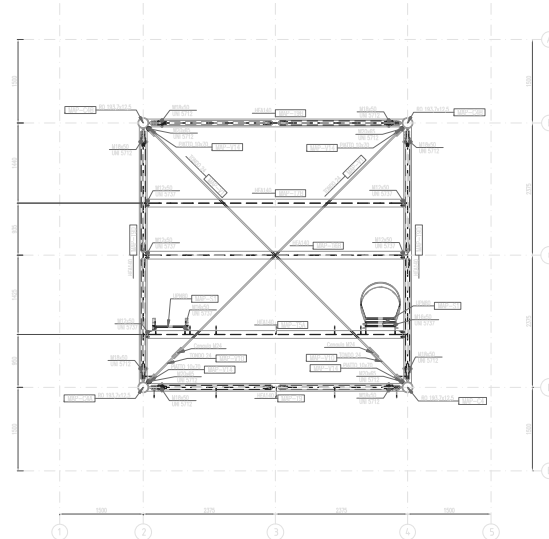


Figure 4.4: Plan view of the gridwork of beams at the elevation of 25 m.

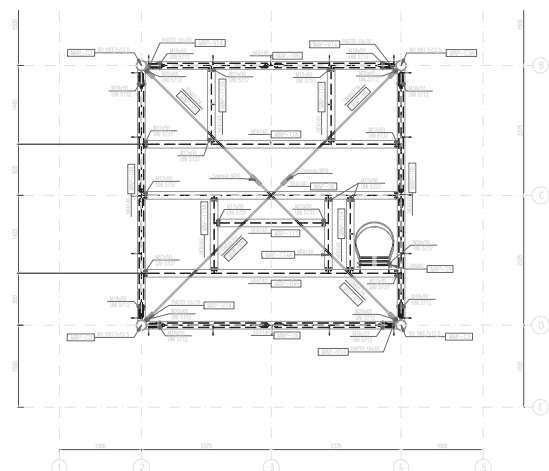
The tower has an intermediate floor at every 5 m height, and three different floor types are used. The difference lies in the grid-work of beams, and their specific elevations are also shown in Figure 4.5. The floor comprises steel modular grilled plates, which are supported by the grid-work of beams with a width of 25 cm or 30 cm.



(a) 15 m, 25 m, 35 m, 45 m, 55 m, 65 m, 75 m, 85 m and 95 m.



(b) 10 m, 30 m, 50 m, 70 m and 90 m.



(c) 20 m, 40 m, 60 m, 80 m and 100 m.

Figure 4.5: Floor plans of all the levels of the tower.

In addition to that, horizontal trusses are provided on each floor in a diagonal direction using steel rods with a diameter of 24 mm. The stairs are made of steel sections denoted as *UPN 80*, and they are provided in an inclined direction with transverse bars that act as steps. For connecting the stairs, *M 16×50* bolts are used, along with fin plates welded to the floor beams.

The parapets are made up of steel frames consisting of plates  $8 \times 70$ , which are used for the vertical walls, while for the horizontal walls, plates of  $6 \times 70$  are used. In addition, the handrail is formed using a steel section of  $42.2 \times 2$ , placed at a height of 80 cm from the floors.

For stiffening the base of the tower, all the inner columns at the base are connected to the outer columns using an *IPE500* beam, which is welded to the web and flanges. The flanges are 40 cm apart from each other. To connect these components, two bolts are provided on each side using *M 20×65* bolts, as shown in Figure 4.6.

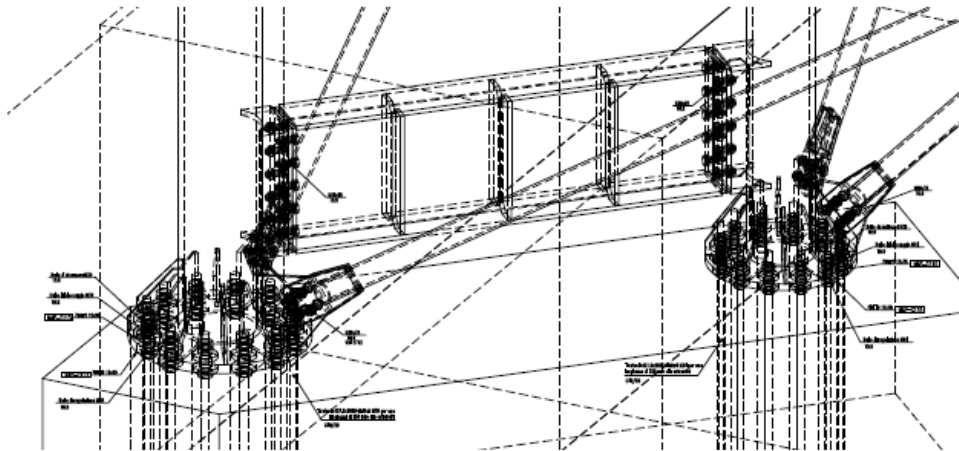


Figure 4.6: Detail view of the *IPE500* beam connecting two corresponding columns.

The tower has an elevator that can raise goods of no more than 1000 kg. The area of the platform of the elevator is about  $1.2 \text{ m} \times 1.2 \text{ m}$  and is raised to about 2 m. The weight of the cabin, the base, and the engine are 650 kg. The mast of this particular elevator is composed of a modular trussed column, and each module is around one and a half meters tall. These modules are triangular and made of two square and circular tubes. A gearing mechanism, allowing the elevator to ride along the mast, is incorporated into the side of one of the square tubes.

The mast is framed to the building on each floor using a tubular member *RO 48 × 3*, which is orthogonally fixed to the *HEA140* beams at the end of each joint. These beams

form the floor grid and are interconnected with bolted plates.

With the aid of a special device, a horizontal tube is connected to the round element of the mast of the elevator. The beam grid is connected to the main structure and the mast at multiple locations. Figure 4.7 shows the elevator and the mast with its configuration to the beam grid.

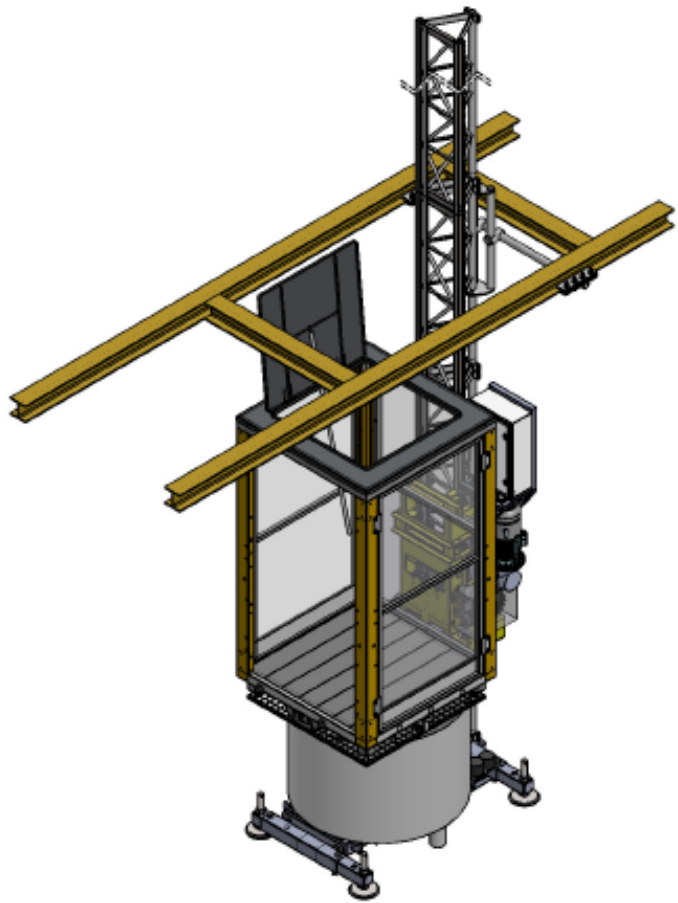


Figure 4.7: Detail view of elevator mast.

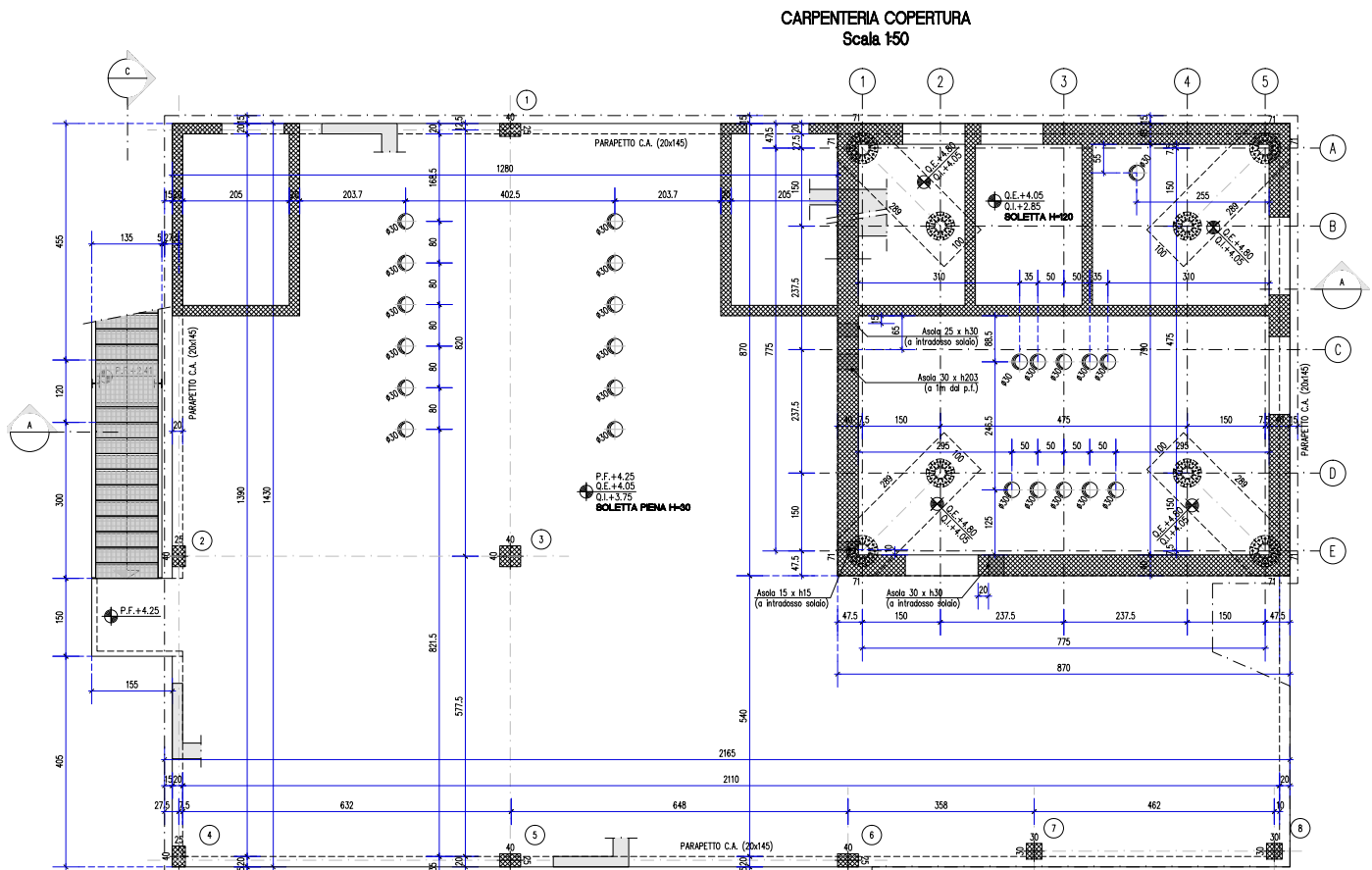
### 4.3. Base Building

The structure beneath the tower is made of reinforced concrete. The area not directly under the tower has a 30 cm thick reinforced concrete slab supported by eight columns of three different section types ( $25mm \times 40mm$ ,  $30mm \times 30mm$ , and  $40mm \times 40mm$ ), along with several reinforced concrete walls, each 20 cm thick, as shown in Figure 4.8.

Underneath the structure, there is a substantial 1.2 m thick reinforced concrete plate, surrounded by perimeter walls that are 40 cm thick, as well as other internal partition

walls, which are also 20 cm thick. The thin and thick plates are reinforced with top and bottom layers arranged in an orthogonal pattern, with additional reinforcements at the intersections of columns and walls. The thick plate has extra diagonal bars that converge at the midpoints of the sides of the plate's perimeter, forming embedded diagonal beams. Figure 4.9 shows an example of the upper reinforcement layout along the y-axis, including the diagonal bars.

The tower is secured to the base structure using long bolts embedded in prismatic concrete shoes, which support the tower. Each concrete shoe has two sets of 12 anchorage bolts arranged in a circular pattern, embedded in the concrete shoes and the underlying 1.2 m thick plate. The bolts for the inner columns are M24,  $21.9 \times 2000$ , with a  $20 \times 545$  bottom anchorage disc also embedded in the concrete. For the outer columns, M30,  $27.6 \times 2000$  bolts are used, along with a  $20 \times 659$  bottom anchorage disc as shown in Figure 4.10. All bolts are securely fastened to the concrete.



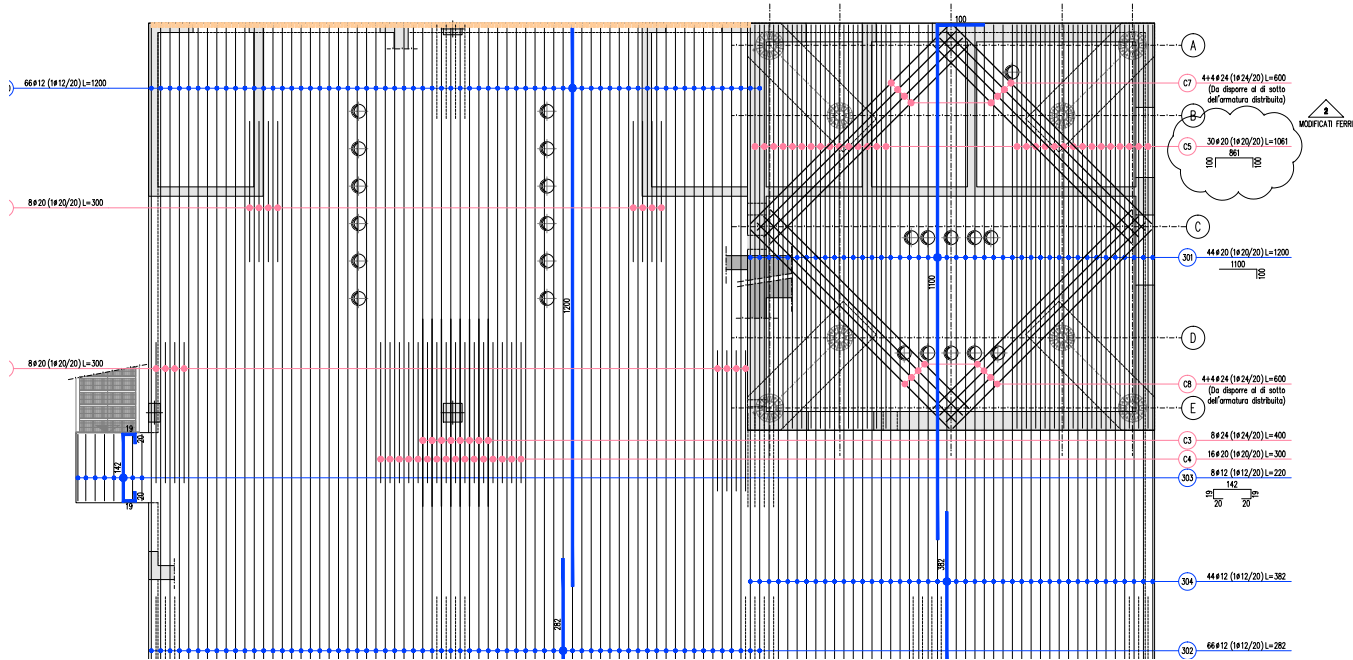


Figure 4.9: Detail plan view of reinforcement at the roof of the base building.

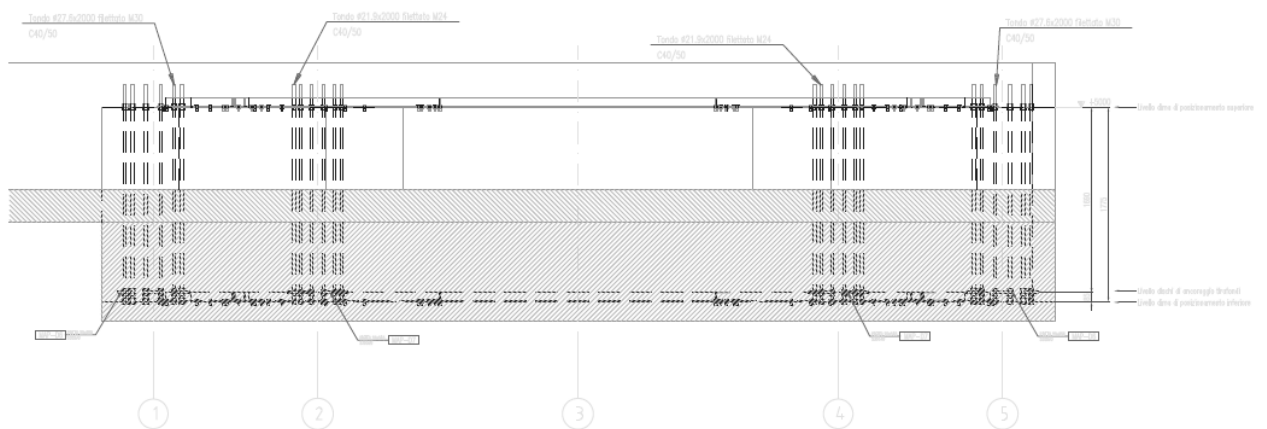


Figure 4.10: Sectional view of the arrangement of anchorage bolts within the concrete shoes.

The matching end plates are welded to the base of each column. The concrete shoes are supported at the corners of the 1.2 m thick plate, which is further reinforced by the walls below and the embedded beams within the plate. These shoes extend 75 cm above the top surface of the roof plate. However, their visible height is about 30 cm since the plate acts as a roof and has been covered with additional non-structural layers, including waterproofing and protective coverings.

The entire structure is built on a foundation plate supported by 91 deep piles, each measuring 60 cm in diameter and 16.5 m in height. The foundation plate features a central square section that measures  $22.0 \times 22.0$  m and has a total depth of  $180 + 20$  cm, centered on the concrete core that supports the tower. Next is a shallow rectangular section measuring  $5.2 \times 16.3$  m, with a depth of  $50 + 20$  cm. These two sections are connected by an intermediate rectangular segment measuring  $1.3 \times 16.3$  m, which varies in thickness from  $50 + 20$  cm to  $180 + 20$  cm. This layout is depicted in the elevation view of the base structure shown in Figure 4.11.

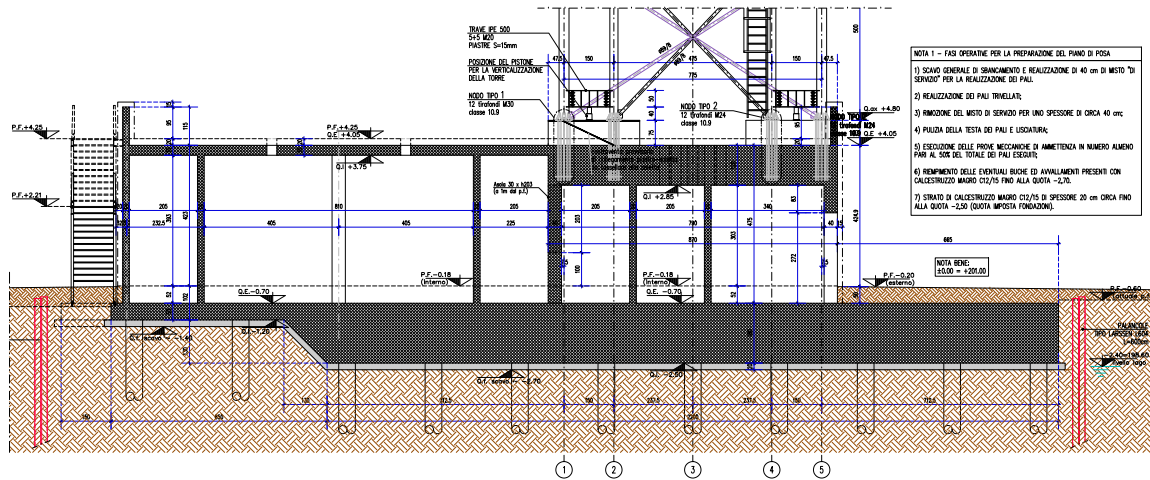


Figure 4.11: Sectional view of the base building.

The tower is built from galvanized steel, which is coated with zinc according to the UNI EN ISO 1462 standard and is made of S275JR steel. The bolts used are classified as grade 8.8, while the corresponding nuts and washers are grade 8 SB and 8.8, respectively, in line with the EN 15048 standard.

The foundation is made up of two layers of concrete: the first layer is 20 cm thick and consists of C40/50 concrete, while the second layer is a reinforced concrete layer made of C32/40 concrete. The deep piles are constructed using C25/30 concrete.

Moreover, C32/40 concrete is also utilized for other reinforced concrete elements, including columns, partition walls, and roof plates. The reinforcement steel employed is B450C.

#### 4.4. Sensors Monitoring for Ambient Vibration Test

The ambient vibration test is a well-established dynamic output-only method for determining a structure's dynamic properties. In this study, we used triaxial accelerometers

with time synchronization precision of  $\pm 32\mu s$ . Initially, three fixed measurement locations were selected at heights of 60 m, 80 m, and 100 m. The data acquisition was carried out using *LORD Microstrain G-Link-200 OEM* sensors, which were housed in an engineered house equipped with an external antenna and a solar panel. This setup enabled the sensors to operate autonomously. The arrangement of the sensors is illustrated in Figure 4.12.

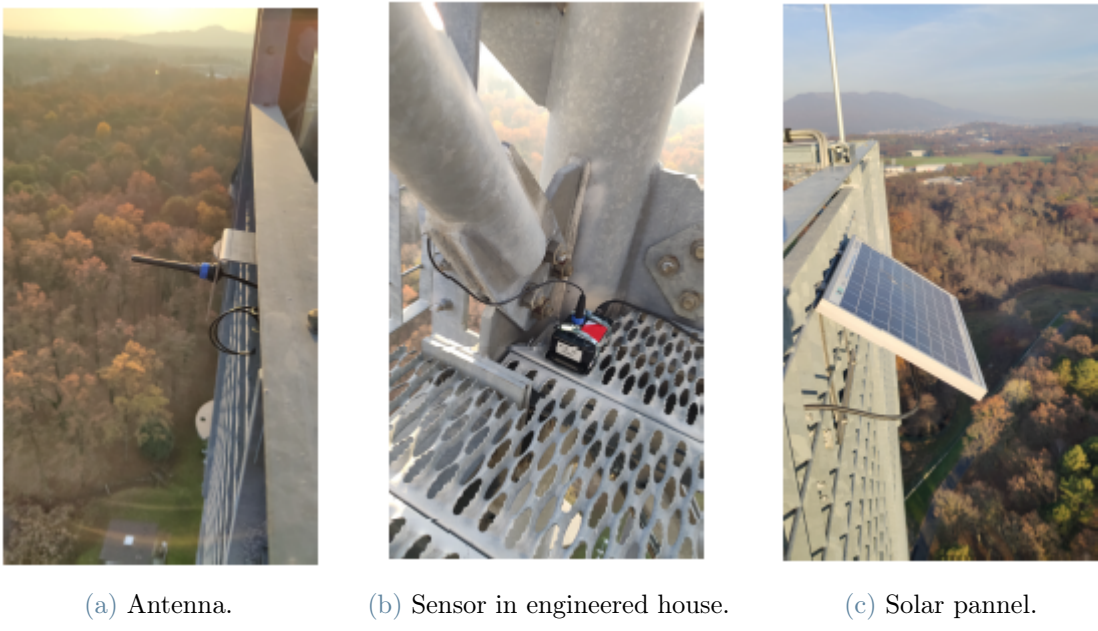


Figure 4.12: Floor plans of all the levels of the tower.

The base station uses the *LXRS* protocol, which works at 2.4 GHz so that our base station will communicate with the sensors wireless. The communication is bidirectional, ensuring the correct data is assembled without any loss from the transmission and retrieving ends. In addition, the untransmitted data will remain in the sensors with the temporary memory of the sensor and be retransmitted back with the correct timestamp.

The receiving base station *LORD Microstarin WSDA-200* is connected to the Ethernet by which all this sensor data will be imported in the *JRC Smart City Platform*.

An accelerometer measures proper acceleration, which is distinct from coordinate acceleration. Proper acceleration is the acceleration experienced by an object relative to its instantaneous rest frame (typically an inertial frame), whereas coordinate acceleration depends on the observer's chosen coordinate system. For example, an accelerometer at rest on the Earth's surface registers an upward proper acceleration of 1 g due to the support force counteracting gravity, even though its coordinate acceleration is zero. Conversely,

during free fall, the accelerometer reads 0 g because the object is in inertial motion, and no proper acceleration is experienced.

The sensors installed on the tower are aligned with their reference frames as shown in Figure 4.13. Importantly, the z-axis points downward, and the accelerations measured along this axis are roughly -1 g, consistent with a vertical downward acceleration of 1 g.

To calculate instantaneous accelerations, it is necessary to process the recorded signals. This involves eliminating constant or low-frequency components from the gravitational acceleration vector. Specifically, apart from the z-axis accelerations (which have an offset of about 1 g), the x and y directions may also exhibit low-frequency noise due to sensor misalignment or tower tilting throughout the day. These issues lead to non-zero projections of the gravitational acceleration vector along these axes.

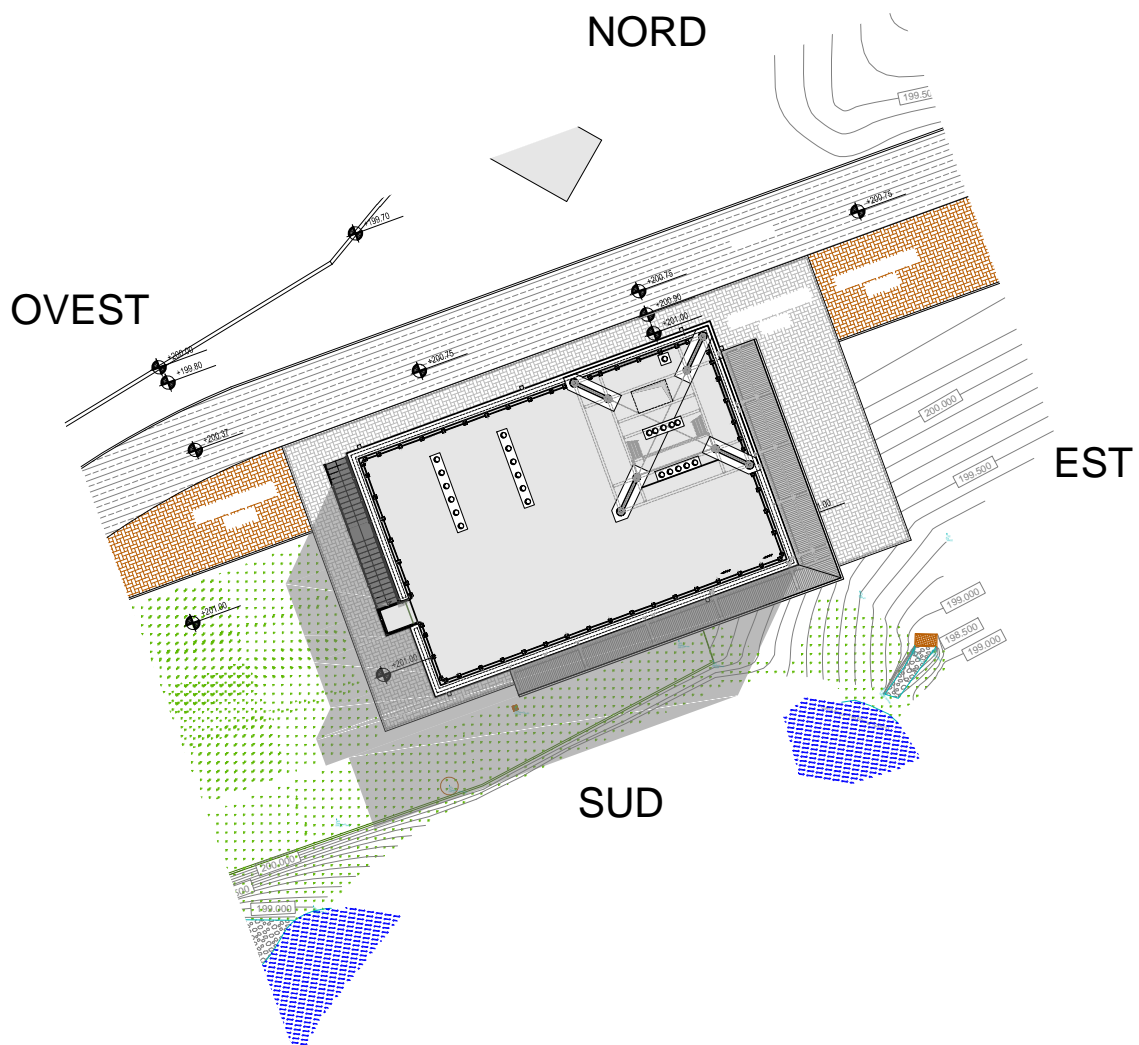


Figure 4.13: Reference frame for sensors along the tower.

## 4.5. Tower Dynamics Assessment during the Delivery Phase

In December 2014, during the delivery phase of the structure, a dynamic characterization test was conducted, and the results are summarized in Table 4.2. This test was conducted by an external company, and at that time, the elevator wasn't present, so the computed model properties are a bit different from the actual dynamic properties now, so we performed the OMA test to compute the dynamic properties of the tower correctly.

The reference frame for the test is depicted in Figure 4.14. A total of 24 mono-directional wired accelerometers were installed, 12 along the X-axis and 12 along the Y-axis. Precisely, two accelerometers were positioned in each horizontal direction across six floors: 5 m, 20 m, 40 m, 60 m, 80 m, and 100 m.

Moreover, an anemometer was installed at the top of the tower to monitor ambient wind excitation, concentrating on both wind direction and intensity.

The acceleration data were analyzed using software that employed the PolyMAX method, a frequency-domain Operational Modal Analysis (OMA) technique based on an extended version of the *Least Squares* algorithm. Additionally, the CFM effectively addressed closely spaced modes [73].

Vibration recordings lasted almost seven days, but only the time histories related to the most consistent excitation periods were examined. OMA techniques assume that the input excitation behaves like white noise.

The sampling frequency was set at 100 Hz, and the measurement system featured an anti-aliasing filter with a cutoff frequency of 20 Hz. Discrete Fourier Transform (DFT) were performed over intervals of 81.92 seconds, resulting in a frequency resolution of 0.012 Hz.

The Modal Assurance Criterion (MAC) index was calculated to confirm the extracted parameters for all possible pairs of mode shape vectors. Ideally, two different mode shapes should have a MAC index of 0, which indicates linear independence, while the MAC index for a mode shape compared to itself should be 1. The Modal Phase Collinearity (MPC) index and the Mean Phase Deviation (MPD) were also computed.

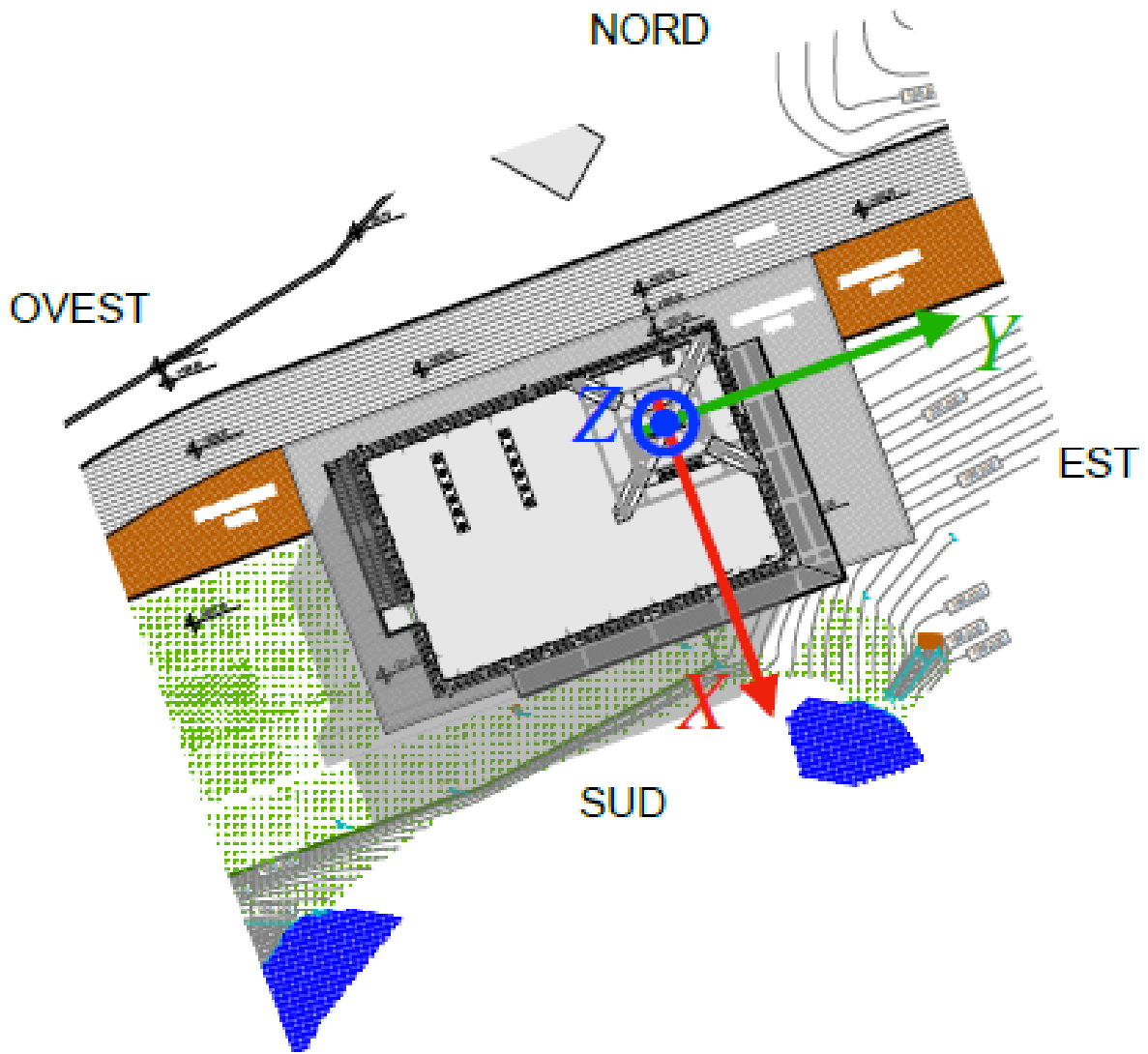


Figure 4.14: Reference frame for dynamics assessment during the delivery phase.

All the computed indices were in agreement, which confirms the reliability of the chosen modes.

Additionally, as the structure ages and its connections gradually loosen, the frequencies measured today may have shifted, particularly toward lower values. This change contrasts the frequencies recorded during the initial dynamic characterization of the tower.

Table 4.2: Dynamic analysis results during the delivery phase.

Mode	Natural Frequency [Hz]	Damping Ratio [%]	Deformed Shape
1	0.83	0.81	X (no sign inversion)
2	0.84	0.79	Y (no sign inversion)
3	2.71	0.28	X (1 sign inversion)
4	2.72	0.26	Y (1 sign inversion)
5	3.15	0.18	T (no sign inversion)
6	5.11	0.22	T (2 sign inversions)
7	6.56	0.31	T (1 sign inversion)
8	11.62	0.49	T (2 sign inversions)
9	15.22	0.12	T (3 sign inversion)

## 4.6. Finite Element Modeling of Tower

For the numerical modelling of the Atmospheric Tower, we used the MIDAS GEN software [57], initially the FE model of the tower structure was modeled in the CEA's *CAST3M* [22] software, in which we wrote the code for the geometrical modelling and analysis of the structure. The programming language used in this is *Gibiane*. For the development detail of the tower in CASTEM software, refer to this thesis [13].

For the geometrical modelling of the tower, which is made of steel truss members, each is a linear finite element, and their connection will be perfectly clamped. As we see previously in section 4.2, we were using the five different geometrical sections for the tower whose sectional properties are given in Table 4.3. On floors with a grid of beams, we also have horizontal stiffeners underneath each floor, each member modeled as the axial member without any flexural stiffness, and the diameter of this bar is 24mm. Different floor grid beam plans are used alternatively on each floor. On top of it, we have the grilled plates, which are constrained by the beams. Here, we assume that this plate will add only the mass in the structure without adding any stiffness to the tower. We model this member as a plate element, and its thickness is identified as a total weight per unit area to the actual weight of the grilled plate by which the resulting thickness of the plate is 5mm.

Table 4.3: Section properties for structural analysis.

Section Type	$A$ [cm $^2$ ]	$I_y$ [cm $^4$ ]	$I_z$ [cm $^4$ ]	$I_t$ [cm $^4$ ]
HEA140	31.42	389.30	1033.00	8.03
RO 298.5 × 20	174.99	17052.95	17052.95	34105.89
RO 244.5 × 20	141.06	8957.20	8957.20	17914.39
RO 193.7 × 12.5	71.16	2934.31	2934.31	5868.62
RO 88.9 × 8	20.33	167.97	167.97	335.93

According to the specified geometrical details, the entire tower is modeled in MIDAS using a perfectly elastic and isotropic material (denoted as **ELASTIC ISOTROPIC**), with Young's modulus of  $E = 210$  GPa, a Poisson's ratio of  $\nu = 0.3$ , and a density of steel  $\rho = 7860$  kg/m $^3$ .

Nodes are added at the footholds on each corresponding floor to model the stairs. A thin plate element is then used to represent the flights of stairs. This element contributes only mass to the structure without adding stiffness, resulting in an effective stair ramp thickness of 7.2 mm, a stair model for a typical floor shown in Figure 4.15.

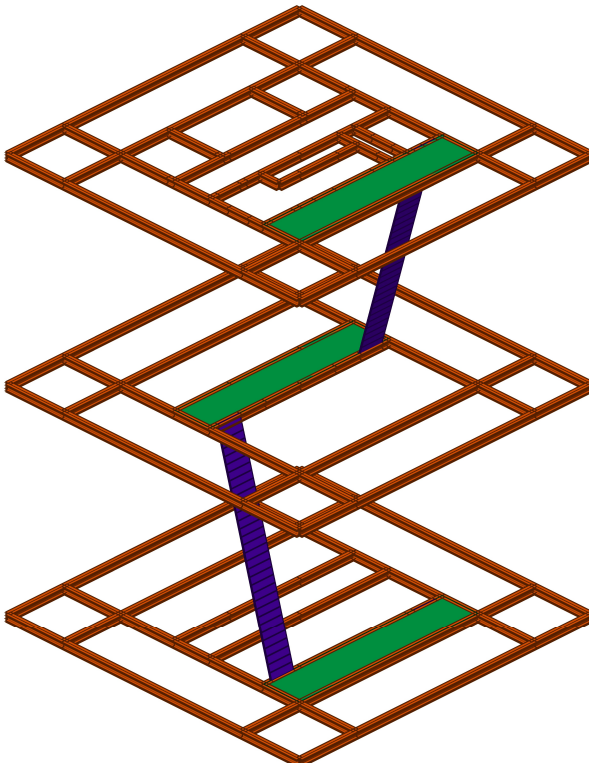


Figure 4.15: Stairs for typical floors in model.

A similar approach is taken for modeling the parapet wall by representing it as a thin plate element with defined support points, thereby avoiding adding extra vertical elements and maintaining proper constraints. This was achieved using the RIGID LINKS command, which was applied individually for each translation ( $UX$ ,  $UY$ ,  $UZ$ ) and rotation ( $RX$ ,  $RY$ ,  $RZ$ ) for every corresponding pair of points (i.e., each lower point is linked to its respective upper point). As in the previous model, the parapets are depicted as thin plates with a thickness of 5 mm, each supported by two pairs of points. This technique was selected because it enables the addition of parapets without introducing excessive spurious modes. The modelling of parapets is shown in Figure 4.16

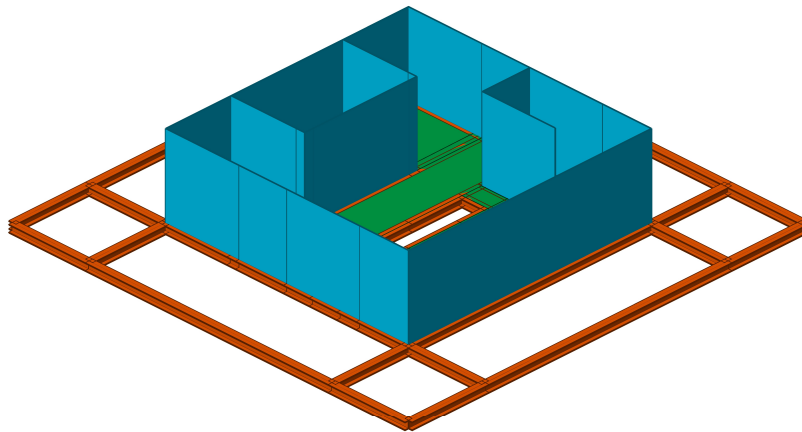


Figure 4.16: Parapets for floor at elevation 20m.

Since the elevator mast consists of many components, incorporating it directly into the primary model would have significantly increased its complexity by adding numerous degrees of freedom. To address this, the elevator mast was modeled separately to determine its equivalent sectional properties, which were then applied to a corresponding line element in the primary model. Two distinct models were developed: one using a truss-type arrangement for the elevator mast and the other employing a simplified uniform cantilever. The objective was to determine the sectional properties of the cantilever so that its behaviour matched that of the truss model. The sectional area was derived based on the weight, with modifications made to the section until the equivalent column's weight equaled that of the trussed columns.

In the same way, the flexural inertias ( $I_y$ ,  $I_z$ ) and the torsional inertia ( $I_x$ ) were calculated by comparing the displacements at the ends of both models when subjected to the same unit forces and torsional moments. Next, the elevator was represented as a lumped mass

of 650 kg and placed at a node on the equivalent column, with its location adjustable via a variable. Once the equivalent column was finalized, it was integrated into the model and secured at each tower floor using transverse tube members. These tube members were modeled as beam elements with sectional properties matching *RO* 48x3.

At this stage, the tower is modeled as firmly anchored to the ground, which means the fixed connection at the ground with no displacement and rotation. The resulting model, based on Figure 4.18 and utilizing a density of 1 m (meaning members are modeled with elements averaging 1 m in length), comprises 57819 nodes, 3463 line elements, and 55280 plane elements, and 278 point elements. The frame of reference adopted for this model and all future iterations is illustrated in Figure 4.17.

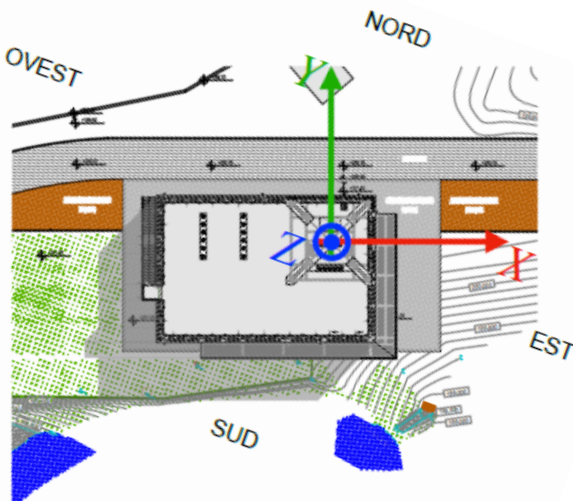


Figure 4.17: Reference frame adopted for the system.

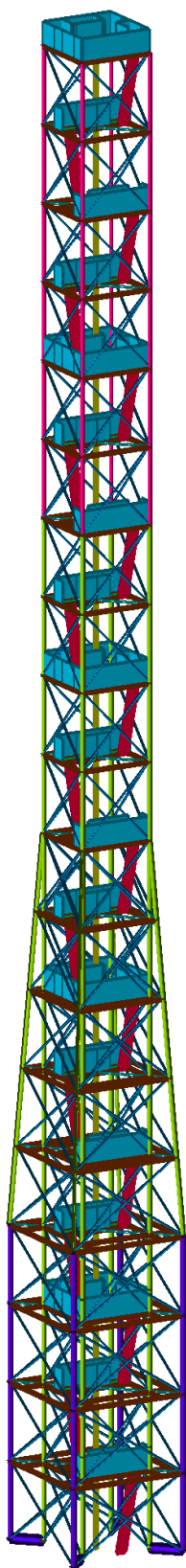


Figure 4.18: Numerical model of the tower.

Considering the geometry, sectional properties, material characteristics, and boundary conditions, the developed model calculates the mass and stiffness matrices of the structure. Subsequently, eigenvalue analysis is performed for  $N$  modes, allowing the determination of the first  $N$  eigenvalues (natural frequencies) and eigenvectors (mode shapes). The Lanczos algorithm, with reorthogonalization, is employed for this analysis, and the results are presented in Table 4.4.

Table 4.4: Natural frequencies of the numerical model of the tower.

Mode	Frequency [Hz]
1	0.70
2	0.71
3	2.77
4	2.80
5	3.53
6	3.59
7	3.62
8	3.68
9	5.86
10	5.92

## 4.7. Finite Element Modelling of Base Building

As outlined in section 4.3, the steel tower is anchored to four reinforced concrete support shoes that extend from the 1.2 m thick roof plate. The initial building modeling utilized 3D elements, mainly 4-node linear cuboid planar elements for all the walls, floors, and columns.

The model is organized into several layers, each corresponding to specific heights:

- **First layer:** 3.55 m high, from the ground to the base of the 1.2 m thick plate.
- **Second layer:** 0.9 m high, from the bottom of the 1.2 m thick plate to the base of the 0.3 m thick plate.
- **Third layer:** Equal to the thickness of the 0.3 m thin plate.
- **Fourth layer:** 0.75 m high, representing the thickness of the support shoes.

The intersection points of overlapping elements were meticulously projected to maintain proper alignment between adjacent elements in each layer. The roof plate, partition walls,

and concrete shoes were modeled considering the projections from all other components. This approach facilitated the development of uniform prismatic macro-elements with consistent geometry throughout their height, ensuring a smooth mesh for these elements.

In terms of materials, assuming the structure stays within the elastic range, uniform elastic homogeneous parameters were applied throughout the model. According to the available documentation, the concrete used in the construction is classified as C32/40, a concrete class defined in the Italian Building Code (NTC 2018) but not in Eurocode 2. Its Young's modulus is 33.3 GPa, with a Poisson's ratio of 0.2 and a specific weight of 25.0 kN/m<sup>3</sup>. For future studies, it might be beneficial to consider the aging of the concrete using the *Age-Adjusted Effective Modulus* and the effects of reinforcement. This could involve either adopting a homogenized modulus that considers both steel and concrete or employing methods to model the reinforcement explicitly.

A second approach was utilized to streamline the model, particularly for integration with the tower model, combining 1D, 2D, and 3D elements. The columns that support the thin roof were modeled using linear beam elements. The thin plate was represented using 4-node planar elements of the shear-plate type. It was placed at an elevation corresponding to the roof's top level. To more accurately reflect the actual geometry, a downward eccentricity equal to half the thickness of the plate was applied to the plate itself. The reinforced concrete walls that support the thick roof plate were modeled with 4-node plane quadrilateral elements of the thin plate with the shear type. Like the roof plate, these walls were positioned to align with the outer perimeter of the structure but were given an eccentricity equal to half their thickness.

The 1.2 m thick plate and the concrete shoes were primarily modelled using 4-node 3D linear cuboid elements, similar to the method used in the full 3D model. In this instance, the thick plate was represented by incorporating the element's projections above and below it. Since elements do not have rotational degrees of freedom at their nodes, ensuring rotational compatibility between the 1.2 m thick plates modelled in 3D and the 2D thin plates of the supporting walls was essential. To accomplish this, fictitious thin plates were introduced, extending from the upper edge of the walls to the top of the thick plate. This addition was vital for aligning the 2D elements with the 3D elements that make up the thick plate and ensuring perfect superposition.

The next step involved eliminating the nodes of the additional 2D elements by merging them with the nodes on the faces of the 3D elements. This ensured proper collaboration—applying this strategy to a simplified structure. In the model, fictitious elements were given null stiffness, effectively negating their influence. This allowed for independent

rotations between the 3D and 2D members. The fictitious plates were assigned the same stiffness as the actual members, facilitating the continuity of rotations at the interface between the 2D and 3D elements.

The resulting model of the base building incorporates this approach. It comprises 4,260 nodes, 80 line elements, 2050 3-node plane elements, 1290 4-node plane elements, 504 prismatic elements, and 1290 cuboid elements.

The model is shown in Figure 4.19, while its natural frequencies are listed in Table 4.5.

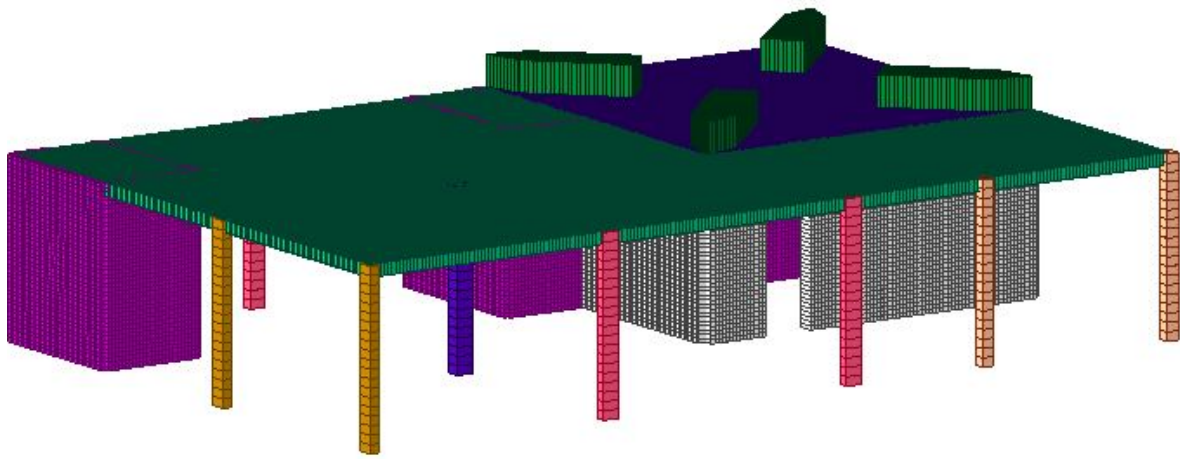


Figure 4.19: Numerical model of the base building.

Table 4.5: Natural frequencies of the numerical model of the base building.

<b>Mode</b>	<b>Frequency [Hz]</b>
1	12.89
2	14.90
3	17.38
4	22.32
5	23.28
6	25.14
7	28.53
8	28.39
9	28.87
10	29.12

## 4.8. Complete Finite Element Model of Structure

The two structures, the JRC Tower and the base building were combined once the two sub-models were finalized and tested to ensure they did not face any convergence issues. These two models were merged into a single file. In the complete model, the tower's base was not directly fixed to the ground but instead anchored to the concrete buildings. To accommodate this, a few additional features were added.

The IPE500 coupling beams, which connect the external and internal columns near the base refer to Figure 4.6, were modeled using beam elements with the appropriate sectional properties. The anchorage of the columns, which is done with long bolts embedded in the concrete refer Figure 4.10, was represented by extending the column elements into the concrete members by a suitable length. The mesh of the concrete members was designed to ensure proper compatibility between the components. Additionally, the beam-like reinforcement embedded within the thick plate referred to Figure 4.9 was modeled using upper and lower as bar elements, each with an area of  $4524 \text{ mm}^2$ . Like the thick concrete plate, its mesh was constructed to ensure compatibility with these additional elements.

The two geometries were merged into a single entity after making these adjustments and accurately translating the tower geometry onto the base building.

The model parameters were standardized, leading to the establishment of global entities. As anticipated, the boundary conditions initially set at the base of the tower were eliminated and exclusively assigned to the base of the concrete structure.

The final comprehensive model includes 4884 nodes, 3615 line elements, 552 3-node plane elements, 916 4-node plane elements, 336 prismatic elements, 540 cuboid elements, and 278 point elements.

For the detailed finite element model and the development of the digital twin in CASTEM software, refer to [13].

Figure 4.20 illustrates the model, while Table 4.6 provides a summary of the resulting natural frequencies, and the deformed configuration of the structure under gravity loading is shown in Figure 4.21

Table 4.6: Natural frequencies of the numerical model of the complete structure.

Mode	Frequency [Hz]
1	0.66
2	0.67
3	2.33
4	2.36
5	3.19
6	3.23
7	4.28
8	4.57
9	5.01
10	5.39

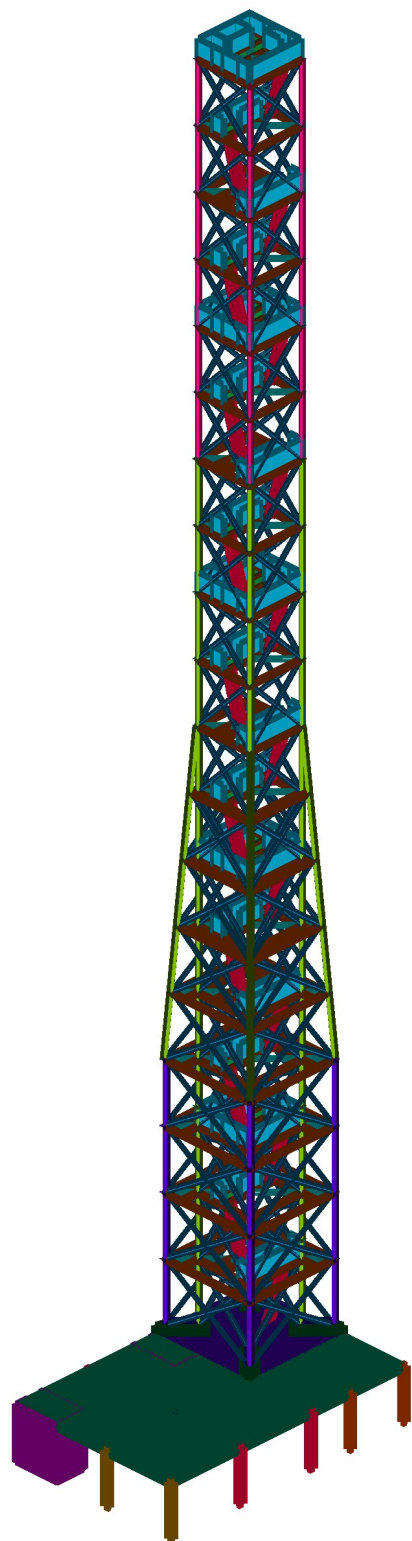


Figure 4.20: Numerical model of the complete structure.

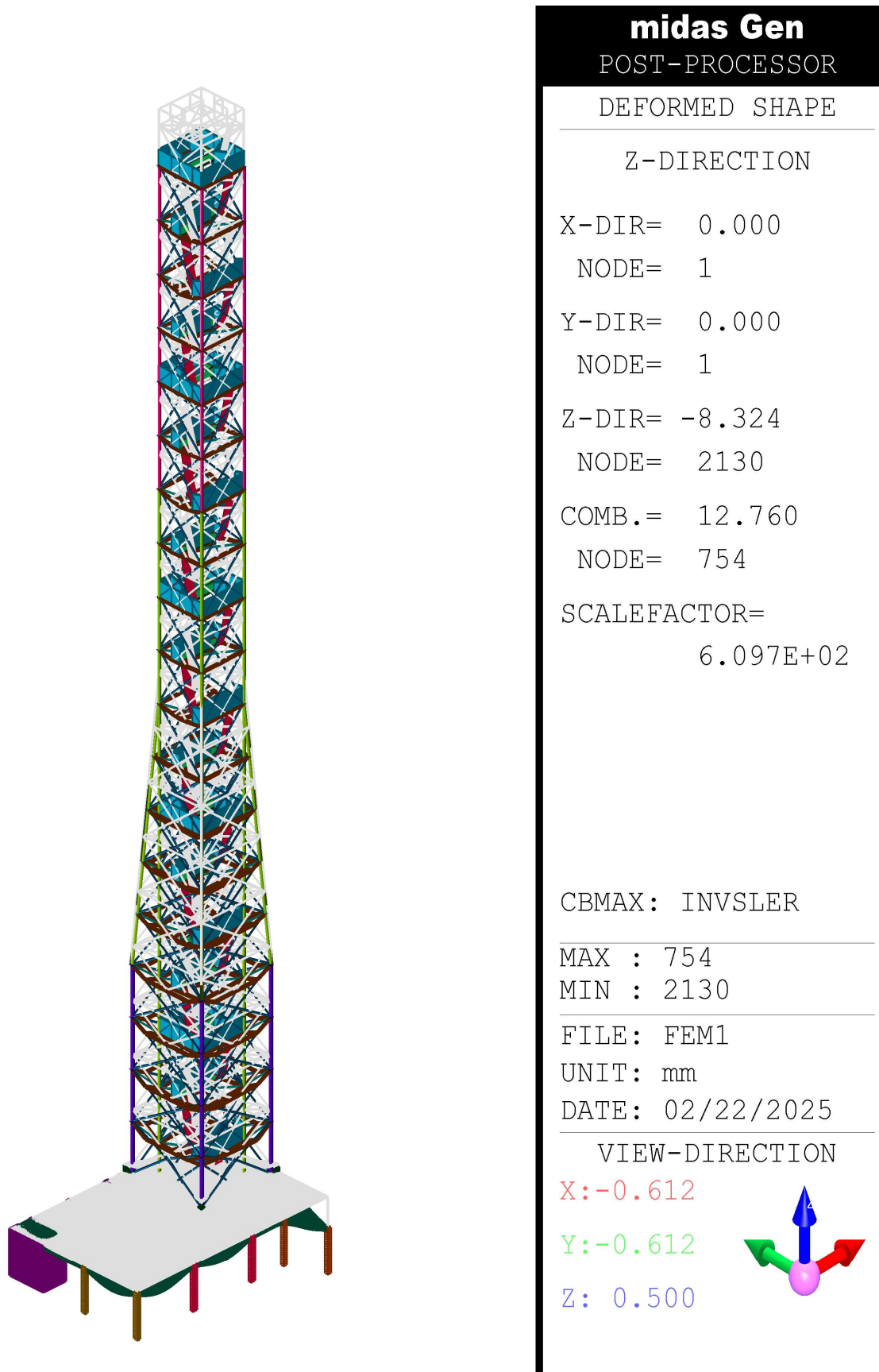


Figure 4.21: Deformed configuration of the structure under gravity loading.

## 4.9. Modal Analysis of Numerical Model of the Complete Structure

Modal analysis is a powerful tool for characterizing a structure's dynamic properties, based on the fact that a structure vibrates with a higher amplitude when it is excited at its resonant frequency. In our approach, the dynamic characteristics of the structure are computed after every iteration of the model updating process. These computed properties are then compared with both the experimental results and the dynamic behaviour observed at the delivery stage of the structure, thereby providing valuable insights into how closely the model represents the actual structural performance.

In this technique, the primary focus is on computing the eigenvalues and eigenvectors of the system. The eigenvalues correspond to the natural frequencies of the structure, which represent the frequencies at which the structure reaches dynamic equilibrium. The eigenvectors, on the other hand, indicate the mode shapes corresponding to each natural frequency, effectively describing the deformation pattern that the structure exhibits during vibration. For this analysis, we employ the MIDAS command to perform the eigenvalue analysis for a predetermined number of modes. This command utilizes the Lanczos algorithm with re-orthogonalization, an iterative method that ensures the accurate and orthogonal computation of the eigenvectors even for large systems.

The analysis produces a set of natural frequencies and mode shapes that include both global and local modes. Global modes are those that involve significant deformation of the entire structure, while local modes are associated with deformations confined to specific regions. To differentiate between these two, we compute the participation masses for each mode; modes with lower participation masses are identified as local. Our findings indicate that after the 7th mode, the majority of the modes exhibit lower participation masses and can therefore be classified as local. Interestingly, the next global mode emerges at the 28th mode, which is identified as a torsional mode characterized by a single sign inversion in its mode shape, as detailed in Table 4.7.

Table 4.7: Natural frequencies and modal participation factors of the numerical model of the complete structure.

Mode	Natural Frequency [Hz]	Mode Shape	Participating Mass (%)
1	0.66	$X$ (no sign inversion)	59.7
2	0.67	$Y$ (no sign inversion)	59.1
3	2.33	$X$ (1 sign inversion)	26.9
4	2.36	$Y$ (1 sign inversion)	26.4
5	3.19	$T$ (no sign inversion)	1.5
6	3.23	$X$ (2 sign inversions)	7.5
7	4.28	$Y$ (2 sign inversions)	7.1
28	5.39	$T$ (1 sign inversion)	42.4

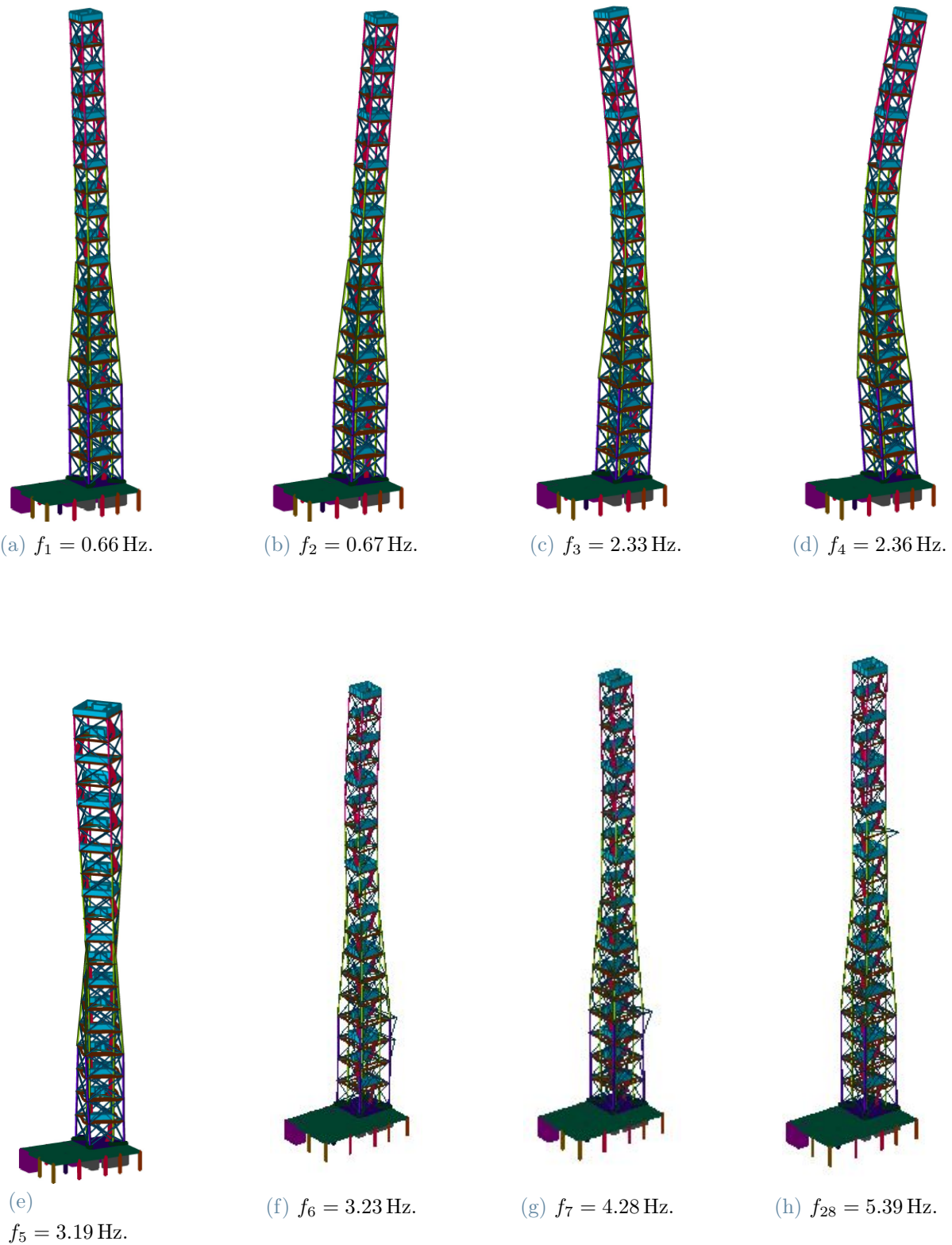


Figure 4.22: Global mode shapes of a complete structure under gravity.



# 5 | Ambient Vibration Testing

## 5.1. Processing of sensor data

### 5.1.1. Detrending

The first step in processing sensor data is to detrend the recorded signals. Sometimes, signals show an underlying spurious trend (due to the temperature effects that accelerometers exhibit, reproducing the titling) that must be removed before further analysis.

One reason for this issue is the sensor's zero-point error. This error arises from the difference between the sensor's actual value measured at rest and the theoretical value expected in that state. For example, this might lead to a measurement of about 1g along the vertical axis. At the same time, the other axes of the accelerometer could show non-zero values if the device is slightly tilted from the horizontal plane.

Removing these components from a signal over a specific duration is quite simple. This can be done by subtracting the average of all samples from each individual sampled value. Figure 5.1 shows how an example signal, recorded by one of the accelerometers on the tower, is recentered around 0g.

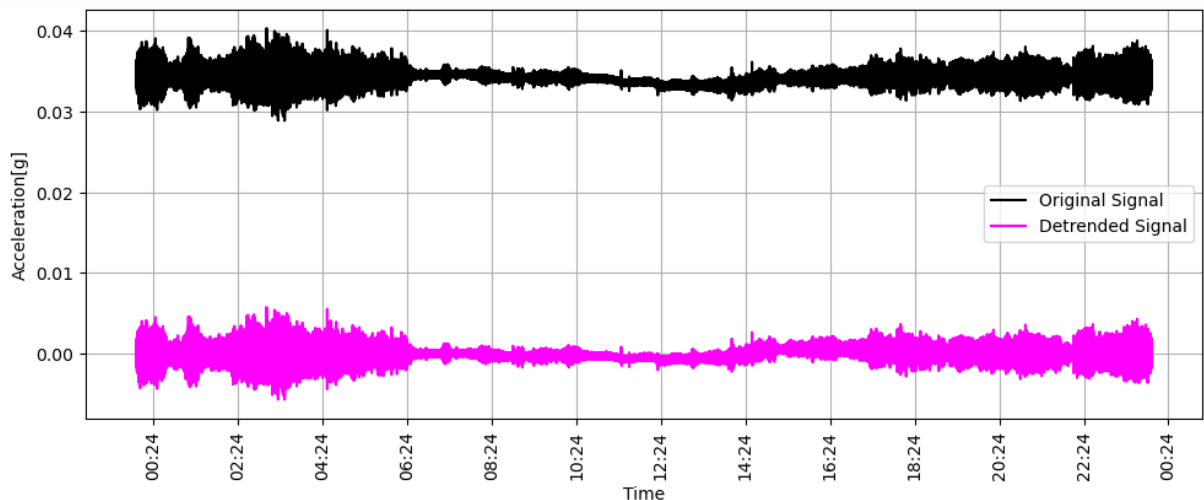
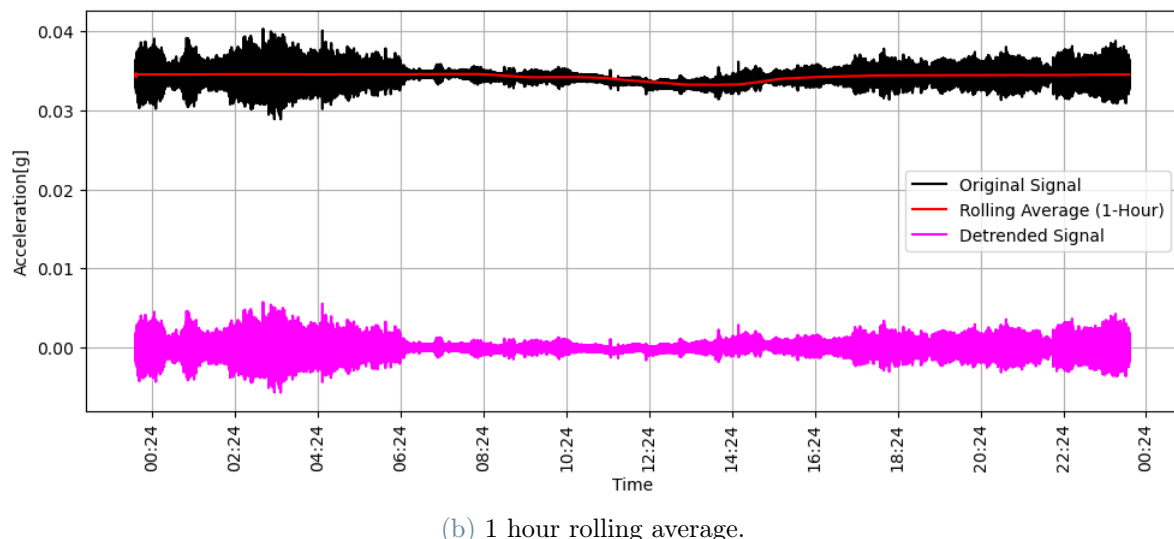
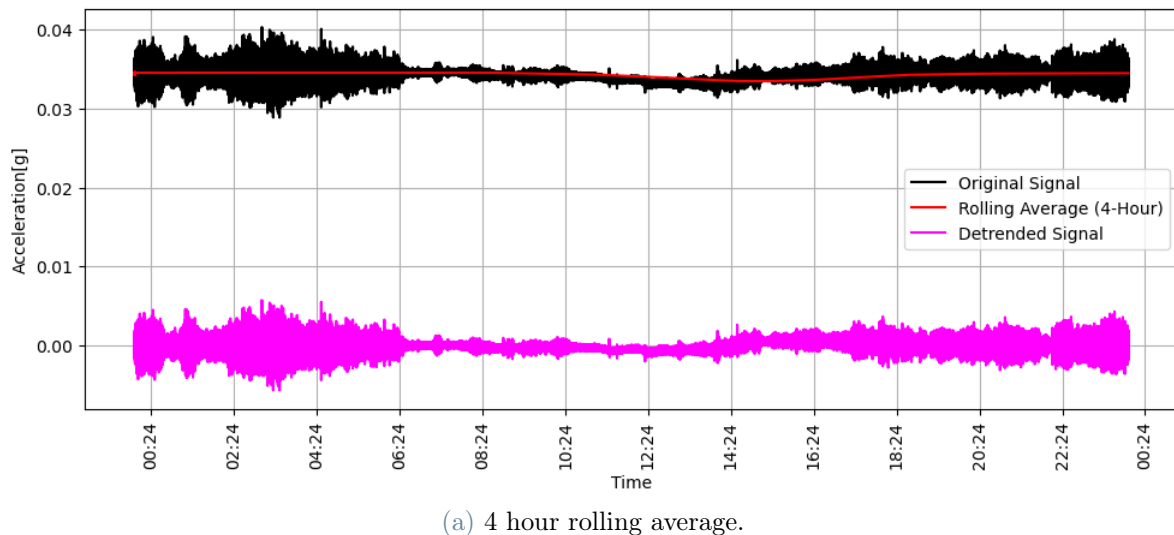


Figure 5.1: Zero-baseline correction of recorded signal.

A signal can show a more intricate and variable trend. This complexity often arises because accelerometers measure proper acceleration, and influences as daily and seasonal temperature changes and tower movements from external forces can lead to gradual tilting of the structure. This tilting produces misleading low-frequency acceleration components due to which the gravitational acceleration vector is projected. In this situation, the signal can be detrended through various techniques.

Figure 5.1 demonstrates the detrending process of the same recorded signal, showcasing results from four different rolling average time windows.



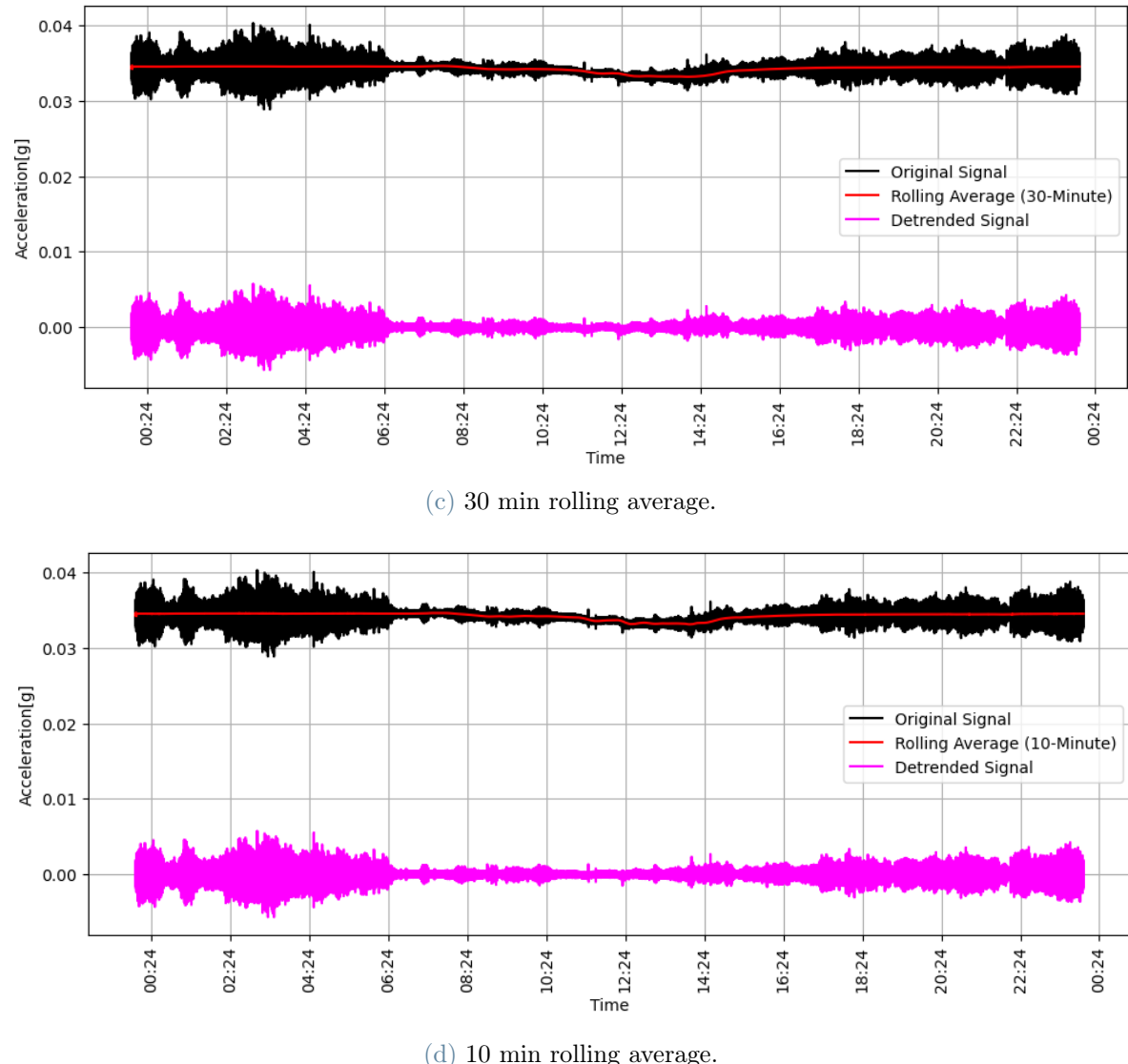


Figure 5.1: Detrending by different rolling averages.

One alternative method is to compute a polynomial of a specific degree that fits the data and then subtract it from the original signal. This can be done in Python using the `numpy.polyfit` function from the NumPy library. As anticipated, choosing a fitting polynomial of degree 0 (which represents a horizontal line) produces results identical to subtracting the average of the signal, as mentioned previously. Figure 5.2 illustrates the detrended signals obtained using fitting polynomials of degrees 0, 1, and 2.

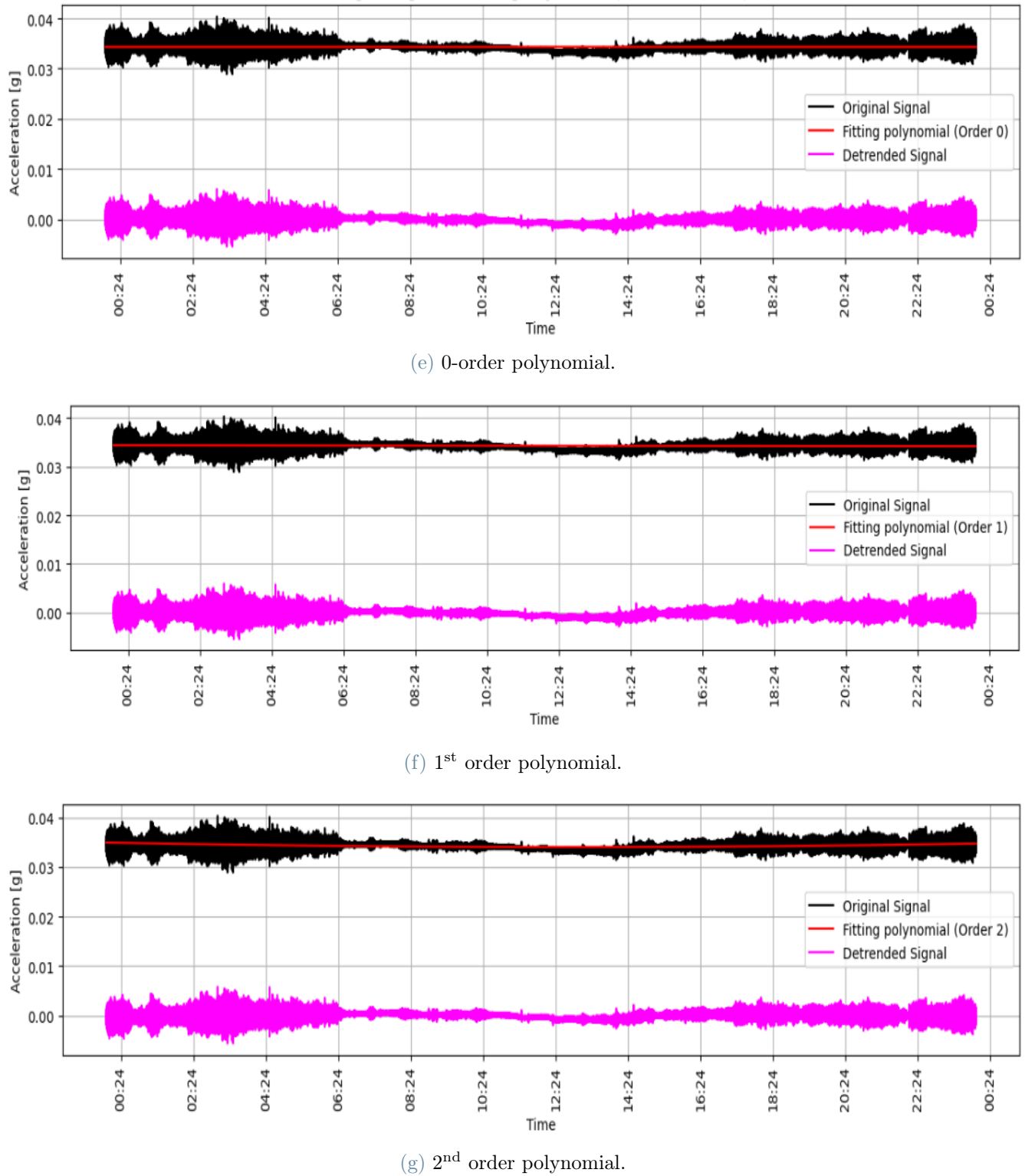


Figure 5.2: Detrending of the same signal by three fitting polynomials.

The script. The signal. As previously mentioned, the detrend module in SciPy automatically removes constant or linear trends from a signal, yielding results similar to those achieved with polynomials of order 0 and 1.

Another method, based on the principles of physics, utilizes filters in the frequency domain. A wide variety of filters are available, many of which are already implemented in different Python libraries and modules. For example, SciPy's `scipy.signal.butter` function can create *Butterworth* filters of any order and type, including low-pass, high-pass, band-pass, and band-stop filters. This technique can detrend a signal by applying a high-pass filter with a carefully selected cutoff frequency.

Filters also enable for more advanced techniques. For instance, a band stop filter can remove specific frequency ranges, such as those associated with daily cycles, while maintaining long-term trends and instantaneous changes. Figure 5.4 demonstrates the use of a 2<sup>nd</sup> order *Butterworth* high-pass filter with a cutoff frequency that corresponds to a period of 10 minutes to detrend the recorded signal.

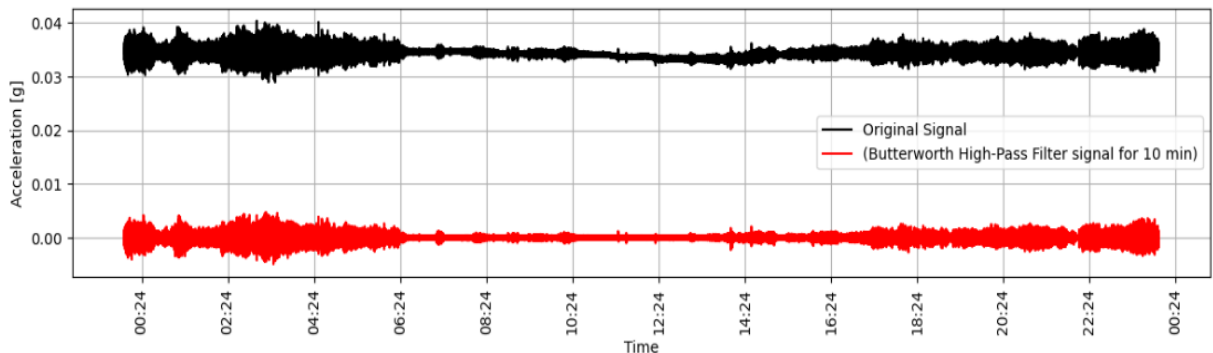


Figure 5.3: Deternding by Butterworth highpass filter signal for 10 min.

### 5.1.2. Noise reduction using smoothing methods

Field-recorded signals frequently have significant noise levels, which renders them inappropriate for direct derivative calculations. As a result, it is crucial to implement smoothing techniques to create sufficiently regular curves that can be derived, all while preserving the essential characteristics of the recorded phenomena.

One fundamental technique is to compute the signal's rolling average using a carefully chosen time window. This window must be short enough to capture the signal's variations while being long enough to provide effective smoothing.

Another technique involves convolution integrals, which can be efficiently calculated using NumPy's `Convolve` module. For a one-dimensional signal, the convolution kernel is

represented as a vector. The length of this vector should be determined based on how much smoothing is desired (similar trade-offs apply as with the rolling average method). All elements of the vector are the same and are selected so that the integration of the vector over time yields a unitary value. This effectively turns the convolution integral into a smoothing filter.

Finally, another method processes the signal using a low-pass filter, eliminating higher-frequency components usually linked to noise. The cutoff frequency must be chosen carefully to ensure effective smoothing while preserving the signal's underlying trend. Figure 5.4 illustrates the results of the smoothing techniques mentioned above, applied to the same signal.

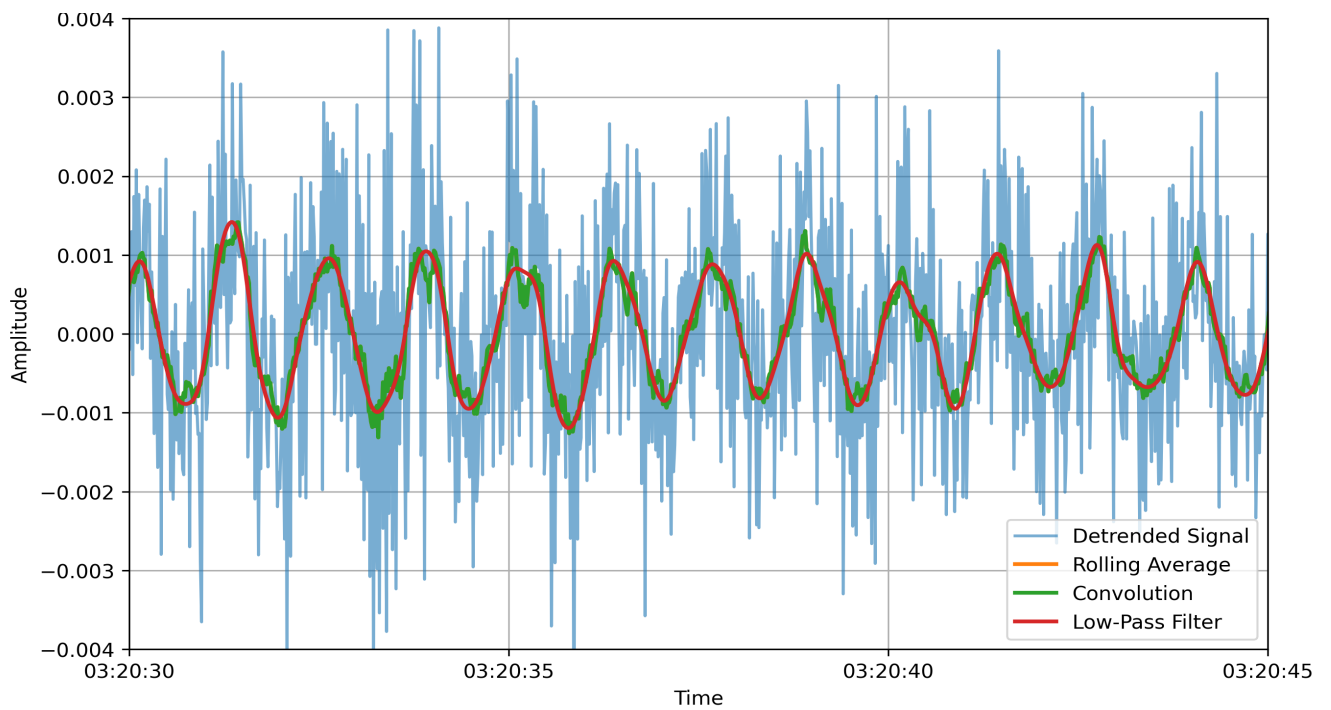


Figure 5.4: Comparison of smoothing technique with different methods.

## 5.2. Modal Parameter Estimation with Operational Modal Analysis

Operational Modal Analysis (OMA) focuses on extracting modal parameters like natural frequencies, mode shapes, and damping ratios from field measurements taken under actual operational conditions, particularly during ambient excitation. In contrast to Experimental Modal Analysis (EMA), OMA does not depend on artificially induced excitation, where the input is known and controlled.

It is essential to analyze the frequency content of the recorded signals to find natural frequencies. In theory, for a continuous signal's  $z(t)$  that changes over time, its Fourier Transform  $X(f)$  as expressed in Equation (5.1):

$$X(f) = \int_{-\infty}^{\infty} z(t)e^{-i2\pi ft} dt \quad (5.1)$$

Since the recorded signal consists of a sequence  $x_n$  made up of  $N$  equally spaced samples in the time domain, rather than being a continuous function, its transform  $X_k$  will also be a sequence of  $N$  equally spaced values in the frequency domain. This transformation is referred to as the DFT, which is defined in Equation (5.2):

$$X_k = \sum_{n=0}^{N-1} x_n e^{-i2\pi kn/N} \quad (5.2)$$

The Fast Fourier Transform (FFT) algorithm is a highly efficient technique for calculating DFT and is available in NumPy's `numpy.fft.fft` module. To estimate the PSD of the signal, we can compute the periodogram of  $x_n$ , which is derived from its DFT  $X_k$ , as illustrated below in Equation (5.3):

$$PSD = \frac{|X_k|^2}{N} \quad (5.3)$$

Calculating the DFT on signal samples with a duration of  $T = 100$  s, sampled at 64 Hz, yields  $N = 6401$ . The frequency resolution of the results is determined by in Equation (5.4):

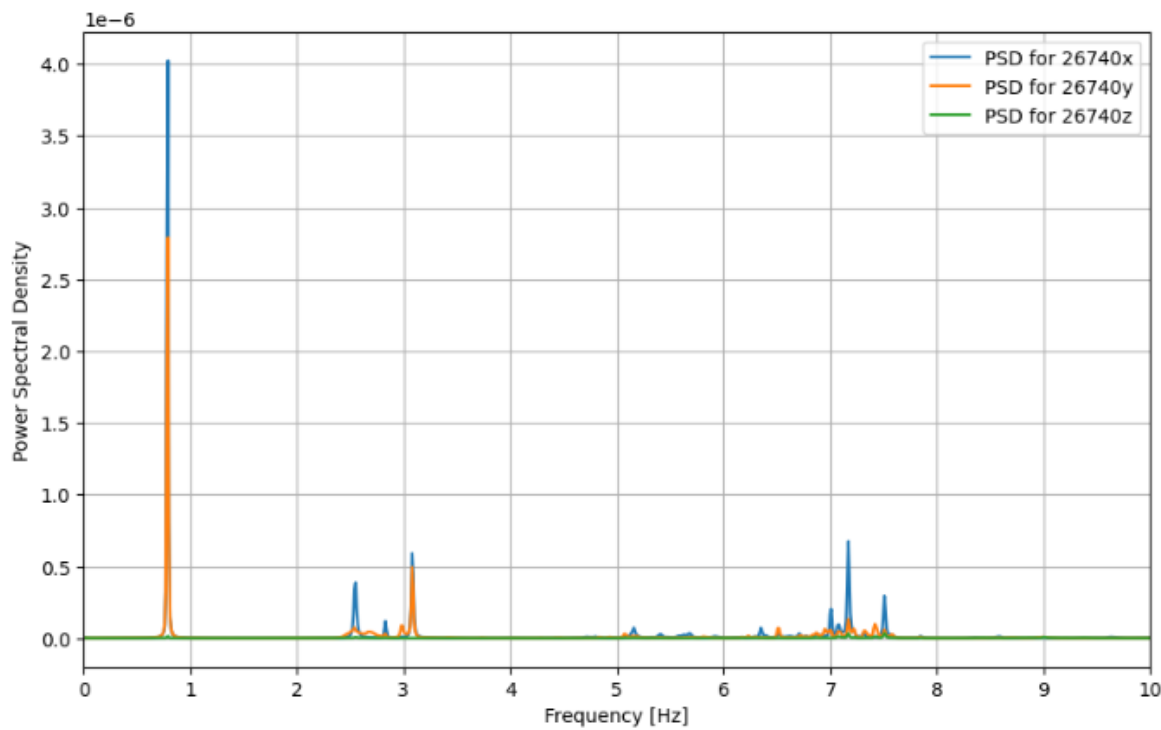
$$\Delta f = \frac{1}{T} = 0.01 \text{ Hz.} \quad (5.4)$$

Figure 5.4 illustrates the power spectral density (PSD) of signal samples collected over

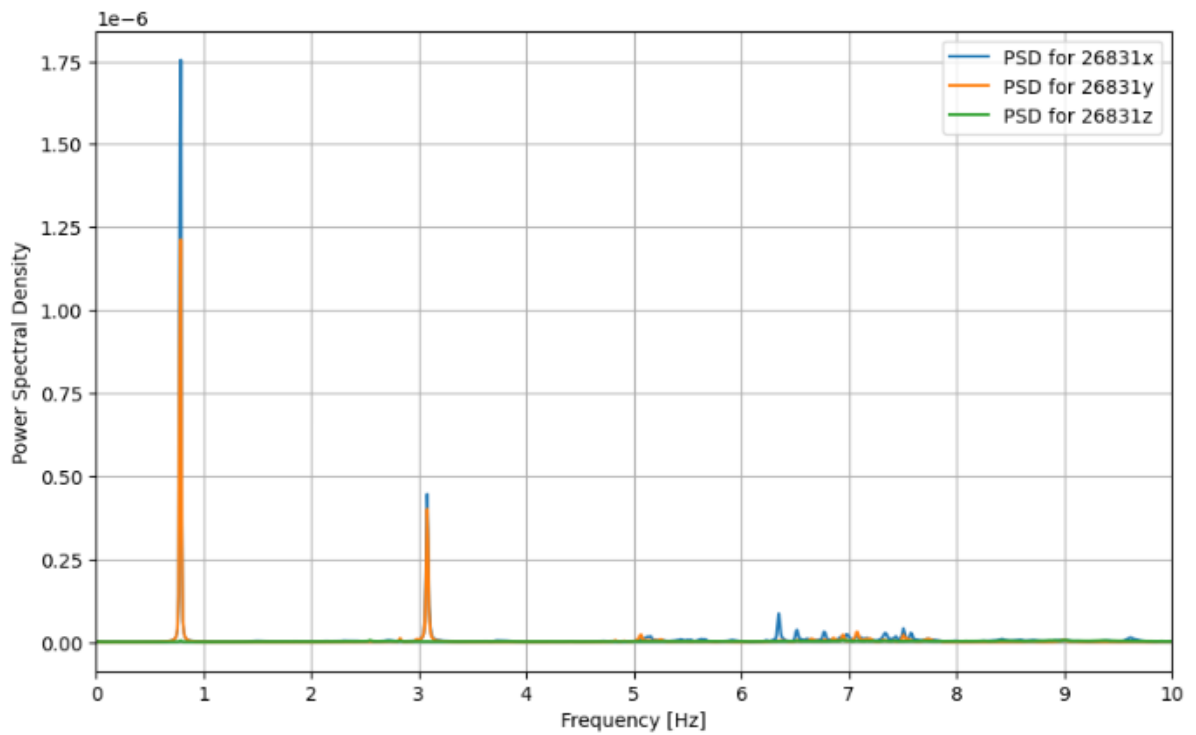
a period of 100 s. These data were recorded between 03:24 and 04:24 on September 22, 2024, and were obtained from the  $y$ -channel of an accelerometer positioned at a height of 100 m.

The accelerograms used in this study are recorded at different elevations as follows:

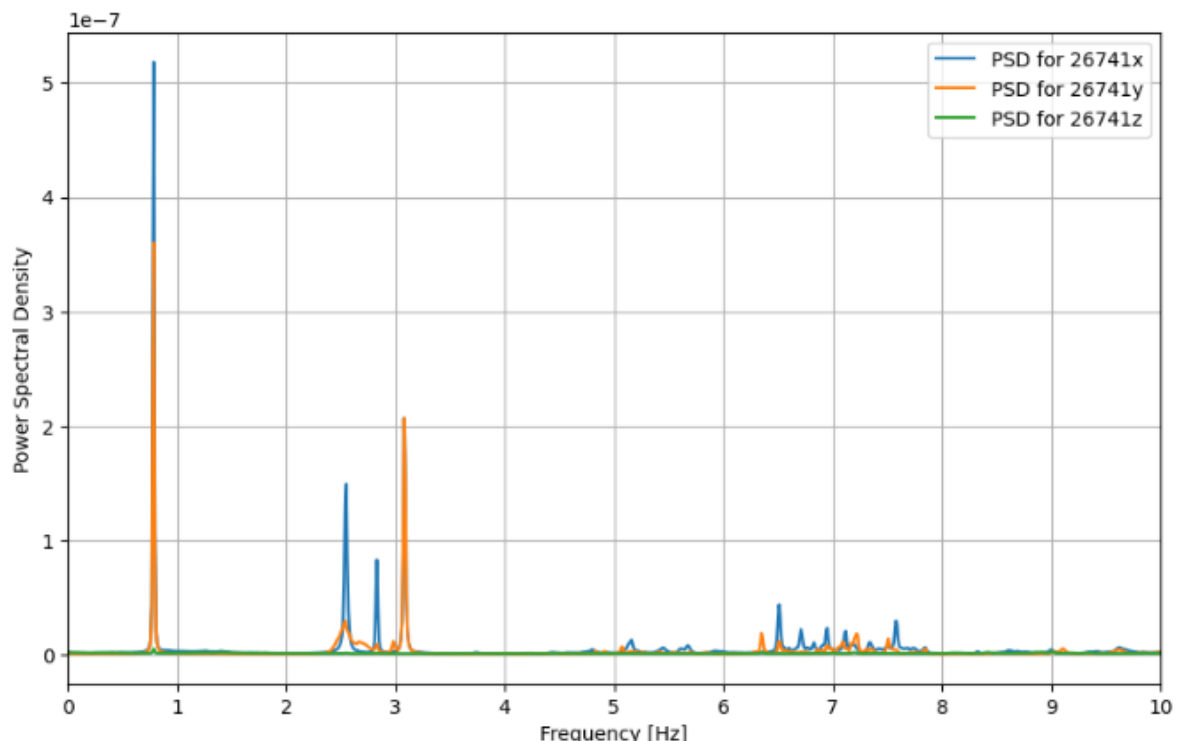
- Accelerogram **26740**: Recorded at an elevation of 100 m.
- Accelerogram **26831**: Recorded at an elevation of 80 m.
- Accelerogram **26741**: Recorded at an elevation of 60 m.



(a) PSD of accelerogram 26740 at 100 m elevation.



(b) PSD of accelerogram 26831 at 80 m elevation.



(c) PSD of accelerogram 26741 at 60 m elevation.

Figure 5.4: Power Spectral Density (PSDs) from tri-axial accelerogram.

The plots reveal two distinct peaks: one at approximately 0.8 Hz and another near 3.1 Hz. When compared with the frequencies from the 2014 dynamic characterization test (see Table 4.2), the first peak likely represents the first-order flexural mode, while the second peak corresponds to the first torsional mode.

The closeness of the first-order flexural modes and the fact that this PSD analysis focuses solely on one axis (the y-axis) likely account for the observation of a single peak near the first frequency. However, the lack of a peak for the second-order flexural mode around 2.7 Hz poses a challenge and highlights the necessity for further investigation, possibly using more advanced techniques.

Advanced methods typically utilize specialized software packages for Operational Modal Analysis (OMA). These tools facilitate the extraction of model properties like natural frequencies, mode shape vectors, and damping ratios. Notable examples include PyOMAc [81], KOMAC [80], and PyOMA [67], which are open-source solutions developed explicitly for OMA tasks.

PyOMA stands out as it offers a Python-based library with a Graphical User Interface (GUI) for its functionalities. It is particularly effective for analyzing signals in both frequency and time domains.

The library can handle multiple time-history inputs corresponding to acceleration data collected simultaneously by various sensors positioned in different directions. For instance, three sensors would yield six input time histories across two directions.

For frequency-domain analysis, the library features the `FDDsvd()` function, which produces an SVD plot from the Power Spectral Density (PSD) matrix of the input signals. This plot is instrumental in identifying peaks that estimate the system's natural frequencies.

After identifying these frequencies, they can be utilized to compute other modal parameters using the Frequency Domain Decomposition (FDD) method or its variants, which we discuss in section 2.8.1. For example, the `FDDmodEX()` function employs the FDD method to determine the natural frequencies and their corresponding mode shapes. Likewise, the `EFDDmodEX()` function applies the Enhanced Frequency Domain Decomposition (EFDD), allowing for the extraction of additional parameters such as modal damping ratios along with natural frequencies and mode shapes. Furthermore, the library provides tools for implementing the Frequency Spatial Domain Decomposition (FSDD) method to refine these estimates further.

Figure 5.5 presents an example of an SVD plot based on 17 minutes of acceleration data col-

lected by sensors on September 22, 2024. The SVD plot can be displayed up to the *Nyquist* frequency, which is 32 Hz for a sampling frequency of 64 Hz. However, in Figure 5.5, only the initial segment is shown to better emphasize the peaks of interest.

The figure indicates that the first notable peaks appear at around 0.8 Hz, 2.5 Hz, 2.8 Hz, and 3.1 Hz. Furthermore, the second singular values also exhibit a peak at the first and second peaks, hinting at the possible existence of closely spaced modes.

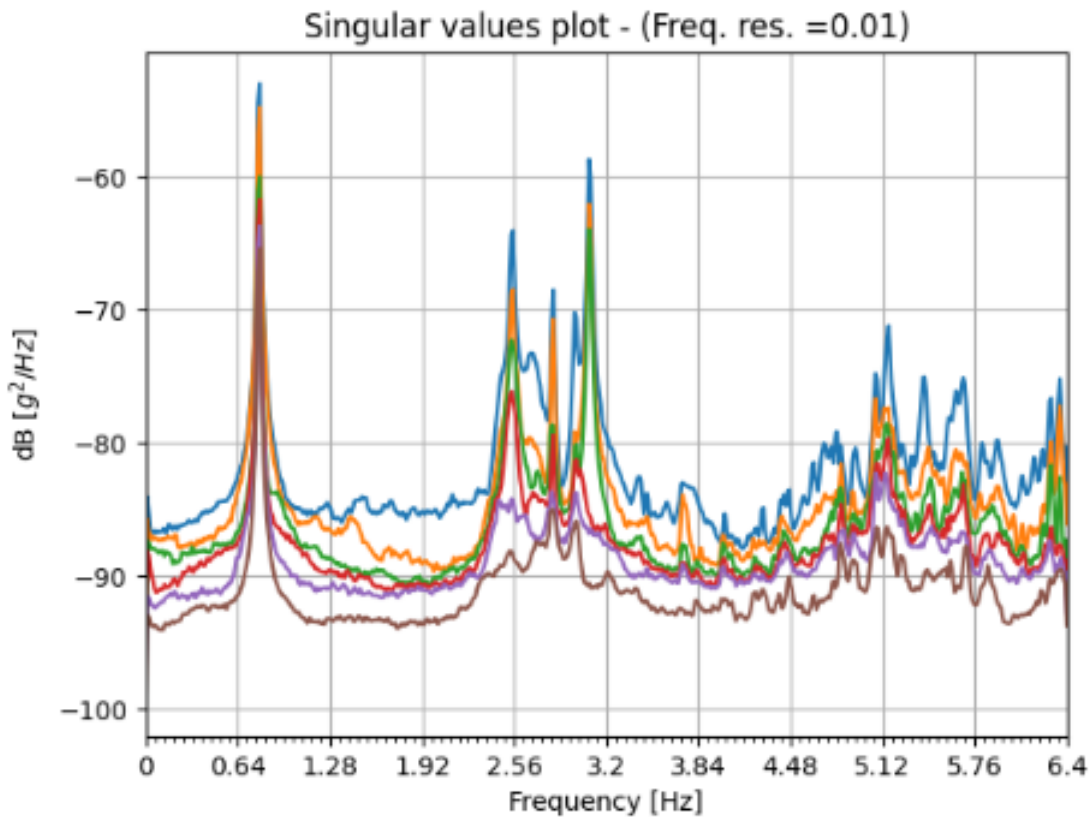


Figure 5.5: SVD frequency plot derived from PSD analysis.

The resulting mode shapes and their corresponding frequencies are shown in Figure 5.6. The FDD method yields  $m$  eigenvectors, each containing  $l$  components. By analyzing the order of the signals, we can link each element to a specific direction and spatial position, allowing for a physical interpretation of the mode shape vectors. Here are some key observations:

- The mode shape at 0.79 Hz exhibits significant components in both the  $X$  and  $Y$  directions, suggesting a combination of the first flexural modes along these axes, which aligns with expectations.
- At 2.48 Hz, the mode shape corresponds to the second flexural mode along the  $Y$

direction.

- The mode shapes at 2.55 Hz and 2.58 Hz may be related to the second flexural mode along the  $X$  direction. The mode at 2.58 Hz also shows some components in the  $Y$  direction, but only one of these two likely represents a true structural mode.
- The mode shape at 3.07 Hz initially seems to resemble a flexural mode involving both the  $X$  and  $Y$  directions. However, based on previous analyses and characterizations, it is more likely linked to the first torsional mode of the structure. This mode shape cannot be accurately captured with the current instrumentation setup, as it requires multiple sensors on the same floor to effectively differentiate between flexural modes in both directions and torsional modes.

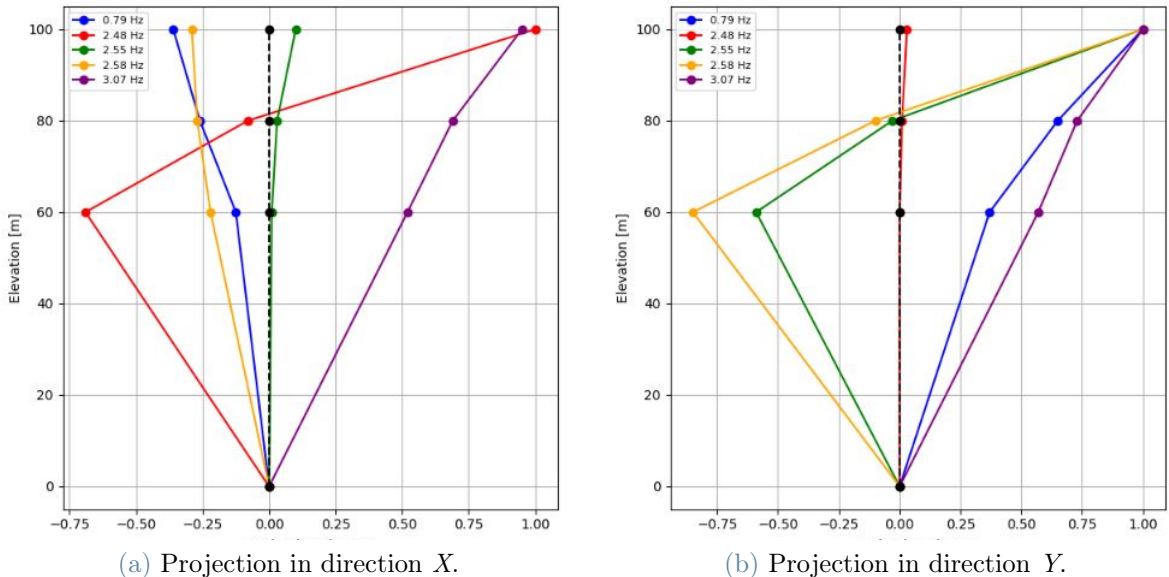


Figure 5.6: Mode Shape Identification Using PyOMA's EFDD Method.

PyOMA also facilitates time domain analysis through the Stochastic Subspace Identification (SSI) method which we discuss in section 2.8.1. The functions `SSICovStaDiag` and `SSIDataStaDiag` specifically allow for the implementation of Cov-SSI or DAT-SSI. These functions produce stabilization diagrams that help identify the structure's natural frequencies. Like the frequency-domain analysis, the `SSIModEX` function is available to calculate modal parameters, including natural frequencies, mode shapes, and damping ratios, based on the SSI results.

Figure 5.7 illustrates a stabilization diagram obtained using Cov-SSI, created from the same time-history data referenced earlier. No upper limit was imposed for constructing the diagram, where system overestimation is viewed as a conservative strategy. However,

this approach may lead to the emergence of nonphysical poles. Typically, spurious poles do not stabilize and tend to be more dispersed.

In the plot, the poles are indicated by five numbers and colors, which have the following interpretations:

- **0.0 / red:** unstable;
- **1.0 / dark orange:** stable in frequency;
- **2.0 / light orange:** stable in frequency and mode shape;
- **3.0 / yellow:** stable in frequency and damping;
- **4.0 / green:** stable in frequency, damping, and mode shape.

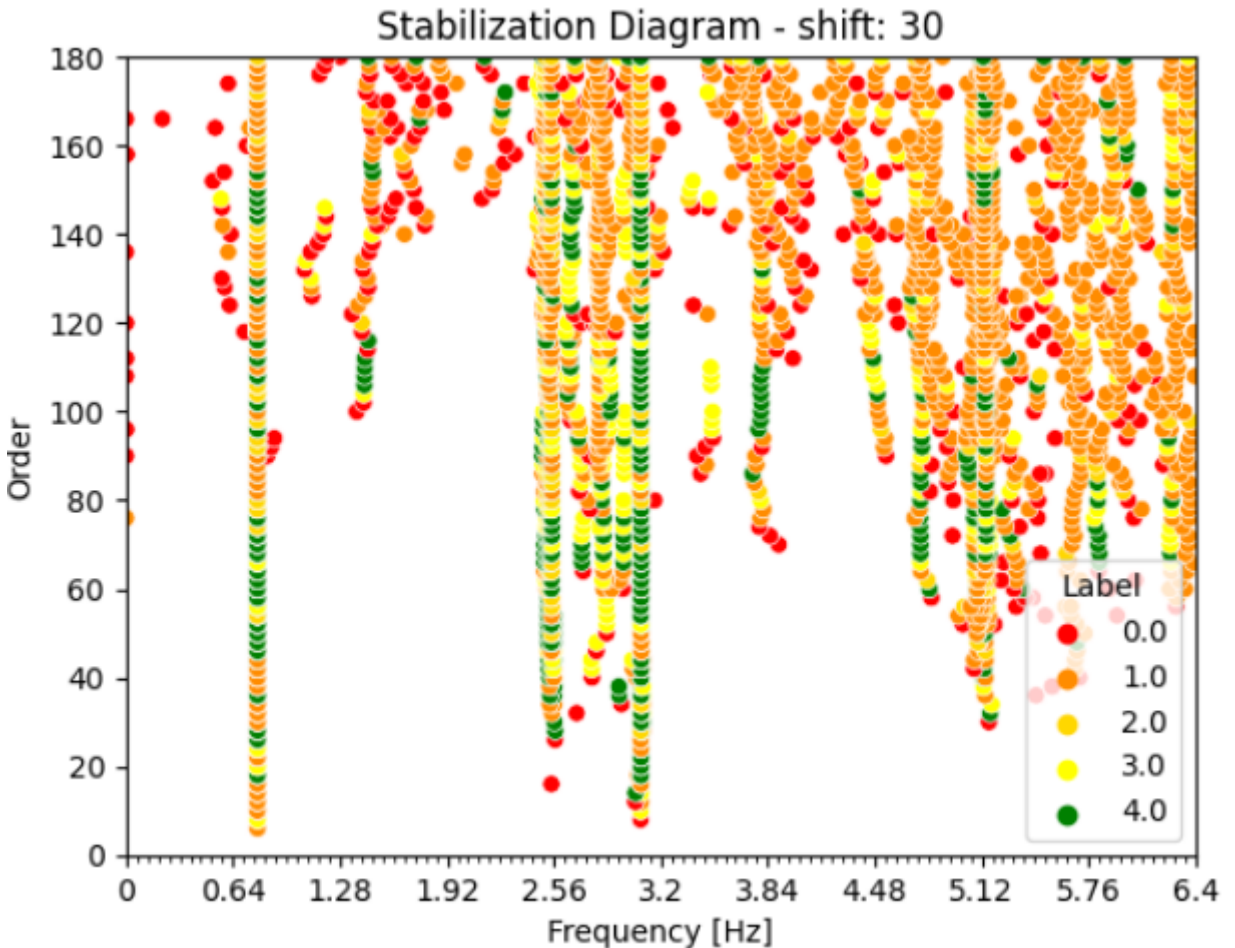


Figure 5.7: Modal stabilisation diagram using Cov-SSI in PyOMA.

The stabilization diagram can also be plotted to the *Nyquist* frequency, similar to the SVD plot. However, in Figure 5.7, only the initial portion is displayed to emphasize the poles of interest more clearly.

Figure 5.8 shows the mode shapes obtained using the Cov-SSI method. The identified frequencies are 0.79 Hz, 2.48 Hz, 2.58 Hz, and 3.07 Hz. Similar to the EFDD method, the program could not distinguish separate mode shapes along the *X* and *Y* directions for the first mode; instead, it produced a combined mode shape featuring characteristics from both directions. The following two frequencies correspond to the second-order flexural modes along *X* and *Y*, although each exhibits some components in both directions. No precise pole alignment was observed near 2.58 Hz, suggesting that the mode shape identified at this frequency using EFDD was likely spurious. Finally, while the frequency of 3.07 Hz appears again for the last mode, its corresponding mode shape was not accurately reproduced due to the limitations discussed earlier.

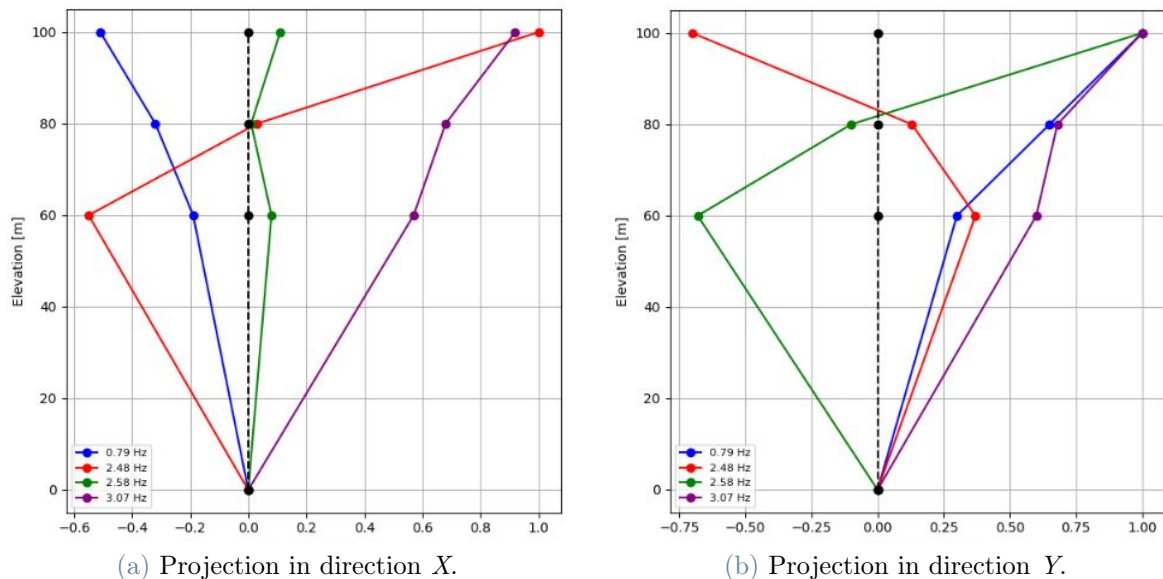


Figure 5.8: Mode shape identification using PyOMA’s Cov-SSI method.

The MAC (Modal Assurance Criterion) index can be used to calculate the correlation between any two mode shapes. This index ranges from 0 to 1, where a value of 0 indicates that the modes are completely independent, and a value of 1 signifies that they are entirely dependent.

In theory, distinct mode shapes should be independent, making the MAC index a valuable tool for initially validating the accuracy of the mode shapes obtained.

A MAC matrix can be created when comparing two sets of mode shapes. This matrix

includes elements represented as  $(i, j)$  the  $MAC_{i,j} = MAC(\phi_i^a, \phi_j^b)$ , where the MAC computed from the  $i$ -th mode shape of set  $a$  and the  $j$ -th mode shape of set  $b$ . Ideally, the MAC matrix will form an identity matrix if the two sets match perfectly. In this scenario, the diagonal elements that represent the MAC of the same mode shapes will equal 1. In contrast, the off-diagonal elements representing the MAC of different mode shapes will equal 0.

For real-valued mode shape vectors, the formula for the element  $(i, j)$  of the MAC matrix is detailed in Equation (5.5).

$$MAC_{i,j} = MAC(\phi_i^a, \phi_j^b) = \frac{|(\phi_i^a)^T \cdot \phi_j^b|^2}{((\phi_i^a)^T \cdot \phi_i^a) \cdot ((\phi_j^b)^T \cdot \phi_j^b)}. \quad (5.5)$$

In this case study, examining the MAC (Modal Assurance Criterion) matrix derived from the mode shapes obtained through a specific analysis method can aid in evaluating the consistency of the computed modes and pinpointing any potential spurious modes.

Furthermore, when comparing eigenvectors obtained from various analysis methods, for instance, one from numerical predictions and another from experimental results, the MAC matrix serves as a tool to assess the correlation between the two approaches.

MAC values exceeding 0.8–0.9 indicate a strong consistency between modes, while values falling below 0.1–0.2 suggest that the modes are independent.

Figures 5.9 and Figures 5.10 display the MAC matrices related to eigenvectors acquired through the EFDD method and the Cov-SSI method, respectively. As anticipated, the diagonal elements of these matrices are all equal to 1.

The off-diagonal elements of the MAC matrix are generally low, except the third and fourth mode shapes, which indicates their independence, as only one of the two corresponds to the actual mode. Figure 5.9 shows a MAC matrix that omits the fourth mode, leading to even lower off-diagonal values and demonstrating a strong independence between the modes.

The MAC matrix for mode shapes calculated using Cov-SSI also reveals low off-diagonal values, apart from the second and third modes, which show slightly elevated MAC indices. This is likely because the mode shape along  $X$  also contains components along  $Y$ .

These findings highlight the importance of employing multiple methods to determine a structure's modal parameters accurately. Cross-checking the results using various techniques ensures the reliability of the derived modal properties.

It is advisable to analyze additional time-history samples and utilize more sensors to enhance further the reliability of identifying the modal parameters.

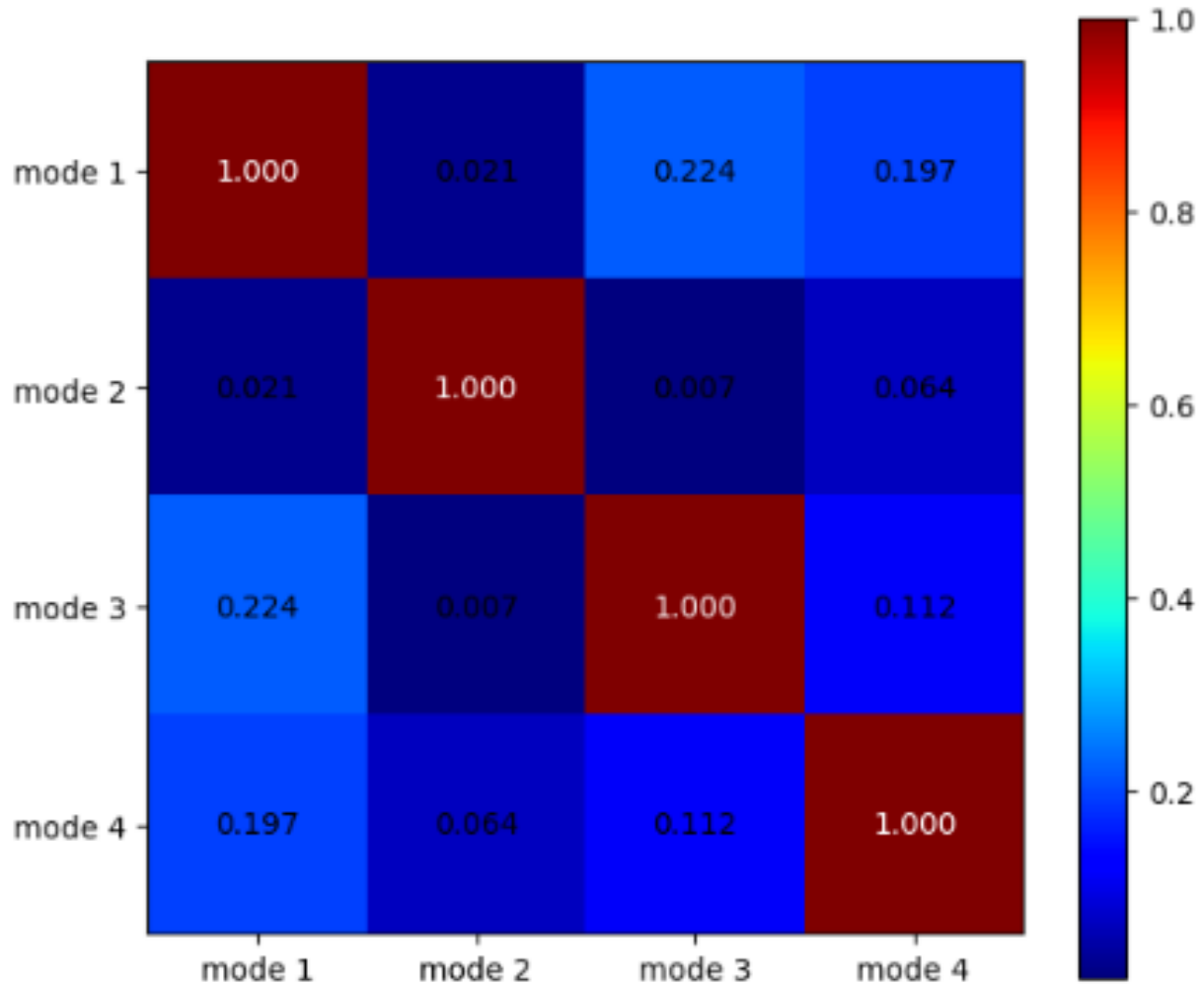


Figure 5.9: Modal Assurance Criterion (MAC) matrix for EFDD results using PyOMA.

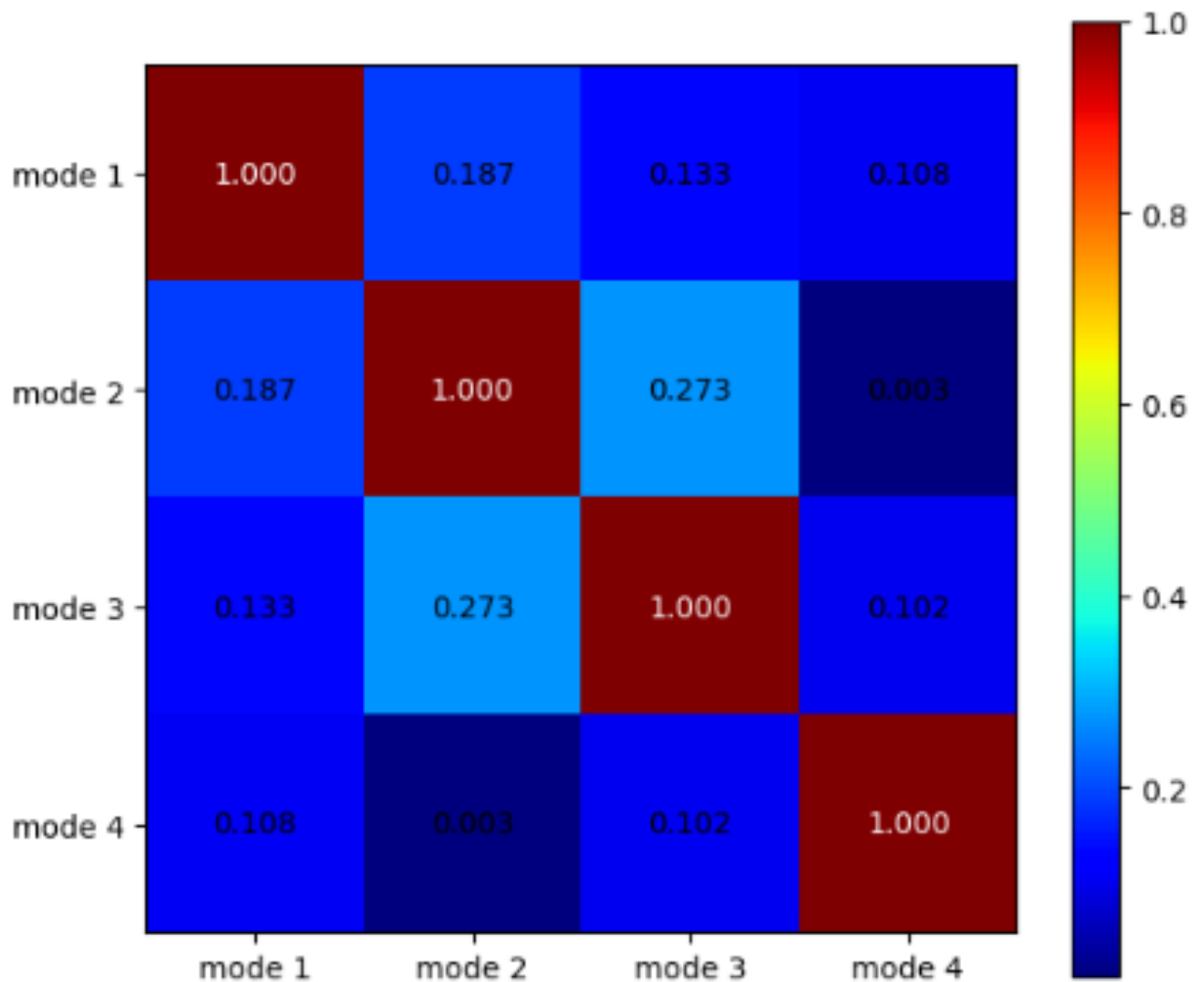


Figure 5.10: Modal Assurance Criterion (MAC) matrix for Cov-SSI results using PyOMA.



# 6 | Model Updating for Real-World Structures

## 6.1. Purpose of Model Updating

The experimental natural frequencies obtained via OMA were compared with those computed from the numerical model. The numerical model frequencies were observed to be lower than the experimental ones. Table 6.1 compares the first five frequencies, including the first two pairs of flexural modes and the first torsional mode.

Table 6.1: Comparison between experimental and numerical natural frequencies.

Mode	Deformed Shape	Natural Frequencies [Hz]			Errors	
		Exp. (EFDD)	Exp. (SSI)	Numerical	EFDD	SSI
1	$X$ (no sign inversion)	0.79	0.79	0.66	16.46%	16.46%
2	$Y$ (no sign inversion)	0.79	0.79	0.67	15.19%	15.19%
3	$X$ (1 sign inversion)	2.48	2.49	2.33	6.05%	6.43%
4	$Y$ (1 sign inversion)	2.55	2.58	2.36	7.45%	8.53%
5	$T$ (no sign inversion)	3.07	3.07	2.55	16.94%	16.94%

Despite accurately replicating the structure's geometry in the numerical model, significant discrepancies persist between the numerical and experimental natural frequencies, as highlighted in Table 6.1. Notably, errors exceeding 10% in the initial modes suggest inaccuracies within the numerical model. To address these discrepancies, implementing model updating techniques is essential. These methods involve adjusting uncertain parameters, such as material properties and boundary conditions, to minimize differences between numerical predictions and experimental observations. By refining the finite element model through this process, we can enhance the accuracy of the numerical simulations, ensuring they more closely align with the actual structural behaviour.

## 6.2. Model Updating of Real-World Structure

As discussed in section 2.3, model updating is an iterative method that we use to reduce the discrepancies in our finite element model with the experimental results obtained through OMA.

In that regard, we manually tuned the updating parameter, which helped us understand the numerical model and identify the parameter controlling its behaviour. We varied the parameters and checked their influence on the numerical model.

Once we understand the behaviour of the structure and its updating parameter through our preliminary analysis, we perform the semi-automatized model updating method, which is the Douglas-Reid method. The complete workflow of model updating is shown in Figure 6.1.

The numerical model of the structure is described in detail in section 4.8. The software used for modeling the structure is MIDAS [57]. The complete model, which includes both the tower and the base building, consists of 4884 nodes, 3615 line elements, 552 three-node plane elements, 916 four-node plane elements, 540 cuboid elements, and 278 point elements.

Initially, the boundary conditions of the numerical model were assumed to be fixed supports, meaning no displacement or rotation at the base. However, a second finite element model was developed since the base building rests on the ground, whose stiffness is not precisely known. In this updated model, the degrees of freedom (DOFs) at the base (i.e., the foundation of the base structure) were released and replaced with three-dimensional springs. This adjustment was made to evaluate the effect of boundary conditions on the model updating process.

Similarly, in the initial finite element, the boundary condition of the joints section of the steel truss tower structure is considered as a rigid joint, but the loosening of the bolts at the joint section does not ensure the complete rigid connection, so a reduced stiffness member is provided to understand the better role of connection. In addition to that, the parameters considered for the model updating are Young's modulus ( $E$ ), density ( $\rho$ ), and 3-dimensional elastic spring ( $K$ ) at the foundation.

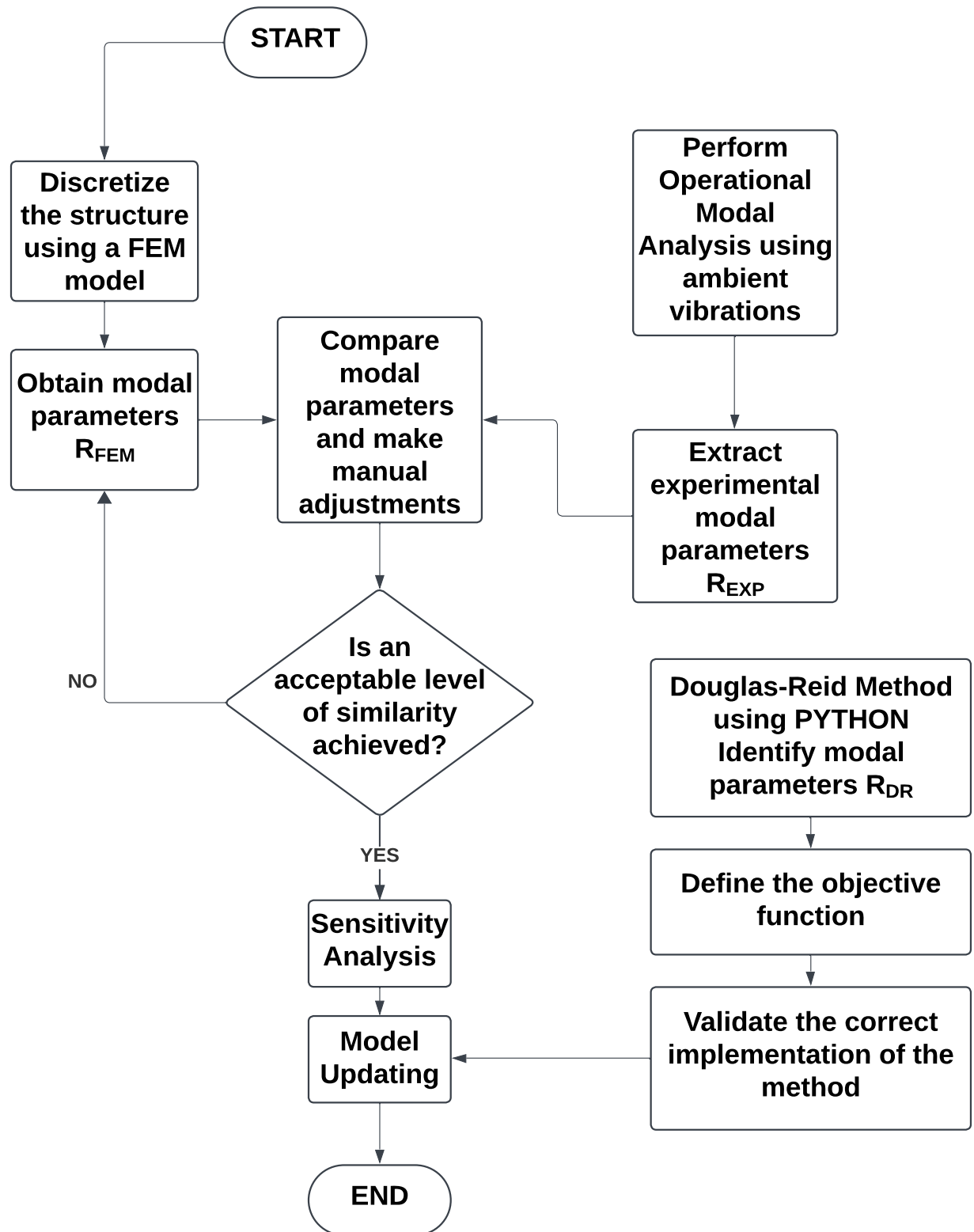


Figure 6.1: Workflow of model updating process.

### 6.2.1. Manual tuning

In model updating, the manual tuning [10] method is commonly used in which the initial optimization is carried out, which means we manually update the parameter and try to understand the behaviour of the structure and the approximated base value for the updating parameter is computed to reduce the error between the numerical and experimental results.

The constraints of the numerical model significantly influence the dynamic behaviour of the structure [78]. Since the building's foundation rests on soil with unknown stiffness properties, assuming a fully fixed base is not an ideal approach. A more realistic representation involves modeling the foundation using a uniform spring stiffness distribution. Given that the foundation consists of pile footings, the base of the footing is considered a rigid body, while linear spring stiffness values  $k_x$ ,  $k_y$ , and  $k_z$  are assigned in kN/mm for all three directions. The stiffness of the foundation is then fine-tuned within a predefined range of 1 to 10 [28] to achieve a more accurate representation.

We will perform the Eigenvalue analysis at each variation and compute the natural frequencies. These computed natural frequencies will be compared with the experimental frequencies as mentioned in Table 4.2 then a variation of error for each mode for the stiffness of the spring at the ground is computed by using the objective function given in Equation (6.1), Figure 6.2 shows the variation of stiffness of spring multiplier between 1-10 for error.

$$\text{Error} = \frac{|f_{\text{exp}} - f_{\text{FEM0}}|}{f_{\text{exp}}} \times 100. \quad (6.1)$$

After performing manual tuning on the elastic springs, we get the multiplier value 7, which has a minimum error of 0.66 % compared to the experimental result.

Initially, the base value of the stiffness of the elastic spring considered for this analysis is 1150 kN/mm. After the analysis or manual tuning, we get the optimal value of 7 for the multiplier, so the new stiffness of the elastic spring is in all directions 8050 kN/mm, which we use in our further analysis.

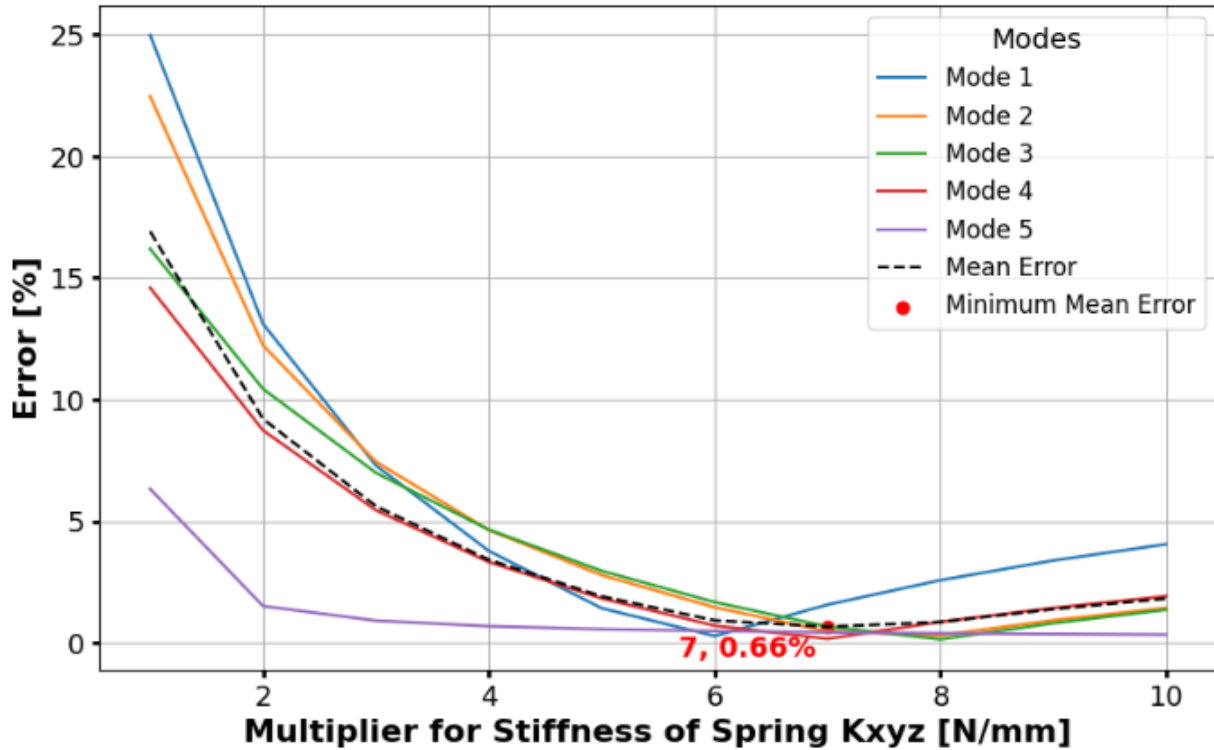


Figure 6.2: Frequency error analysis with varying stiffness in elastic spring supports.

### 6.2.2. Sensitivity analysis

Sensitivity analysis involves identifying the most influential variables affecting the model's response. In the context of a finite element model (FEM), the impact of input parameters on the overall structural behaviour is influenced by the heterogeneity of steel and concrete materials, varying levels of damage, and the interaction between different structural components. In a sensitivity analysis, we generally measure the sensitivity of the particular parameter that defines the dynamic characteristic of the structure. Here, the steel truss structure with the base building creates heterogeneity in the structure's dynamic behaviour, and the aim is to find that parameter that improves the output from the dynamic analysis of the numerical model.

In addition to studying the influence of one parameter on the other, the individual behaviour of the updating parameter is initially examined in relation to the structure. Afterward, varying multiple variables at a time to find the optimal solution for different updating parameters is also considered.

In sensitivity analysis, we will compute the sensitivity coefficient for each model updating parameter  $S_{i,j}$  as shown in Equation (6.2). According to this coefficient, we will better

understand the influence of that updating parameter on defining the dynamic behaviour of the structure. For this, we vary each updating variable by 5% and compute its sensitivity coefficient.

$$S_{i,j} = 100 \cdot \frac{X_j}{R_i^{\text{FEM}}} \cdot \frac{\Delta R_i^{\text{FEM}}}{\Delta X_j},$$

$i = 1, \dots, M \quad M = \text{Frequencies},$

$j = 1, \dots, N \quad N = \text{Parameters}.$

(6.2)

Here,

$X_j$  represents the updating parameter we will consider for the model updating.

$R_i^{\text{FEM}}$  represent the output we get from the numerical model which is a natural frequency.

$\Delta X_j$  represent the updating parameter value after a 5% variation.

$\Delta R_i^{\text{FEM}}$  represents the output natural frequency we get for the updated parameter.

Table 6.2 shows the updating parameter we were considering in this numerical model, which is Young's modulus, density, and the boundary condition considered for an elastic foundation.

Table 6.2: Sensitivity analysis for various tower parameters.

Name	Parameter	Initial Value	Sensitivity coefficient ( $S_{i,j}$ )
Floor Beams of Tower	$E1 [MPa]$	210000	0.9%
External Column of Tower	$E2 [MPa]$	210000	7%
Internal Column+Inclined Column of Tower	$E3 [MPa]$	210000	20%
Internal Column last 6 Floors of Tower	$E4 [MPa]$	210000	3%
Vertical Bracing of Tower	$E5 [MPa]$	210000	20.8%
Columns of Base Building	$E6 [MPa]$	33000	0.9%
Elastic Foundation at base	$K [kN/mm]$	1150	4.2%
Floor Beams of Tower	$\rho_1 [kg/m^3]$	7860	10.2%
Internal Column+Inclined Column of Tower	$\rho_2 [kg/m^3]$	7860	11.5%
Internal Column last 6 Floors of Tower	$\rho_3 [kg/m^3]$	7860	8.3%
External Shaft of Tower	$\rho_4 [kg/m^3]$	7860	1.4%
Vertical Bracing of Tower	$\rho_5 [kg/m^3]$	7860	10.7%

Only those parameters with the highest frequency sensitivity for the lower modes are considered. The sensitivity coefficients are reported in the last column of Table 6.2. It can be observed how the  $E_3$  steel Young's modulus (internal plus inclined columns) and the  $E_5$  one (vertical truss elements) have the highest influence (20 and 20.8 % respectively) in defining the dynamic behaviour of the structure. The least influencing update parameters, with a value of 0.9 %, are  $E_1$  and  $E_6$  (Young's modulus of the tower's floor beams and the base building's columns, respectively). The remaining other parameters have a comparatively intermediate influence on the structure. Note that a larger number of parameters were considered in the initial stage, but their influence was negligible, so they have not been reported here. They will not be considered as updating parameters for the subsequent analysis. After discarding the non-relevant parameters, the ones included in the procedure are the elastic moduli, stiffness, and densities, as shown in Figure 6.3.

It must be observed that the elastic moduli here considered must be intended as fictitious variables, taking the overall stiffness of the element into account, which is affected by a number of phenomena, mainly related to the joint's behaviour. A similar comment applies to densities, whose value fictitiously incorporates the effect of additional masses.

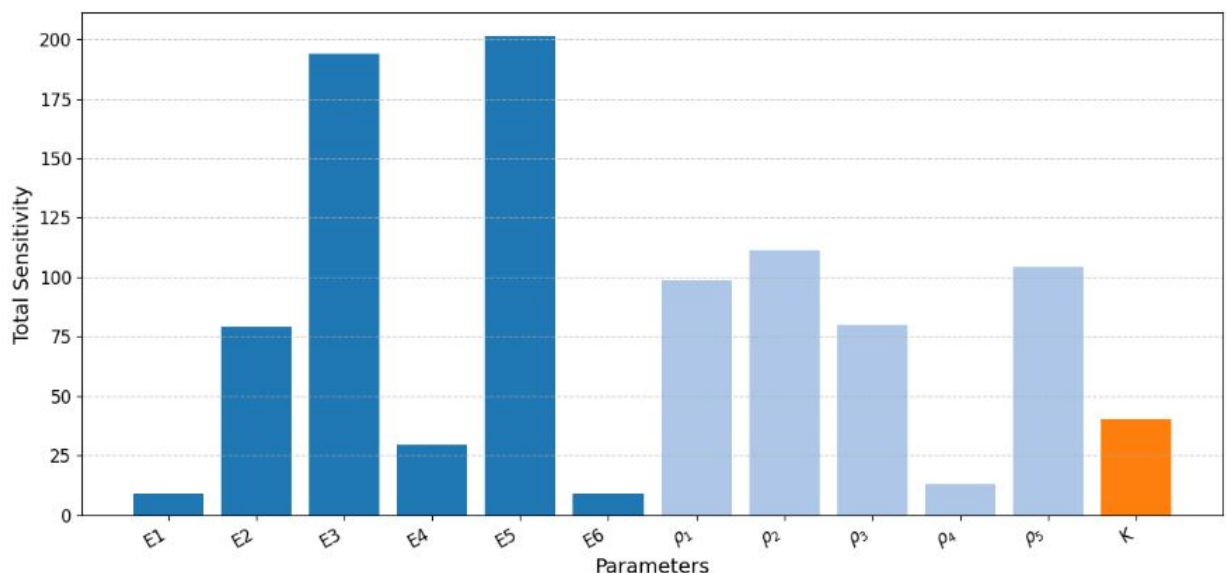


Figure 6.3: Total sensitivities of parameters.

### 6.3. Model Updating Results

Table 6.3 presents the results of the basic finite element model (FEM1), where a fixed constraint is applied at the base of the building. The table displays 11 updating parameters, specifically Young's moduli and material densities, along with their initial values, updated values after the model updating process, and the corresponding percentage variations. Notably,  $E_2$  (Young's modulus for the external columns of the steel tower) exhibits the highest variation at 57%, while  $\rho_1$  shows no variation at 0%.

Table 6.3: Updating parameter values after model updating in FEM1.

Parameter	Initial Value	Updated Value	Variation [%]
$E_1 [MPa]$	210000	315000	50.0
$E_2 [MPa]$	210000	329700	57.0
$E_3 [MPa]$	210000	285600	36.0
$E_4 [MPa]$	210000	197400	-6.0
$E_5 [MPa]$	210000	138600	-34.0
$E_6 [MPa]$	330000	23760	-28.0
$\rho_1 [kg/m^3]$	7860	7860	0.0
$\rho_2 [kg/m^3]$	7860	8410.2	7.0
$\rho_3 [kg/m^3]$	7860	6523.8	-17.0
$\rho_4 [kg/m^3]$	7860	8253	5.0
$\rho_5 [kg/m^3]$	7860	6547.3	-16.7

Similarly, in the advanced finite element model (FEM2), the building's base is not fixed; instead, it is in this case supported by a three-dimensional elastic spring. This approach is adopted because a complete analysis of the site's soil behaviour is unavailable, making the elastic spring support the most appropriate representation of the foundation. Table 6.4 displays the variation of 12 updating parameters, which include Young's moduli, material densities, and the elastic spring at the foundation. For each parameter, the table lists the initial value, the updated value after the model updating process, and the corresponding percentage variation. Notably,  $E_2$  (Young's modulus for the external columns of the steel tower) exhibits the highest variation at 67%, while  $E_4$  shows the least variation at -4%.

Table 6.4: Updating parameter values after model updating in FEM2.

Parameter	Initial Value	Updated Value	Variation [%]
$E1 [MPa]$	210000	302400	44.0
$E2 [MPa]$	210000	350700	67.0
$E3 [MPa]$	210000	247800	18.0
$E4 [MPa]$	210000	201600	-4.0
$E5 [MPa]$	210000	180600	-14.0
$E6 [MPa]$	33000	27720	-16.0
$K [kN/mm]$	1150	8050	-
$\rho_1 [\text{kg/m}^3]$	7860	7702.80	-12.0
$\rho_2 [\text{kg/m}^3]$	7860	8410.20	7.0
$\rho_3 [\text{kg/m}^3]$	7860	8960.40	14.0
$\rho_4 [\text{kg/m}^3]$	7860	4951.80	-37.0
$\rho_5 [\text{kg/m}^3]$	7860	6547.38	-16.7

Table 6.5 summarizes the errors for the initial finite element model (FEM1) across the first five modes, using experimental data from Operational Modal Analysis (OMA) as a reference. In comparison, Table 6.6 presents the errors for the advanced finite element model (FEM2), where all errors are below 2% for the five modes. This indicates that FEM2 can effectively serve as a digital twin of the experimental structure. Additionally, Tables 6.3 and 6.4 provide the updated structural parameter values for FEM1 and FEM2, respectively. Overall, the advanced model (FEM2) accurately replicates the dynamic response of the fundamental structure, representing the most precise outcome achieved through the model updating process.

Table 6.5: Comparison between experimental and numerical natural frequencies of FEM1.

Mode	Exp. (EFDD)	Exp. (SSI)	Numerical	EFDD Error [%]	SSI Error [%]
1	0.79	0.79	0.7685	2.792%	2.792%
2	0.79	0.79	0.7751	2.532%	2.532%
3	2.48	2.49	2.4842	3.874%	3.143%
4	2.55	2.58	2.4885	2.685%	4.136%
5	3.07	3.07	3.2757	8.073%	8.073%

Table 6.6: Comparison between experimental and numerical natural frequencies of FEM2.

Mode	Exp. (EFDD)	Exp. (SSI)	Numerical	EFDD Error [%]	SSI Error [%]
1	0.79	0.79	0.8013	1.41%	1.41%
2	0.79	0.79	0.8078	2.20%	2.20%
3	2.48	2.49	2.5197	1.57%	1.17%
4	2.55	2.58	2.5580	0.31%	0.86%
5	3.07	3.07	3.1115	1.33%	1.33%

In November 2024, preventive maintenance inspections and interventions on the JRC Atmospheric Tower revealed that some bolts had loosened, resulting in a reduction of joint stiffness. To simulate this behaviour, an additional finite element model, FEM3, was developed. This model specifically targets the assessment of joint loosening within the structure. The critical joint sections were identified at the intersections of vertical trusses with beams and columns, as shown in Figure 6.4. The modeling approach aims to determine whether these joints behave as rigid connections, hinge-like connections, or exhibit an intermediate behaviour between these two extremes.

To analyze the structure's response under varying conditions, seven scenarios were considered, each corresponding to different levels of joint stiffness reduction: 0%, 5%, 10%, 15%, 20%, 25%, and 30%. For each scenario, after applying the model updating process within FEM3, the numerical modal frequencies were computed and compared with the experimental natural frequencies for the first five vibration modes. As illustrated in Figure 6.5, the comparison showed that a 15% reduction in joint stiffness resulted in the minimum error relative to the experimental data. This finding suggests that the actual condition of the joints following maintenance is best represented by a 15% stiffness reduction.

The analysis underscores the importance of accurately modeling the joint behaviour to reflect the real dynamic response of the structure. By calibrating the finite element model against experimental measurements, the approach validates that even moderate reductions in stiffness, such as observed 15%, can significantly influence the vibrational characteristics of the structure. This detailed assessment provides a robust foundation for further investigations into structural integrity and helps guide future maintenance strategies.

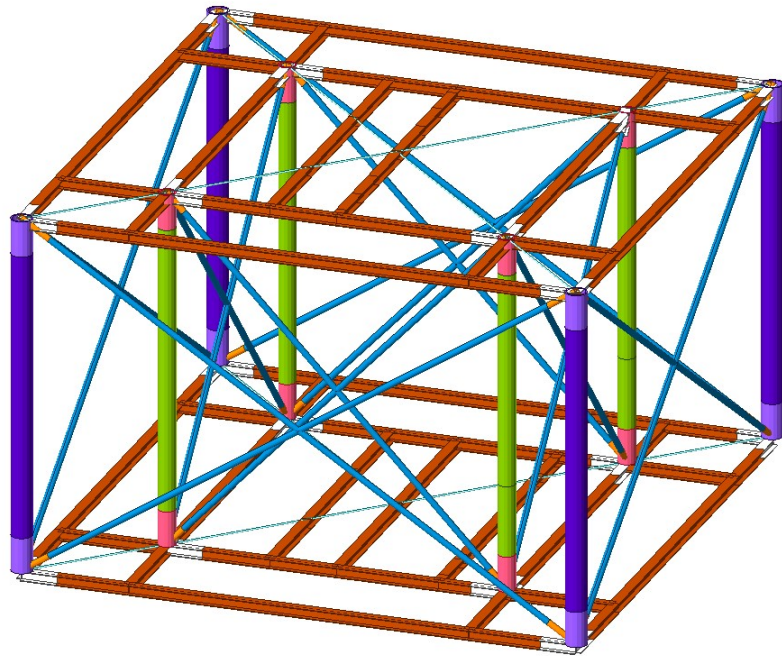
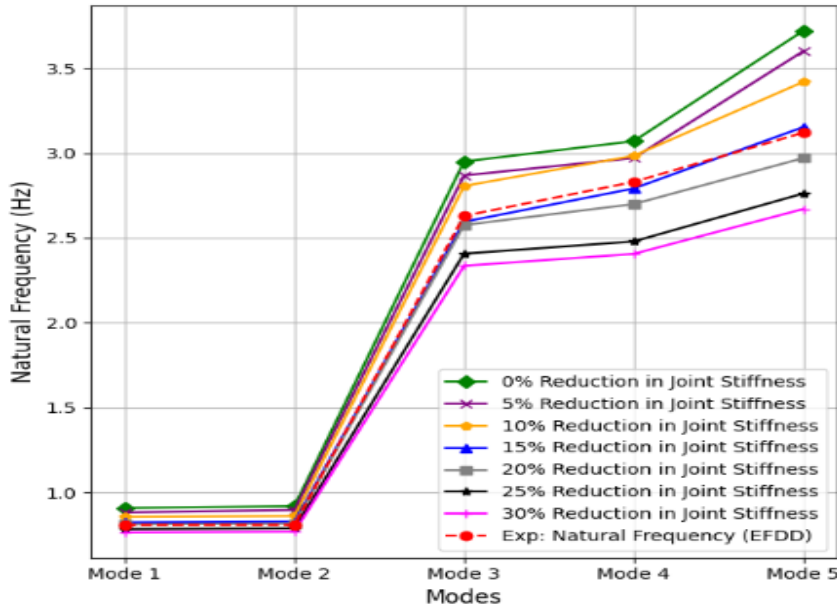
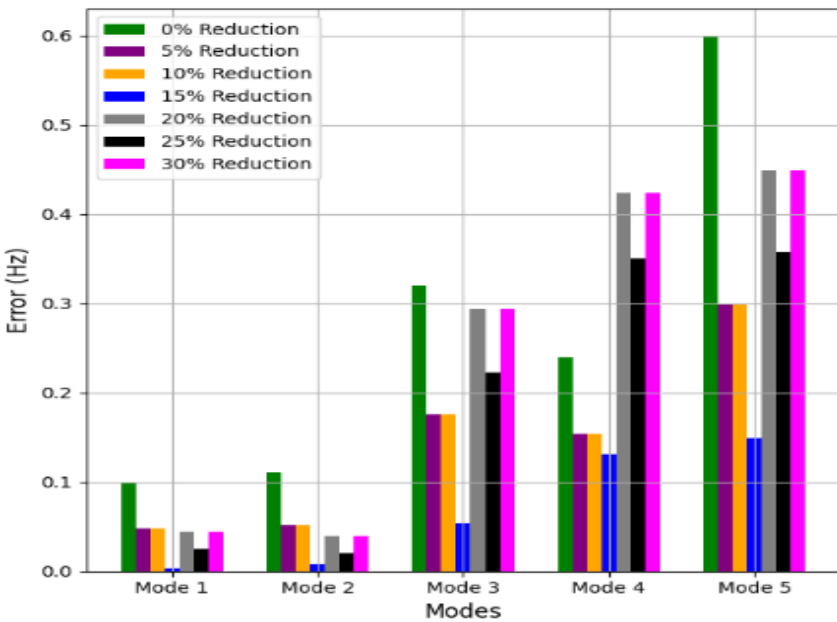


Figure 6.4: End sections in FEM for vertical truss, columns, and beams.

The results of the model updating due to a variation of element stiffness are shown in Figure 6.6 where the colour indicates the amount of stiffness variation of each structural component. The most accurate FEM model is associated with the 15 % reduction in joint stiffness. This can be regarded as the most accurate model obtained from the overall model updating process.



(a) Natural frequency for each mode



(b) Error in natural frequency for each mode

Figure 6.5: Effect of joint bending stiffness reduction on natural frequency.

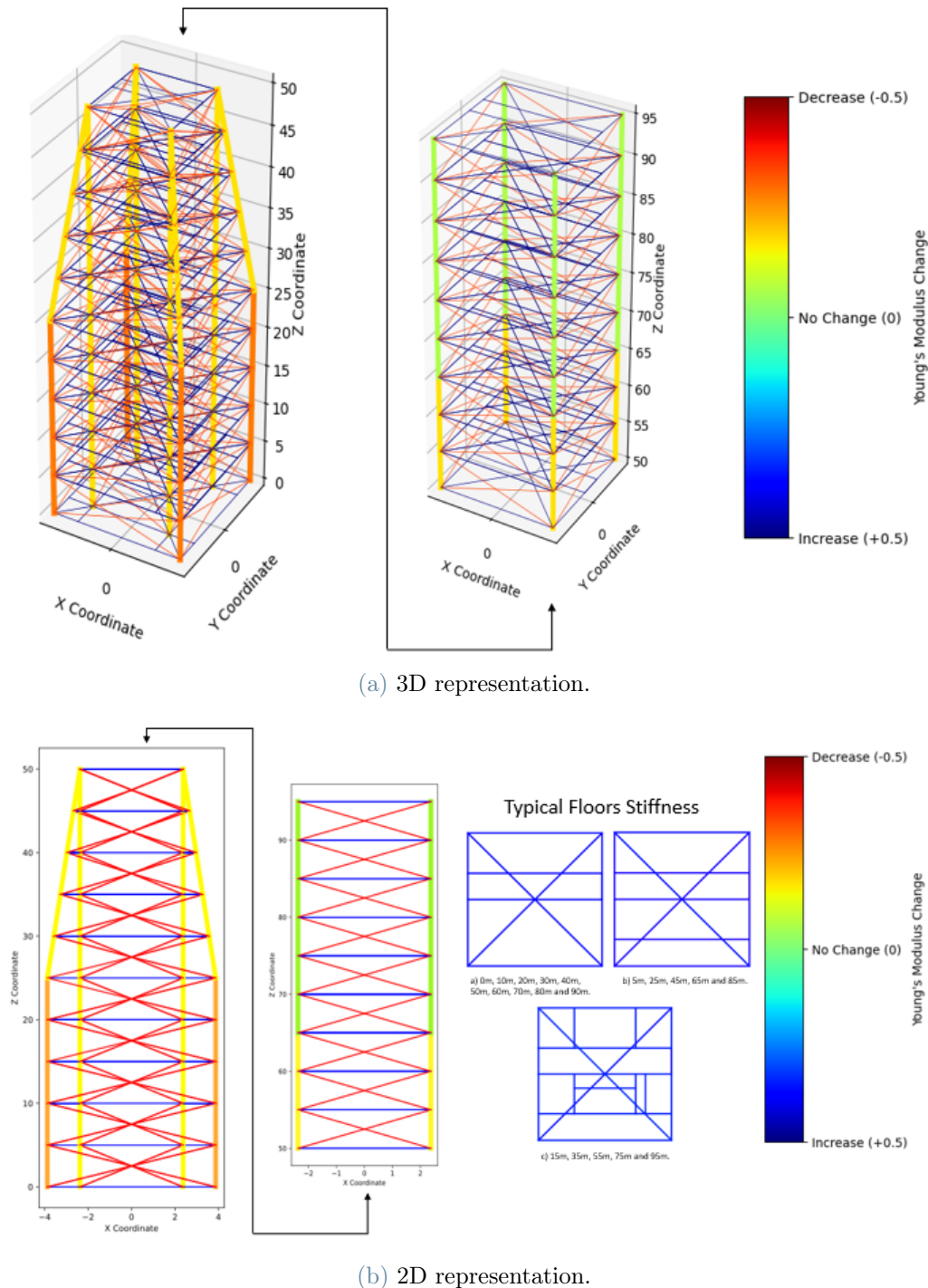


Figure 6.6: Variation in Young's modulus for each member of the steel truss tower after model updating, with updated values obtained from FEM2.



# 7 | Wind Analysis of Atmospheric Tower

After the development of the numerical model of the JRC Atmospheric Tower that can accurately replicate the dynamic behaviour of the actual structure, it is then possible the next development in that is to perform the dynamic analysis of the of the structure under wind loading. According to the Eurocode description, gravity and wind loads are important to consider in the design of the steel tower structure. Given the site's location of the JRC Atmospheric Tower, wind load significantly affects the dynamic properties of the structure also, given that the structure is significantly tall. For the analysis here presented, the reference wind speed for this project was taken as  $v_{ref} = 25 \text{ m/s}$ , as specified in Eurocode 1. The wind speed and zone can also be seen in *Dubal Software*[79] website as shown in Figure 7.1.

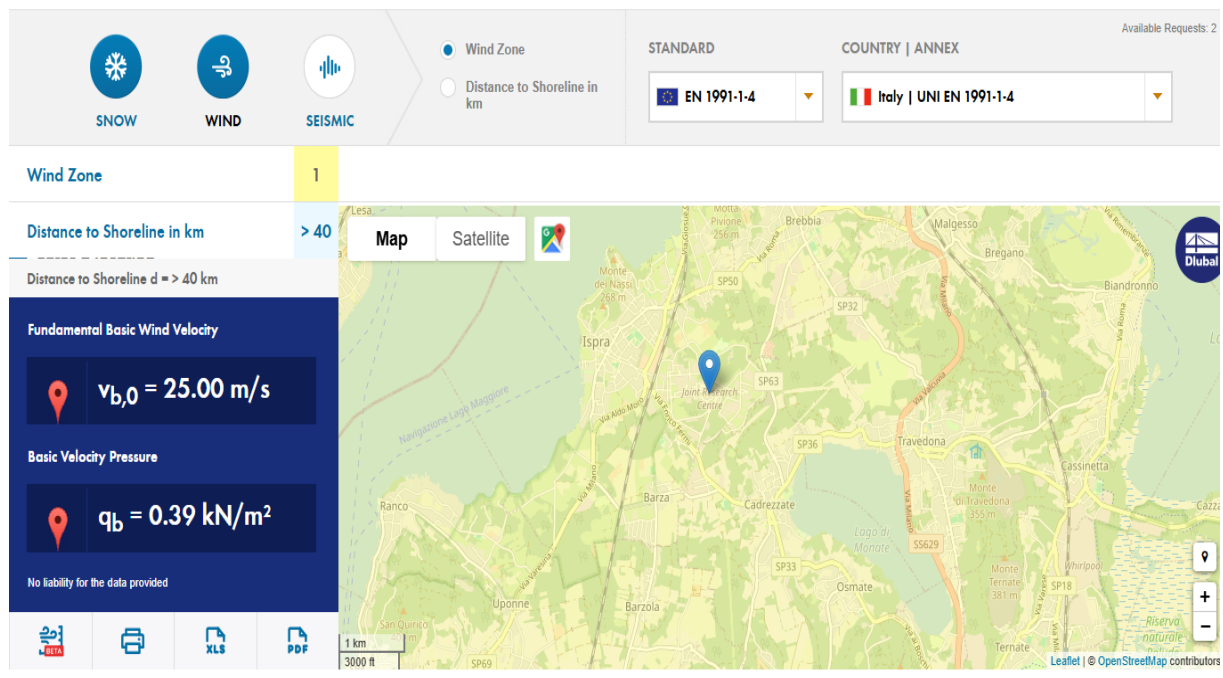


Figure 7.1: Wind zoning of Lombardy region.

## 7.1. Wind Load Calculation

Wind is a variable load that produces a dynamic force that fluctuates over time and space. Wind load is computed by a simple method equivalent to static loads for tall structures. The wind pressure acting on a structure depending on its geographic position, elevation, and relative height of a structure above mean sea level. It can be evaluated according to the Italian National Annex to UNI EN 1991-1-4:2007, Eurocode 1 – *Action on structures – Parts 1-4: General actions - Wind actions* as follows in Equation 7.1:

$$p = q_b \cdot c_e \cdot c_p \cdot c_d \quad (7.1)$$

Where:

- $q_b$ : is the peak velocity pressure
- $c_e$ : is the exposure coefficient
- $c_p$ : is an aerodynamic coefficient depending on the geometry and orientation of the building. This value is obtained by wind tunnel test
- $c_d$ : is the dynamic coefficient that takes into account of the reductive effects associated with the non-contemporaneity of maximum local pressures and amplification effects due to structural vibration

### 7.1.1. Peak velocity pressure

The peak velocity pressure can be evaluated based on the following expression in Equation 7.2:

$$q_b = \frac{1}{2} \rho V_b^2 \quad (7.2)$$

Where:

- $\rho$ : air density = 1.25 [kg/m<sup>3</sup>]
- $V_b$ : basic wind velocity [m/s]

### 7.1.2. Basic wind velocity

The basic wind velocity,  $V_b$ , is the characteristic value of the wind speed at 10 m above the ground on a plot of category II exposure, averaged over ten minutes and referred to

a return period of 50 years.

According to NTC-18, we can use this table to verify the essential wind velocity given by the website, as shown in the above Figure 7.1, and by this formula, we can find that  $V_b$  is given in Equation 7.3 and 7.4.

$$V_b = V_{b,0} \quad \text{for } a_s \leq a_0 \quad (7.3)$$

$$V_b = V_{b,0} + k_a(a_s - a_0) \quad \text{for } a_0 < a_s \leq 1500m \quad (7.4)$$

Table 7.1: Basic wind velocities with Italian regions.

Zona	Descrizione	$v_{b,0}$ [m/s]	$a_0$ [m]	$k_a$ [1/s]
1	Valle d'Aosta, Piemonte, Lombardia, Trentino Alto Adige, Veneto, Friuli Venezia Giulia (con l'eccezione della provincia di Trieste)	25	1000	0.010
2	Emilia Romagna	25	750	0.015
3	Toscana, Marche, Umbria, Lazio, Abruzzo, Molise, Puglia, Campania, Basilicata, Calabria (esclusa la provincia di Reggio Calabria)	28	750	0.015
4	Sicilia e provincia di Reggio Calabria	28	1000	0.020
5	Sardegna (zona a oriente della retta congiungente Capo Teulada con l'Isola di Maddalena)	28	750	0.015
6	Sardegna (zona a occidente della retta congiungente Capo Teulada con l'Isola di Maddalena)	28	1000	0.020
7	Liguria	30	1500	0.015
8	Provincia di Trieste	30	1500	0.015
9	Isole (con l'eccezione di Sicilia e Sardegna) e mare aperto	31	500	0.020

As we are in the city of Ispra, located in the Lombardy region, and our site is at an elevation of 220 m above sea level (which is below 1000 m), we can take  $V_{b,0} = 25$  m/s.

$$V_b = V_{b,0} \quad \text{for } a_s \leq a_0$$

$$V_b = 25 \text{ m/s}$$

Data collected from *Dubal Software* website refer to the same value of wind velocity.

Peak velocity pressure can be found with the formula given in Equation 7.2:

$$q_b = \frac{1}{2} \rho \cdot V_b^2$$

$$\begin{aligned} q_b &= \frac{1}{2} \cdot 1.25 \cdot 25^2 \\ q &= 390.625 \text{ N/m}^2 \end{aligned}$$

The website refers to the same amount of velocity pressure  $0.39 \text{ KN/m}^2$ .

### 7.1.3. Exposure coefficient:

The exposure coefficient  $c_e$  in wind load depends on the roughness class of the location, which is determined based on the characteristics of the surrounding terrain and structures. The exposure coefficient increases with the increasing of the roughness class, as locations with rougher terrain and more buildings will experience higher wind pressures. The exposure coefficient is an essential factor to consider in wind load calculations, as it can significantly impact the design of a structure. It can be evaluated as follows:

$$c_e(z) = k_r z^2 c_t \ln \left( \frac{z}{z_0} \right) [7 + c_t \ln \left( \frac{z}{z_0} \right)] \quad \text{for } z \geq Z_{min} \quad (7.5)$$

$$c_e(z) = c_e[Z_{min}] \quad \text{for } z < Z_{min} \quad (7.6)$$

Where:  $k_r, z_0, Z_{min}$  are functions of the exposure category of the site located the construction; They are marked in Table 7.2.

**Table 7.2:**  $K_r$ ,  $Z_0$ , and  $Z_{min}$  values and categories.

Categoria di esposizione del sito	$k_r$	$z_0$ [m]	$z_{min}$ [m]
I	0.17	0.01	2
II	0.19	0.05	4
III	0.20	0.10	5
IV	0.22	0.30	8
V	0.23	0.70	12

According to the location of the site's terrain, category IV is considered for the analysed structure, and accordingly, the parameters are defined like  $c_t$  is the topography coefficient, generally set equal to 1, and the exposure coefficient  $c_e(z)$  depends on the height of a structure  $Z$ , as shown in the below Figure 7.2.

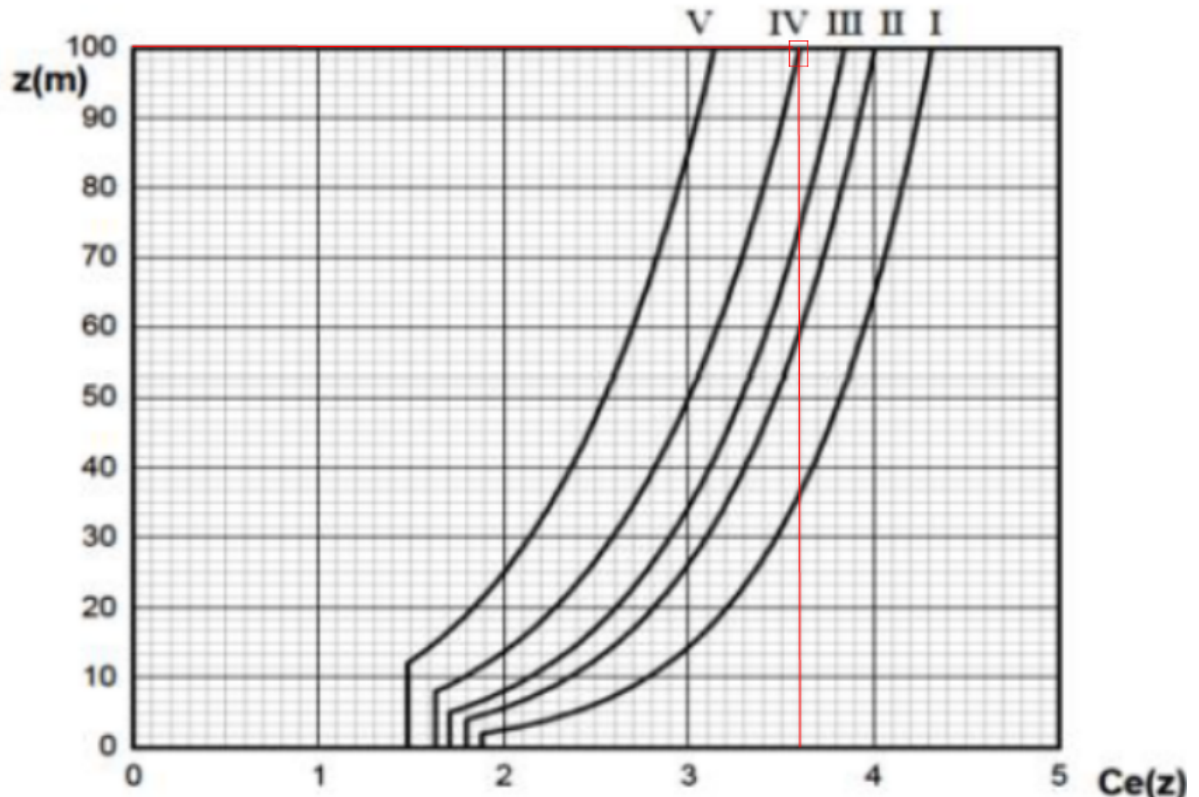


Figure 7.2: Exposure coefficient w.r.t height.

The height of the Tower structure is 100m, so the exposure coefficient  $c_e(z)$  is 3.6.

#### 7.1.4. Aerodynamic coefficient

To evaluate the aerodynamic coefficient, only the wind load inclination of  $90^\circ$  is considered, as it directly impacts the exposed parts of the tower structure. A shape coefficient of  $c_p = 0.8$  is used for windward surfaces where the wind directly acts. In contrast, a reduced shape coefficient of  $c_p = 0.4$  is applied for leeward surfaces, which are not directly exposed to the wind.

### 7.1.5. Dynamic coefficient

The dynamic coefficient  $c_d$  takes account of the reducing effects associated with non-contemporaneity, the maximum local pressures, and amplification effects due to the dynamic response of the structure. It is assumed to be equal to 1.

The wind pressure acting on the structure at the roof level  $z = 100$  m (windward) is:

$$\begin{aligned} p &= q_b \cdot c_e \cdot c_p \cdot c_d \\ p &= 1.123 \text{ kN/m}^2 \end{aligned}$$

The action of wind loading on EC JRC *Atmospheric Tower* according to Eurocode is shown in Figure 7.3.

## 7.2. Wind Load Calculation in Midas Gen

Midas Gen calculates wind loads using a set of input parameters, including terrain category, friction coefficient, basic wind velocity, and force coefficients. The process involves determining the peak velocity pressure  $q_p(z)$  at height  $z$  using:

$$q_p(z) = (1 + 7 \cdot l_s(z)) \cdot \frac{1}{2} \cdot \rho \cdot v_m^2(z) \quad (7.7)$$

The wind force  $F_w$  on a structure is then calculated using the formula:

$$F_w = c_s \cdot c_d \cdot c_t \cdot q_p(z_e) \cdot A_{\text{ref}} \quad (7.8)$$

The calculation also includes adjustments for orographic effects, neighboring structures, and displacement height. These factors ensure the wind load is accurately determined for the structure's location and design.

## 7.3. Response of Structure Under Wind Loading

After calculating the wind pressure acting on the structure, we apply this loading to our advanced finite element model, that is FEM3, in MIDAS from the loads section, we choose the "wind loads" command, which induces the wind pressure calculated in section 7.1, then perform the static wind analysis on the structure. The wind loads acting on the

structure computed from the software are shown in Figure 7.3.

Figure 7.4 shows the deformed shape of the tower under the wind loading in the windward direction, which is north-south.

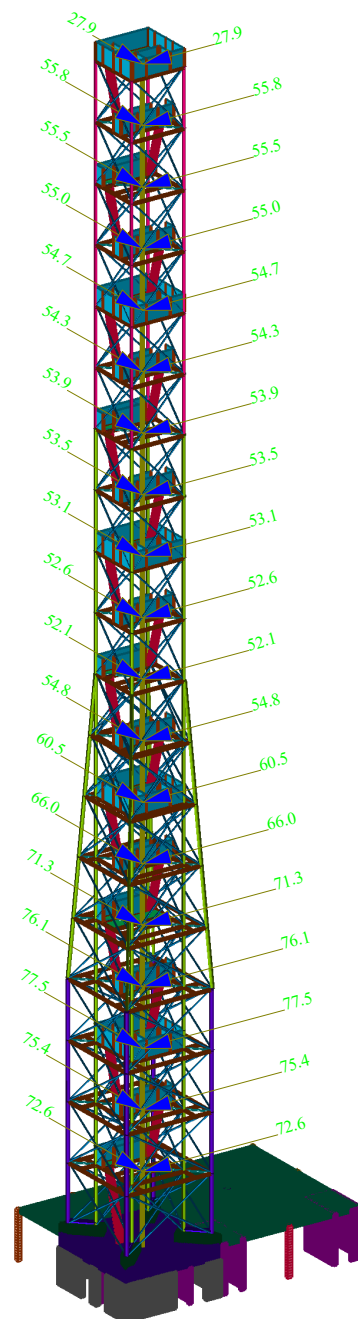


Figure 7.3: Static wind load calculation (Eurocode 1 - EN 1991-1-4) in kN.

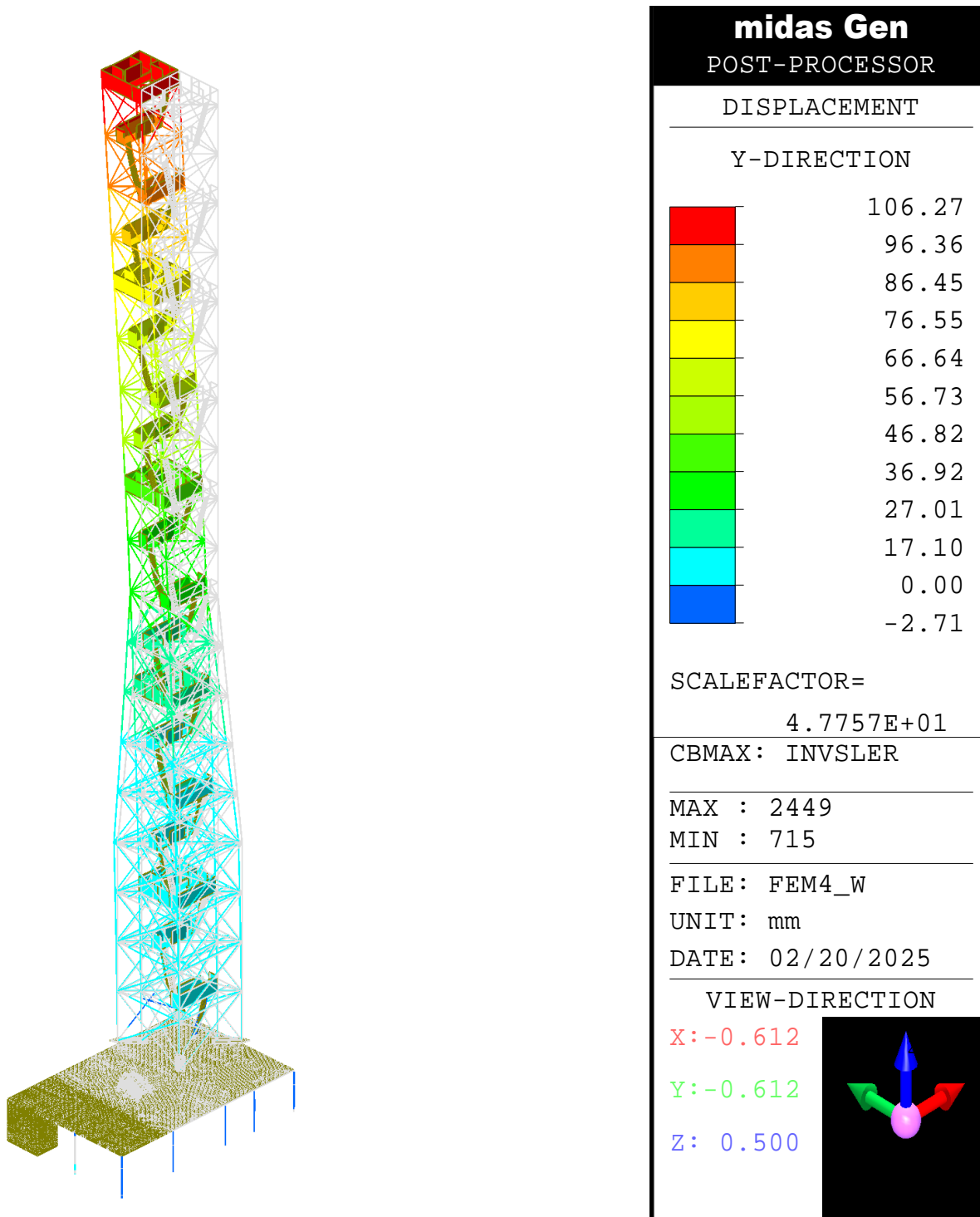


Figure 7.4: Deformed shape of the tower under wind loading on global Y-direction.

## 7.4. Modal Updating for FEM4

In the FEM4 model, we consider the FEM3 model, which includes the effects of joint sections and elastic spring supports at the foundation. In addition to gravity loads, wind loads are also applied to the tower structure in this model.

Initially, we updated the model properties of the tower structure and identified the optimal parameters for the FEM3 model, which accurately reproduced the dynamic properties of the structure. Now, we perform another model update by including the wind load acting on the tower. The updated parameters for the tower structure are presented in Table 7.3, which can be compared with the model properties obtained from Operational Modal Analysis (OMA). The errors computed for each mode are shown in Table 7.4.

**Table 7.3:** Updating parameter values after model updating in FEM4.

Parameter	Initial Value	Updated Value	Variation [%]
$E1 [MPa]$	210000	260400	24.0
$E2 [MPa]$	210000	308700	47.0
$E3 [MPa]$	210000	174300	-17.0
$E4 [MPa]$	210000	281400	34.0
$E5 [MPa]$	210000	180600	-14.0
$E6 [MPa]$	33000	38940	18.0
$K [kN/mm]$	1150	8050	-
$\rho_1 [\text{kg/m}^3]$	7860	8017.20	2.0
$\rho_2 [\text{kg/m}^3]$	7860	9196.20	17.0
$\rho_3 [\text{kg/m}^3]$	7860	10060.80	28.0
$\rho_4 [\text{kg/m}^3]$	7860	5973.60	-24.0
$\rho_5 [\text{kg/m}^3]$	7860	6460.92	-17.8

The FEM1 and FEM2 models, with their updated parameters presented in Table 6.3 and Table 6.4, provide a robust baseline for evaluating the structure's dynamic response under gravity loading. However, these models do not account for the additional complexities introduced by wind forces. In contrast, the FEM4 model incorporates significant parameter updates that capture the influence of wind loads, necessitating a recalibration of both stiffness and mass distribution to reflect experimental behaviour accurately. Ultimately, while the gravity-only models effectively capture lower-order dynamics, incorporating wind load in the FEM4 model requires a more refined approach to fully represent the dynamic effects, especially in the higher modes.

Table 7.4: Comparison between experimental and numerical natural frequencies of FEM4.

Mode	Exp. (EFDD)	Exp. (SSI)	Numerical	EFDD Error [%]	SSI Error [%]
1	0.79	0.79	0.808	2.28%	2.28%
2	0.79	0.79	0.813	2.91%	2.91%
3	2.48	2.49	2.583	4.15%	3.73%
4	2.55	2.58	2.791	9.45%	8.15%
5	3.07	3.07	3.212	4.63%	4.63%

## 7.5. Modal Analysis with wind loading

After calculating the wind loads and applying them to the structure, the modal analysis is performed again to compute the dynamic properties of the structure, which are natural frequency and the mode shapes under wind loading. The natural frequency is given in Table 7.5, and mode shapes are shown in Figure 7.5.

Table 7.5: Natural frequencies of the numerical model FEM4.

Mode	Natural Frequency [Hz]	Mode Shape
1	0.81	X (no sign inversion)
2	0.81	Y (no sign inversion)
3	2.58	X (1 sign inversion)
4	2.79	Y (1 sign inversion)
5	3.21	T (no sign inversion)

Under wind loading, the structure's natural frequency decreases because second-order effects, such as P-Delta effects in MIDAS, introduce additional bending moments from axial forces, effectively reducing the structure's stiffness while its mass remains unchanged. Since the natural frequency is proportional to the square root of the stiffness-to-mass ratio, a reduction in stiffness results in lower natural frequencies, thereby altering the structure's dynamic behaviour.

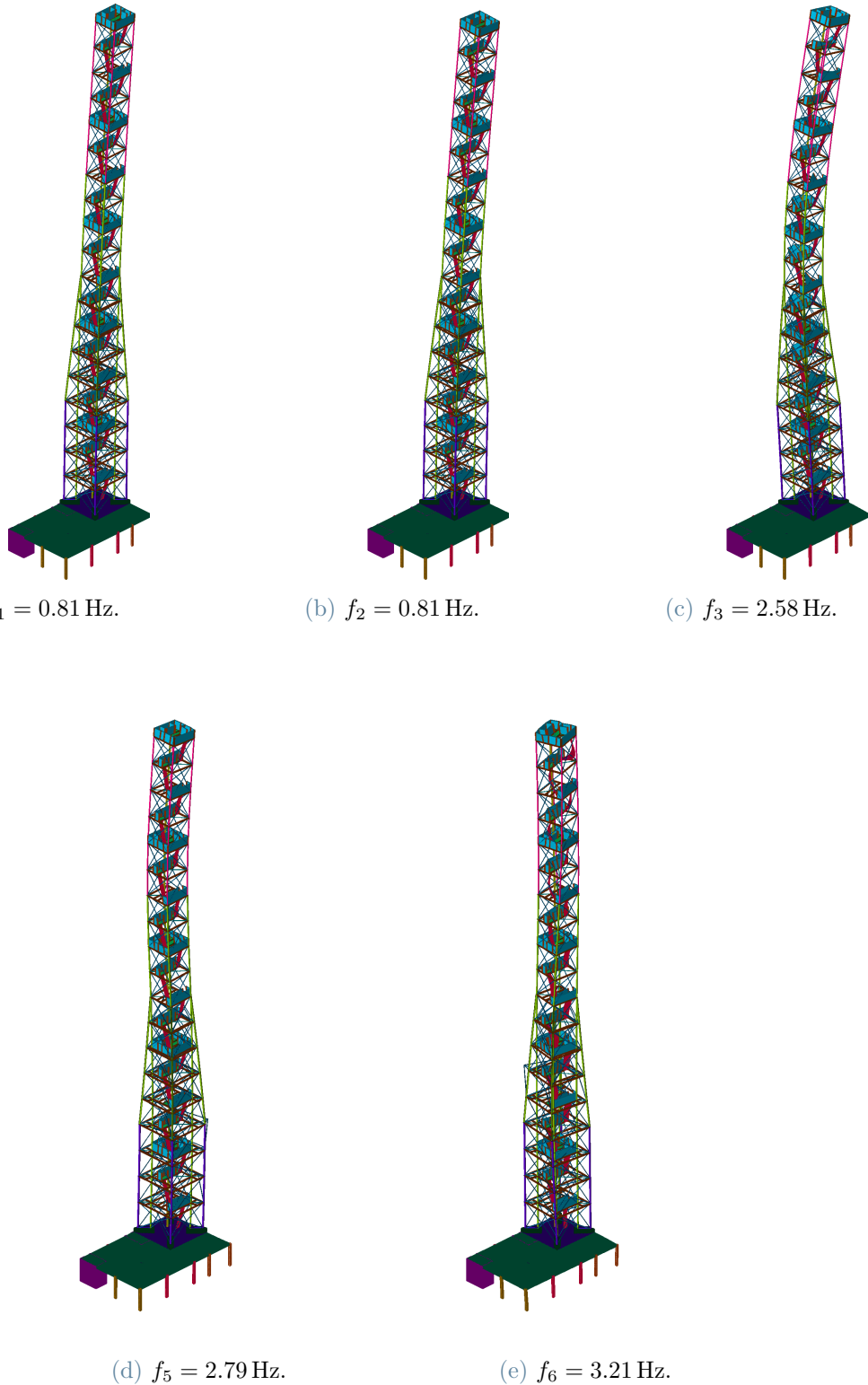


Figure 7.5: Mode shapes of a global tower model under wind loading.



## 8 | Conclusion and Way Forward

The increasing number of significant structures still in use beyond their intended lifespans highlights the growing necessity for practical tools to evaluate their structural integrity. By integrating reliable Finite Element (FE) model updating into a Structural Health Monitoring (SHM) system, the quality of data used to assess the integrity of monitored structures can be significantly improved. This thesis presents the implementation of FE model updating using the Douglas-Reid (DR) framework. Additionally, the proposed method has been rigorously analyzed and tested across various updating scenarios. The outcomes of these tests demonstrate the potential of this approach as a valuable asset for SHM.

The primary goal of this research is to assess the effectiveness of combining Operational Modal Analysis (OMA) and Finite Element Model Updating (FEMU) techniques to achieve accurate FE models in support of digital twin development. A FE model of the *JRC Atmospheric Tower* was created, and the dynamic properties of the structure were identified using OMA techniques based on wireless sensor data collected at different levels of the structure. FEMU was then performed using the semi-optimized DR method, where the updating parameters were optimized, and the updated values were computed by minimizing the objective function.

Three distinct FE models, **FEM1**, **FEM2**, and **FEM3**, were considered in this work. Two initial models (**FEM1** and **FEM2**) were created with different constraint conditions (fixed constraints and elastic spring support), as the type of constraint applied significantly impacts the model's dynamic behaviour.

A manual tuning process was conducted to estimate the stiffness of the base springs by minimizing the average frequency error. A sensitivity analysis was also performed to assess how model parameters influence the dynamic behaviour of the structure, identifying the most critical parameters for model updating.

The final updated model, **FEM2**, takes into account the effects of different stiffness reductions in the joints. The numerical response of the model was compared with the experimental results, and the final updated mechanical properties of the updating parameters

were computed.

The optimized parameters yielded reasonable values that were consistent with the local results. The model updating process resulted in only minor variations in the modulus of elasticity, supporting the estimation of unstressed structural elements. The change in the updated modulus of elasticity was attributed to the reduction in stiffness models.

The accuracy of results obtained through the DR method tends to decrease as the level of under-determinism in the updating problem increases. This is particularly relevant in SHM, where the number of sensors installed on a structure is limited, and larger structures often require more updating parameters. Additionally, increasing noise levels in experimental modal data can negatively affect the accuracy of updating results. Given the inherent noise in modal properties identified using OMA techniques, the effectiveness of a finite element model updating method is primarily influenced by its ability to manage disturbances caused by data noise.

This thesis outlines a general procedure for analyzing raw data acquired during an extensive local monitoring campaign. The integrated strategy aims to develop a reliable FE model.

## Suggestions for Future Work

This thesis aims to demonstrate the effectiveness and reliability of the DR method for updating FE models. Several specific aspects of this method could be explored in greater detail. Here are some suggestions for potential next steps to further enhance the DR FE model updating process:

- In this study, a static wind analysis was performed to assess the structural response under wind loading. For future research, it would be valuable to undertake a comprehensive nonlinear analysis of the structure subjected to both wind and seismic loads. This approach would capture complex behaviours such as material and geometric nonlinearity, inelastic deformations, and the interactions between wind-induced forces and seismic excitations. By considering these factors, the analysis would provide a more realistic depiction of the structure's performance under extreme loading conditions and help inform more robust design recommendations.
- When updating real structures, the regularization parameters should be heuristically selected. Understanding the impact of these parameters on the updating results is an essential area for future research. Ideally, future work could provide guidelines for selecting appropriate regularization parameters.

- In this thesis, the DR model updating approach yielded only point estimates for the updating parameters. Investigating methods to quantify the uncertainty associated with these estimates would be beneficial. This exploration could be extended to analyze residuals related to various experimental modal data points.
- The experimental modal data used in this study were obtained using Operational Modal Analysis (OMA). It is important to evaluate the performance of the DR model updating method when applied to modal data derived from Experimental Modal Analysis (EMA). For better accuracy, it is recommended to first use modal data from prototype structures, as their physical properties are more specific and easier to control compared to those of larger structures.



# Bibliography

- [1] *Front Matter*, pages i–xxi. John Wiley & Sons, Ltd, 2010. ISBN 9781118032428. doi: <https://doi.org/10.1002/9781118032428.fmatter>. URL <https://onlinelibrary.wiley.com/doi/abs/10.1002/9781118032428.fmatter>.
- [2] Identification of dynamic displacements and modal frequencies of a medium-span suspension bridge using multimode gnss processing. *Engineering Structures*, 81:432–443, 2014. ISSN 0141-0296. doi: <https://doi.org/10.1016/j.engstruct.2014.10.010>. URL <https://www.sciencedirect.com/science/article/pii/S0141029614006154>.
- [3] *Frequency-Domain Identification*, chapter 10, pages 261–280. John Wiley & Sons, Ltd, 2015. ISBN 9781118535141. doi: <https://doi.org/10.1002/9781118535141.ch10>. URL <https://onlinelibrary.wiley.com/doi/abs/10.1002/9781118535141.ch10>.
- [4] N. A. Z. Abdullah, M. S. M. Sani, M. M. Rahman, and I. Zaman. A review on model updating in structural dynamics. In *IOP Conference Series: Materials Science and Engineering*, volume 100, page 012015. IOP Publishing, 2015.
- [5] P. Andersen, R. Brincker, and P. H. Kirkegaard. *Identification of Civil Engineering Structures using Vector ARMA Models*, pages 19–38. Number R9808 in R / Institut for Bygningsteknik. Dept. of Building Technology and Structural Engineering, Aalborg University, Denmark, 1998.
- [6] A. L. Caballero Arcos. *Finite element model updating for civil engineering structures*. PhD thesis, Technical University of Denmark, 2022.
- [7] V. Arora, P. Hoogt, R. Aarts, and A. de Boer. Identification of stiffness and damping characteristics of axial airfoil bearings. *International Journal of Mechanics and Materials in Design*, 7(3):231–243, 2011. doi: 10.1007/s10999-011-9161-7.
- [8] P. Asadollahi, Y. Huang, and J. Li. Bayesian finite element model updating and assessment of cable-stayed bridges using wireless sensor data. *Sensors*, 18(9):3057, 2018. doi: <https://doi.org/10.3390/s18093057>.
- [9] S. Atamturktur, F. Hemez, and C. Unal. Calibration under uncertainty for finite element models of masonry monuments. Technical report, Los Alamos National Laboratory (LANL), Los Alamos, NM (United States), 2010.

- [10] C. Baggio, V. Sabbatini, S. Santini, and C. Sebastiani. Comparison of different finite element model updates based on experimental onsite testing: The case study of san giovanni in macerata. *Journal of Civil Structural Health Monitoring*, 11:767–790, 2021.
- [11] J. L. Beck and Ka-Veng Yuen. Model selection using response measurements: Bayesian probabilistic approach. *Journal of Engineering Mechanics*, 130(2):192–203, 2004. doi: 10.1061/(ASCE)0733-9399(2004)130:2(192). URL <https://ascelibrary.org/doi/abs/10.1061/%28ASCE%290733-9399%282004%29130%3A2%28192%29>.
- [12] J. K. Blitzstein and J. Hwang. *Introduction to Probability*. 2019.
- [13] G. D. Bocchino, F. Perotti, F. Bono, and L. Martinelli. Structural health monitoring: Ec jrc atmospheric tower. 2023.
- [14] J. Bodeux and J. C. Golinval. Application of armav models to the identification and damage detection of mechanical and civil engineering structures. *Smart Materials and Structures*, 10:479, 06 2001. doi: 10.1088/0964-1726/10/3/309.
- [15] A. Brandt. *Noise and Vibration Analysis: Signal Analysis and Experimental Procedures*. EBL-Schweitzer. Wiley, 2011. ISBN 9780470978115. URL <https://books.google.it/books?id=-1DSxr1hL5sC>.
- [16] R. Brincker, L. Zhang, and P. Andersen. Modal identification from ambient responses using frequency domain decomposition. *Proceedings of the International Modal Analysis Conference - IMAC*, 1, 01 2000.
- [17] R. Brincker, C. Ventura, and P. Andersen. Damping estimation by frequency domain decomposition. *Proceedings of the International Modal Analysis Conference - IMAC*, 1, 01 2001.
- [18] R. Brincker, P. Andersen, and N. J. Jacobsen. Automated frequency domain decomposition for operational modal analysis. 01 2007.
- [19] R. Brincker, P. Olsen, S. Amador, M. Juul, A. Malekjafarian, and M. Ashory. Modal participation in multiple input ibrahim time domain identification. *Mathematics and Mechanics of Solids*, 24(1):168–180, 2019. doi: 10.1177/1081286517733034. URL <https://doi.org/10.1177/1081286517733034>.
- [20] P. Bruneau, O. Parisot, and B. Otjacques. A heuristic for the automatic parametrization of the spectral clustering algorithm. In *2014 22nd International Conference on Pattern Recognition*, pages 1313–1318, 2014. doi: 10.1109/ICPR.2014.235.
- [21] A. L. Caballero Arcos. *Finite element model updating for civil engineering structures: Applying convex optimization*. PhD thesis, 2022.
- [22] Cast3M. Cast3m. <http://www-cast3m.cea.fr/index.php?page=notices>.

- [23] Á. Bautista-De Castro, L. Sánchez-Aparicio, L. Ramos, J. Sena-Cruz, and D. González-Aguilera. Integrating geomatic approaches, operational modal analysis, advanced numerical and updating methods to evaluate the current safety conditions of the historical bôco bridge. *Construction and Building Materials*, 158, 11 2017. doi: 10.1016/j.conbuildmat.2017.10.084.
- [24] M. Chandravanshi and A. Mukhopadhyay. Analysis of variations in vibration behavior of vibratory feeder due to change in stiffness of helical springs using fem and ema methods. *Journal of the Brazilian Society of Mechanical Sciences and Engineering*, 39, 03 2017. doi: 10.1007/s40430-017-0767-z.
- [25] J. Chiachío, M. Chiachío, A. Saxena, S. Sankararaman, G. Rus, and K. Goebel. Bayesian model selection and parameter estimation for fatigue damage progression models in composites. *International Journal of Fatigue*, 70:361–373, 2015. doi: <https://doi.org/10.1016/j.ijfatigue.2014.08.003>.
- [26] I. D. Craiu and M. Nedelcu. *Combining iFEM and GBT for accurate shape sensing and damage detection in truncated conical shells with circular cross-section*. PhD thesis, 2024. URL <https://doi.org/10.1016/j.oceaneng.2024.118811>.
- [27] B. M. Douglas and W. H. Reid. Dynamic tests and system identification of bridges. *Journal of the Structural Division*, 108(10):2295–2312, 1982. doi: 10.1061/JSDEAG.0006057. URL <https://ascelibrary.org/doi/abs/10.1061/JSDEAG.0006057>.
- [28] A. Elyamani. Integrated monitoring and structural analysis strategies for the study of large historical construction. application to mallorca cathedral. Phd thesis, Technical University of Catalonia, Barcelona, 2015. URL [https://www.researchgate.net/publication/281897106\\_Integrated\\_monitoring\\_and\\_structural\\_analysis\\_strategies\\_for\\_the\\_study\\_of\\_large\\_historical\\_construction\\_Application\\_to\\_Mallorca\\_cathedral](https://www.researchgate.net/publication/281897106_Integrated_monitoring_and_structural_analysis_strategies_for_the_study_of_large_historical_construction_Application_to_Mallorca_cathedral).
- [29] A. Elyamani and P. Roca Fabregat. A review on the study of historical structures using integrated investigation activities for seismic safety assessment. part ii: model updating and seismic analysis. *Scientific Culture*, 4(1):29–51, 2018.
- [30] M. Esposito. *A novel shape sensing approach based on the coupling of Modal Virtual Sensor Expansion and iFEM: Numerical and experimental assessment on composite stiffened structures*. PhD thesis, 2024. URL <https://doi.org/10.1016/j.compstruc.2024.107520>.
- [31] E. Forstner and H. Wenzel. The application of data mining in bridge monitoring projects: Exploiting time series data of structural health monitoring. *2011 22nd International Workshop on Database and Expert Systems Applications*, pages 297–301, 2011. URL <https://api.semanticscholar.org/CorpusID:15613220>.
- [32] M. Friswell and J.E. Mottershead. *Finite Element Model Updating in Structural Dynamics*.

- Solid Mechanics and Its Applications. Springer Netherlands, 2013. ISBN 9789401585088. URL <https://books.google.it/books?id=WGgPCQAAQBAJ>.
- [33] M.I. Friswell. The adjustment of structural parameters using a minimum variance estimator. *Mechanical Systems and Signal Processing*, 3(2):143–155, 1989. ISSN 0888-3270. doi: [https://doi.org/10.1016/0888-3270\(89\)90013-7](https://doi.org/10.1016/0888-3270(89)90013-7). URL <https://www.sciencedirect.com/science/article/pii/0888327089900137>.
  - [34] H. P. Gavin, R. Morales, and K. Reilly. Drift-free integrators. *Review of Scientific Instruments*, 69(5):2171–2175, 05 1998. ISSN 0034-6748. doi: 10.1063/1.1148918. URL <https://doi.org/10.1063/1.1148918>.
  - [35] C. Gentile. Modal and structural identification of a r.c. arch bridge. *Structural Engineering and Mechanics*, 22:53–70, 01 2006. doi: 10.12989/sem.2006.22.1.053.
  - [36] C. Gentile, A. Saisi, and A. Cabboi. Structural identification of a masonry tower based on operational modal analysis. *International Journal of Architectural Heritage*, 9(2):98–110, 2015.
  - [37] M. Ghalishooyan and A. Shooshtari. Operational modal analysis techniques and their theoretical and practical aspects: A comprehensive review and introduction. *6th International Operational Modal Analysis Conference, IOMAC 2015*, 01 2015.
  - [38] Y. Govers and M. Link. Stochastic model updating—covariance matrix adjustment from uncertain experimental modal data. *Mechanical Systems and Signal Processing*, 24, 04 2010. doi: 10.1016/j.ymssp.2009.10.006.
  - [39] P. C. Hansen. *Discrete inverse problems. Insight and algorithms*, volume 7. 01 2010. doi: 10.1137/1.9780898718836.
  - [40] L. Hermans and H. Van Der Auweraer. Modal testing and analysis of structures under operational conditions: Industrial applications. *Mechanical Systems and Signal Processing*, 13(2):193–216, 1999. ISSN 0888-3270. doi: <https://doi.org/10.1006/mssp.1998.1211>. URL <https://www.sciencedirect.com/science/article/pii/S0888327098912110>.
  - [41] G. W. Housner, L. A. Bergman, T. K. Caughey, A. G. Chassiakos, R. O. Claus, S. F. Masri, R. E. Skelton, T. T. Soong, B. F. Spencer, and J. T. P. Yao. Structural control: Past, present, and future. *Journal of Engineering Mechanics*, 123(9):897–971, September 1997. ISSN 0733-9399. doi: 10.1061/(ASCE)0733-9399(1997)123:9(897).
  - [42] R. A. Ibrahim. Engineering applications of correlation and spectral analysis- julius s. bendat and allan g. piersol. *AIAA Journal*, 31(11):2190–2191, 1993. doi: 10.2514/3.49131. URL <https://doi.org/10.2514/3.49131>.
  - [43] G. James, T. Carne, and J. Laufer. The natural excitation technique (next) for modal

- parameter extraction from operating structures. *Journal of Analytical and Experimental Modal Analysis*, 10, 01 1995.
- [44] J. Jang and A. W. Smyth. Model updating of a full-scale fe model with nonlinear constraint equations and sensitivity-based cluster analysis for updating parameters. *Mechanical Systems and Signal Processing*, 83:337–355, 2017. ISSN 0888-3270. doi: <https://doi.org/10.1016/j.ymssp.2016.06.018>. URL <https://www.sciencedirect.com/science/article/pii/S0888327016302023>.
  - [45] A. Jindal and M. Liu. Networked computing in wireless sensor networks for structural health monitoring. *IEEE/ACM Transactions on Networking*, 20(4):1203–1216, 2012. doi: 10.1109/TNET.2011.2175450.
  - [46] A. Kaveh. Optimizing the conditioning of structural flexibility matrices. *Computers & Structures*, 41(3):489–494, 1991. ISSN 0045-7949. doi: [https://doi.org/10.1016/0045-7949\(91\)90142-9](https://doi.org/10.1016/0045-7949(91)90142-9). URL <https://www.sciencedirect.com/science/article/pii/0045794991901429>.
  - [47] A. Kaveh and I. Ghaderi. Conditioning of structural stiffness matrices. *Computers & Structures*, 63(4):719–725, 1997. ISSN 0045-7949. doi: [https://doi.org/10.1016/S0045-7949\(96\)00073-9](https://doi.org/10.1016/S0045-7949(96)00073-9). URL <https://www.sciencedirect.com/science/article/pii/S0045794996000739>. Computing in Civil and Structural Engineering.
  - [48] B. H. Kim and N. Stubbs. A new method to extract modal parameters using output-only responses. *Journal of Sound and Vibration - J SOUND VIB*, 282:215–230, 04 2005. doi: 10.1016/j.jsv.2004.02.026.
  - [49] V. Kumar and R. Aarts. *Finite-element-model Updating Using a Multi-criteria Method*, pages 143–160. Springer London, 2010. ISBN 978-1-84996-323-7. doi: [https://doi.org/10.1007/978-1-84996-323-7\\_8](https://doi.org/10.1007/978-1-84996-323-7_8).
  - [50] T. P. Le and P. Paultre. Modal identification based on the time-frequency domain decomposition of unknown-input dynamic tests. *International Journal of Mechanical Sciences*, 71:41–50, 06 2013. doi: 10.1016/j.ijmecsci.2013.03.005.
  - [51] J. J. Lee and M. Shinozuka. Real-time displacement measurement of a flexible bridge using digital image processing techniques. *Experimental Mechanics*, 46:105–114, 02 2006. doi: 10.1007/s11340-006-6124-2.
  - [52] F. Liu, J. Wu, F. Gu, and Andrew Ball. An introduction of a robust oma method: Cosssi and its performance evaluation through the simulation and a case study. *Shock and Vibration*, 2019:1–14, 01 2019. doi: 10.1155/2019/6581516.
  - [53] F. Magalhães and Alvaro Cunha. Explaining operational modal analysis with data from an

- arch bridge. *Mechanical Systems and Signal Processing - MECH SYST SIGNAL PROCESS*, 25:1431–1450, 07 2011. doi: 10.1016/j.ymssp.2010.08.001.
- [54] C. Mares, J. Mottershead, and M. Friswell. Stochastic model updating: Part 1—theory and simulated example. *Mechanical Systems and Signal Processing*, 20:1674–1695, 10 2006. doi: 10.1016/j.ymssp.2005.06.006.
- [55] T. Marwala, I. Boulkaibet, and S. Adhikari. *Probabilistic finite element model updating using Bayesian statistics: Applications to aeronautical and mechanical engineering*. John Wiley & Sons, 2016.
- [56] M. H. Masjedian and M. Keshmiri. A review on operational modal analysis researches: Classification of methods and applications. *IOMAC 2009 - 3rd International Operational Modal Analysis Conference*, pages 707–716, 01 2009.
- [57] MIDAS IT. Midas gen version 1.1 software, 2015. URL <https://www.midasoft.com/>.
- [58] R.S. Minette, S.F. SilvaNeto, L.A. Vaz, and U.A. Monteiro. Experimental modal analysis of electrical submersible pumps. *Ocean Engineering*, 124:168–179, 2016. ISSN 0029-8018. doi: <https://doi.org/10.1016/j.oceaneng.2016.07.054>. URL <https://www.sciencedirect.com/science/article/pii/S0029801816303067>.
- [59] B. De Moor, P. Van Overschee, and P. Suykens. Subspace algorithms for system identification and stochastic realization. 1, 10 1998.
- [60] J. Mottershead and M. Friswell. Model updating in structural dynamics: A survey. *Journal of Sound and Vibration - J SOUND VIB*, 167:347–375, 1993. doi: 10.1006/jsvi.1993.1340.
- [61] J. Mottershead, M. Link, and M. Friswell. The sensitivity method in finite element model updating: A tutorial. *Mechanical Systems and Signal Processing*, 25:2275–2296, 10 2011. doi: 10.1016/j.ymssp.2010.10.012.
- [62] Y. Q. Ni, Y. Xia, W. Y. Liao, and J. M. Ko. Technology innovation in developing the structural health monitoring system for guangzhou new tv tower. *Structural Control and Health Monitoring*, 16(1):73–98, February 2009. ISSN 1545-2255, 1545-2263. doi: 10.1002/stc.303. URL <https://onlinelibrary.wiley.com/doi/10.1002/stc.303>.
- [63] P. Van Overschee and B. De Moor. Subspace algorithms for the stochastic identification problem. *Automatica*, 29(3):649–660, 1993. ISSN 0005-1098. doi: [https://doi.org/10.1016/0005-1098\(93\)90061-W](https://doi.org/10.1016/0005-1098(93)90061-W). URL <https://www.sciencedirect.com/science/article/pii/000510989390061W>.
- [64] P. Van Overschee and B. De Moor. N4sid: Subspace algorithms for the identification of combined deterministic-stochastic systems. *Automatica*, 30(1):75–93, 1994. ISSN 0005-1098. doi: [https://doi.org/10.1016/0005-1098\(94\)90230-5](https://doi.org/10.1016/0005-1098(94)90230-5). URL <https://www.sciencedirect.com/science/article/pii/0005109894902305>.

- [com/science/article/pii/0005109894902305](https://www.sciencedirect.com/science/article/pii/0005109894902305). Special issue on statistical signal processing and control.
- [65] P. Van Overschee and B. De Moor. Continuous-time frequency domain subspace system identification. *Signal Processing*, 52(2):179–194, 1996. ISSN 0165-1684. doi: [https://doi.org/10.1016/0165-1684\(96\)00052-7](https://doi.org/10.1016/0165-1684(96)00052-7). URL <https://www.sciencedirect.com/science/article/pii/0165168496000527>. Subspace Methods, Part II: System Identification.
  - [66] P. Van Overschee and B. De Moor. *Subspace identification for linear systems: Theory—Implementation—Applications*. Springer Science & Business Media, 2012.
  - [67] Aloisio A. Rosso M. M. & Sotiropoulos S. Pasca, D. P. Pyoma and pyoma\_gui: A python module and software for operational modal analysis. *SoftwareX*, 20:101216, December 2022. doi: 10.1016/j.softx.2022.101216. URL <https://doi.org/10.1016/j.softx.2022.101216>.
  - [68] B. Peeters and G. De Roeck. Reference-based stochastic subspace identification for output-only modal analysis. *Mechanical Systems and Signal Processing*, 13(6):855–878, 1999. ISSN 0888-3270. doi: <https://doi.org/10.1006/mssp.1999.1249>. URL <https://www.sciencedirect.com/science/article/pii/S0888327099912499>.
  - [69] B. Peeters and G. De Roeck. Stochastic system identification for operational modal analysis: A review. *Journal of Dynamic Systems Measurement and Control-transactions of The Asme - J Dyn Syst Meas Contr*, 123, 12 2001. doi: 10.1115/1.1410370.
  - [70] F. Peña, P. B. Lourenço, N. Mendes, and D. V. Oliveira. Numerical models for the seismic assessment of an old masonry tower. *Engineering Structures*, 32(5):1466–1478, 2010.
  - [71] S. Pietrzko and R. Cantieni. Modal testing of a steel/concrete composite bridge with a servo-hydraulic shaker. *Proc. 14th Int. Modal Analysis Conference*, 01 1996.
  - [72] S. Qin, J. Kang, and Q. Wang. Operational modal analysis based on subspace algorithm with an improved stabilization diagram method. *Shock and Vibration*, 2016:1–10, 01 2016. doi: 10.1155/2016/7598965.
  - [73] C. Rainieri and G. Fabbrocino. *Operational modal analysis of civil engineering structures: An introduction and guide for applications*. Springer, New York, NY, 2014. ISBN 978-1-4939-0766-3. doi: 10.1007/978-1-4939-0767-0. URL <https://link.springer.com/10.1007/978-1-4939-0767-0>.
  - [74] C. Rainieri, G. Fabbrocino, and E. Cosenza. "operational modal analysis and earthquake engineering". 01 2009.
  - [75] E. Reynders. System identification methods for (operational) modal analysis: Review and

- comparison. *Archives of Computational Methods in Engineering*, 19:51–124, 03 2012. doi: 10.1007/s11831-012-9069-x.
- [76] E. Reynders and K. Maes. Uncertainty quantification of modal characteristics identified from frequency-domain stochastic subspace identification. *Procedia Engineering*, 199:996–1001, 12 2017. doi: 10.1016/j.proeng.2017.09.231.
- [77] Fabbrocino G. & Rainieri C. Rosati, I. A discussion about the douglas-reid model updating method and its prospective application to continuous vibration-based shm of a historical building. *Engineering Structures*, 273:115058, 2022. doi: <https://doi.org/10.1016/j.engstruct.2022.115058>. URL <https://doi.org/10.1016/j.engstruct.2022.115058>.
- [78] S. Santini, C. Baggio, E. Da Gai, V. Sabbatini, and C. Sebastiani. Automated model updating of a masonry historical church based on operational modal analysis: the case study of san giovanni in macerata. Master’s thesis. URL [https://www.scipedia.com/public/Santini\\_et\\_al\\_2021a](https://www.scipedia.com/public/Santini_et_al_2021a).
- [79] Dlubal Software. Load zones for snow, wind, earthquake: Wind – uni en 1991-1-4. [https://www.dlubal.com/en/load-zones-for-snow-wind-earthquake/wind-uni-en-1991-1-4.html?srsltid=AfmB0orlsyzau94H45o7sjMzvCfdGP\\_P1oaSnCZUj10YzCHqni5BegAV](https://www.dlubal.com/en/load-zones-for-snow-wind-earthquake/wind-uni-en-1991-1-4.html?srsltid=AfmB0orlsyzau94H45o7sjMzvCfdGP_P1oaSnCZUj10YzCHqni5BegAV).
- [80] KOMA Development Team. Welcome to the koma documentation - koma 1.0.1, 2024. URL <https://koma.readthedocs.io/en/latest/>. Retrieved December 12, 2024.
- [81] PYOMAC Development Team. Pyomac - operational modal analysis of civil structures, 2024. URL <https://pyomac.readthedocs.io/en/latest/>. Retrieved December 12, 2024.
- [82] S. Thenozhi, W. Yu, and R. Garrido. A novel numerical integrator for velocity and position estimation. *Transactions of the Institute of Measurement and Control*, 35(6):824–833, 2013. doi: 10.1177/0142331213476987. URL <https://doi.org/10.1177/0142331213476987>.
- [83] B. Titurus and M. I. Friswell. Regularization in model updating. *International Journal for Numerical Methods in Engineering*, 75(4):440–478, 2008. doi: <https://doi.org/10.1002/nme.2257>. URL <https://onlinelibrary.wiley.com/doi/abs/10.1002/nme.2257>.
- [84] N. J. van Eck and L. Waltman. Vosviewer: A computer program for bibliometric mapping. *Scientometrics*, 84(2):523–538, 2010. ISSN 0138-9130, 1588-2861. doi: 10.1007/s11192-009-0146-3. URL <https://link.springer.com/10.1007/s11192-009-0146-3>.
- [85] Y. L. Xu and Baiyu Chen. Integrated vibration control and health monitoring of building structures using semi-active friction dampers: Part i—methodology. *Engineering Structures*, 30:1789–1801, 07 2008. doi: 10.1016/j.engstruct.2007.11.013.
- [86] T. Yin, H.P. Zhu, and S.J. Fu. Model selection for dynamic reduction-based structural health monitoring following the bayesian evidence approach. *Mechanical Systems*

- and *Signal Processing*, 127:306–327, 2019. ISSN 0888-3270. doi: <https://doi.org/10.1016/j.ymssp.2019.03.009>. URL <https://www.sciencedirect.com/science/article/pii/S0888327019301621>.
- [87] Z. Yuan, P. Liang, T. Silva, K. Yu, and J. E. Mottershead. Parameter selection for model updating with global sensitivity analysis. *Mechanical Systems and Signal Processing*, 115: 483–496, 2019. ISSN 0888-3270. doi: <https://doi.org/10.1016/j.ymssp.2018.05.048>. URL <https://www.sciencedirect.com/science/article/pii/S0888327018303078>.
- [88] K. V. Yuen. Recent developments of bayesian model class selection and applications in civil engineering. *Structural Safety*, 32(5):338–346, 2010. ISSN 0167-4730. doi: <https://doi.org/10.1016/j.strusafe.2010.03.011>. URL <https://www.sciencedirect.com/science/article/pii/S0167473010000305>.
- [89] F. B. Zahid, O. Chao, and S. Khoo. A review of operational modal analysis techniques for in-service modal identification. *Journal of the Brazilian Society of Mechanical Sciences and Engineering*, 42, 08 2020. doi: 10.1007/s40430-020-02470-8.
- [90] L. Zhang, R. Brincker, and P. Andersen. An overview of operational modal analysis: Major development and issues. *Proceedings of the 1st International Operational Modal Analysis Conference, IOMAC 2005*, 01 2005.
- [91] L. Zhang, T. Wang, and Y. Tamura. A frequency–spatial domain decomposition (fsdd) method for operational modal analysis. *Mechanical Systems and Signal Processing*, 24(5): 1227–1239, 2010. ISSN 0888-3270. doi: <https://doi.org/10.1016/j.ymssp.2009.10.024>. URL <https://www.sciencedirect.com/science/article/pii/S0888327009003744>. Special Issue: Operational Modal Analysis.
- [92] A. Zona. Vision-based vibration monitoring of structures and infrastructures: An overview of recent applications. *Infrastructures*, 6:4, 12 2020. doi: 10.3390/infrastructures6010004.
- [93] T. Zordan, B. Briseghella, and T. Liu. Finite element model updating of a tied-arch bridge using douglas-reid method and rosenbrock optimization algorithm. *Journal of Traffic and Transportation Engineering (English Edition)*, 1(4):280–292, 2014.



# A | Appendix A

Table A.1: Keyword thesaurus of VOSviewer.

No.	Keyword	Occurrences
1	acoustic emission	8
2	ambient vibration	10
3	artificial neural network	7
4	computer vision	7
5	condition assessment	10
6	convolutional neural network	9
7	corrosion	5
8	crack detection	9
9	damage	5
10	damage detection	85
11	damage identification	26
12	damage index	6
13	damage localization	14
14	data fusion	8
15	deep learning	20
16	deformation	5
17	dynamic characteristics	6
18	earthquake	7
19	experimental modal analysis	5
20	fatigue	7
21	feature extraction	6
22	field measurement	13
23	finite element analysis	6
24	finite element model	7
25	genetic algorithm	5
26	guided waves	6

Continued on next page

No.	Keyword	Occurrences
27	health monitoring	23
28	high-rise building	16
29	high-rise buildings	11
30	high-rise structure	5
31	image processing	5
32	kalman filter	6
33	machine learning	21
34	modal analysis	7
35	modal identification	11
36	modal strain energy	5
37	model updating	18
38	monitoring	6
39	numerical simulation	5
40	operational modal analysis	16
41	optimal sensor placement	12
42	optimization	10
43	principal component analysis	5
44	seismic interferometry	5
45	sensor	6
46	shaking table test	5
47	shanghai tower	7
48	shm	20
49	steel frame	11
50	steel structure	12
51	steel structures	18
52	stochastic subspace identification	8
53	strain	7
54	structural damage detection	9
55	structural damage identification	5
56	structural dynamics	9
57	structural health monitoring	328
58	structural health monitoring (shm)	29
59	structural system identification	10
60	super high-rise building	8
61	super-tall building	8

Continued on next page

No.	Keyword	Occurrences
62	supertall building	6
63	system identification	27
64	tall building	14
65	tall buildings	13
66	typhoon	12
67	uncertainty quantification	6
68	vibration	5
69	wave propagation in buildings	6
70	wavelet analysis	7
71	wind effect	8
72	wind tunnel test	6
73	wireless sensor network	10



# B | Appendix B

Table B.1: List of acronyms.

Acronym	Definition
<b>FEM</b>	Finite Element Method
<b>FE</b>	Finite Element
<b>IoT</b>	Internet of Things
<b>JRC</b>	Joint Research Centre
<b>OMA</b>	Operational Modal Analysis
<b>SHM</b>	Structural Health Monitoring
<b>EC</b>	European Commission
<b>FEMU</b>	Finite Element Model Updating
<b>DR</b>	Douglas-Reid
<b>EMA</b>	Experimental Modal Analysis
<b>IDFT</b>	Inverse Discrete Fourier Transform
<b>DFT</b>	Discrete Fourier Transform
<b>FFT</b>	Fast Fourier Transform
<b>TDD</b>	Time Domain Decomposition
<b>SDOF</b>	Single Degree of Freedom System
<b>MDOF</b>	Multi Degree of Freedom System
<b>PP</b>	Peak Picking
<b>SVD</b>	Singular Value Decomposition
<b>PSD</b>	Power Spectral Density
<b>FDD</b>	Frequency Domain Decomposition
<b>EFDD</b>	Enhanced Frequency Domain Decomposition
<b>FSDD</b>	Frequency Spatial Domain Decomposition
<b>SSI</b>	Stochastic Subspace Identification
<b>SSI-Cov</b>	Covariance-Driven Stochastic Subspace Identification
<b>SSI-Dat</b>	Data-Driven Stochastic Subspace Identification

Continued on next page

Acronym	Definition
<b>CoS-SSI</b>	Component-Specific Stochastic Subspace Identification
<b>iSMA</b>	Impact Synchronous Modal Analysis
<b>FRF</b>	Frequency Response Function
<b>NExT</b>	Natural Excitation Technique
<b>ARMA</b>	Auto-Regressive Moving Average
<b>CVA</b>	Canonical Variant Analysis
<b>UPC</b>	Unweighted Principal Component
<b>PC</b>	Principal Component
<b>CFM</b>	Complex Frequency Method
<b>MAC</b>	Modal Assurance Criterion
<b>MPC</b>	Modal Phase Collinearity
<b>MPD</b>	Mean Phase Deviation

# List of Figures

2.1	Yearly trend of structural health monitoring (SHM). . . . .	8
2.2	Yearly trend of model updating in (SHM). . . . .	9
2.3	Yearly trend of model updating tall structures in (SHM). . . . .	10
2.4	VOSviewer analysis map on keyword co-occurrence of Structural Health Monitoring (SHM). . . . .	11
2.5	VOSviewer analysis map on important keyword co-occurrence of Structural Health Monitoring (SHM). . . . .	12
2.6	VOSviewer analysis map on keyword co-occurrence of modal analysis of tall and steel structure. . . . .	13
2.7	VOSviewer analysis map on keyword co-occurrence of model updating of tall structure. . . . .	15
2.8	VOSviewer analysis map on keyword co-occurrence of damage detection in structure. .	16
3.1	3D model of dual design structure. . . . .	42
3.2	Shorter caption . . . . .	43
3.3	Shorter caption . . . . .	44
3.4	Initial numerical model of testing structure. . . . .	48
3.5	Shorter caption . . . . .	50
3.6	Predicted natural frequencies for ( $E_c$ ). . . . .	53
3.7	Minimization of objective function for ( $E_c$ ). . . . .	54
3.8	Comparison between the predicted and optimal natural frequencies with the experimental results for ( $E_c$ ). . . . .	54
3.9	Absolute error between the $E_{nom}$ and $E_{opt}$ . . . . .	55
3.10	Predicted natural frequencies for ( $EI_b$ ). . . . .	56
3.11	Minimization of objective function for ( $EI_b$ ). . . . .	57
3.12	Comparison between the predicted and optimal natural frequencies with the experimental results for ( $EI_b$ ). . . . .	57
3.13	Absolute error between the $EI_{nom}$ and $EI_{opt}$ . . . . .	58
4.1	Orientation of the tower according to the cardinal directions. . . . .	62
4.2	Plan view at the elevation of 5 m,. . . . .	64
4.3	Elevation view of the whole tower. . . . .	65

4.4	Plan view of the gridwork of beams at the elevation of 25 m. . . . .	66
4.5	Floor plans of all the levels of the tower. . . . .	67
4.6	Detail view of the <i>IPE500</i> beam connecting two corresponding columns. . . . .	68
4.7	Detail view of elevator mast. . . . .	69
4.8	Reinforced concrete vertical elements of the base building. . . . .	70
4.9	Detail plan view of reinforcement at the roof of the base building. . . . .	71
4.10	Sectional view of the arrangement of anchorage bolts within the concrete shoes. .	71
4.11	Sectional view of the base building. . . . .	72
4.12	Floor plans of all the levels of the tower. . . . .	73
4.13	Reference frame for sensors along the tower. . . . .	74
4.14	Reference frame for dynamics assessment during the delivery phase. . . . .	76
4.15	Stairs for typical floors in model. . . . .	78
4.16	Parapets for floor at elevation 20m. . . . .	79
4.17	Reference frame adopted for the system. . . . .	80
4.18	Numerical model of the tower. . . . .	81
4.19	Numerical model of the base building. . . . .	84
4.20	Numerical model of the complete structure. . . . .	87
4.21	Deformed configuration of the structure under gravity loading. . . . .	88
4.22	Global mode shapes of a complete structure under gravity. . . . .	91
5.1	Zero-baseline correction of recorded signal. . . . .	93
5.1	Detrending by different rolling averages. . . . .	95
5.2	Detrending of the same signal by three fitting polynomials. . . . .	96
5.3	Deternding by Butterworth highpass filter signal for 10 min. . . . .	97
5.4	Comparison of smoothing technique with different methods. . . . .	98
5.4	Power Spectral Density (PSDs) from tri-axial accelerogram. . . . .	101
5.5	SVD frequency plot derived from PSD analysis. . . . .	103
5.6	Mode Shape Identification Using PyOMA's EFDD Method. . . . .	104
5.7	Modal stabilisation diagram using Cov-SSI in PyOMA. . . . .	105
5.8	Mode shape identification using PyOMA's Cov-SSI method. . . . .	106
5.9	Modal Assurance Criterion (MAC) matrix for EFDD results using PyOMA. . . . .	108
5.10	Modal Assurance Criterion (MAC) matrix for Cov-SSI results using PyOMA. . . . .	109
6.1	Workflow of model updating process. . . . .	113
6.2	Frequency error analysis with varying stiffness in elastic spring supports. . . . .	115
6.3	Total sensitivities of parameters. . . . .	117
6.4	End sections in FEM for vertical truss, columns, and beams. . . . .	121
6.5	Effect of joint bending stiffness reduction on natural frequency. . . . .	122
6.6	Variation in Young's modulus for each member of the steel truss tower after model updating, with updated values obtained from FEM2. . . . .	123

7.1	Wind zoning of Lombardy region. . . . .	125
7.2	Exposure coefficient w.r.t height. . . . .	129
7.3	Static wind load calculation (Eurocode 1 - EN 1991-1-4) in kN. . . . .	131
7.4	Deformed shape of the tower under wind loading on global Y-direction. . . . .	132
7.5	Mode shapes of a global tower model under wind loading. . . . .	135



# List of Tables

2.1	Summary of different OMA techniques with their pros and cons.	39
3.1	Table of members geometry.	44
3.2	Concrete cylindrical strength (MPa).	45
3.3	Strength and ultimate elongation of steel bars.	46
3.4	Experimental natural frequencies of the structure under its self-weight.	47
3.5	Properties of different section types.	47
3.6	Mode shape properties.	49
3.7	The first updating parameter is $E_c$ .	53
3.8	The second updating parameter is $EI_b$ .	56
4.1	Sensor information for dynamic behaviour analysis.	63
4.2	Dynamic analysis results during the delivery phase.	77
4.3	Section properties for structural analysis.	78
4.4	Natural frequencies of the numerical model of the tower.	82
4.5	Natural frequencies of the numerical model of the base building.	84
4.6	Natural frequencies of the numerical model of the complete structure.	86
4.7	Natural frequencies and modal participation factors of the numerical model of the complete structure.	90
6.1	Comparison between experimental and numerical natural frequencies.	111
6.2	Sensitivity analysis for various tower parameters.	116
6.3	Updating parameter values after model updating in FEM1.	118
6.4	Updating parameter values after model updating in FEM2.	119
6.5	Comparison between experimental and numerical natural frequencies of FEM1.	119
6.6	Comparison between experimental and numerical natural frequencies of FEM2.	120
7.1	Basic wind velocities with Italian regions.	127
7.2	$K_r$ , $Z_0$ , and $Z_{min}$ values and categories.	128
7.3	Updating parameter values after model updating in FEM4.	133
7.4	Comparison between experimental and numerical natural frequencies of FEM4.	134
7.5	Natural frequencies of the numerical model FEM4.	134

A.1 Keyword thesaurus of VOSviewer. . . . .	151
B.1 List of acronyms. . . . .	155

## List of Symbols

Variable	Description	SI unit
$f$	Natural frequency	Hz
$E$	Young's modulus	MPa
$\rho$	Density	kg/m <sup>3</sup>
$K$	Elastic spring stiffness	kN/mm
$f_{ck}$	Characteristic strength of concrete	MPa



## Acknowledgements

I want to take this opportunity to express my deepest gratitude to all those who have contributed to the successful completion of this thesis. Their guidance, support, and encouragement have been invaluable throughout this journey.

First and foremost, I would like to extend my heartfelt thanks to Flavio BONO for his exceptional mentorship and unwavering support. His profound knowledge, insightful feedback, and constant encouragement were instrumental in shaping this work. Without his guidance, this thesis would not have reached its full potential. I am truly grateful for the time and effort he dedicated to helping me navigate the challenges of this research.

I am also deeply indebted to Graziano RENALDI and Giovanni VAGLICA for their invaluable assistance in handling sensors, data acquisition, and IT infrastructure. Their technical expertise and willingness to help at every stage of the project were crucial in overcoming numerous obstacles. Their patience and dedication made the experimental phase of this work possible, and for that, I am sincerely grateful.

I want to extend my sincere appreciation to Professor Luca MARTINELLI and Professor Federico PEROTI for their inspiring courses, which laid the foundation for this thesis. Their teachings not only sparked my interest in this field but also provided the theoretical framework that guided my research. Their continuous support, constructive feedback, and encouragement throughout the development of this thesis have been invaluable. I am truly honored to have had the opportunity to learn from such esteemed mentors.

Additionally, I would like to acknowledge the support of my colleagues and friends, who have been a source of motivation and inspiration throughout this journey. Their camaraderie and encouragement helped me stay focused and motivated during challenging times.

Lastly, I would like to express my deepest gratitude to my family for their unconditional love, support, and understanding. Their belief in me and their encouragement have been my driving force, and I am forever thankful for their presence in my life.

This thesis is a culmination of the collective efforts of all those who have supported me along the way, and I am profoundly grateful to each and every one of them. Thank you.

